

**“Mechanisms of resistance of tumor cells
in response to treatment with the vacuolar
H⁺-ATPase inhibitor archazolid B”**

Dissertation

zur Erlangung des Grades

“Doktor der Naturwissenschaften”

im Promotionsfach Pharmazie

**am Fachbereich Chemie, Pharmazie und
Geowissenschaften der Johannes Gutenberg-Universität in
Mainz**

**vorgelegt von Dipl. Chemikerin Rebecca Hamm
geboren am 15.02.1985 in Lahnstein**

Mainz, September 2014

Betreuer: Prof. Dr. [REDACTED]

Gutachter der Arbeit: Prof. Dr. [REDACTED]

Prof. Dr. [REDACTED]

Datum der mündlichen Prüfung: 19.11.2014 (Prüfung vorverlegt auf den 17.11.2014)

Prüfer: Prof. Dr. [REDACTED]

Prof. Dr. [REDACTED]

Prof. Dr. [REDACTED]

Publications

Original publications as lead author

- R. Hamm, M. Zeino, R. Müller, T. Efferth, "Up-regulation of cholesterol associated genes as novel resistance mechanism in glioblastoma cells in response to archazolid B," submitted at *Toxicol Appl Pharmacol*, accepted 2 September 2014.
- R. Hamm, Y. Sugimoto, H. Steinmetz, T. Efferth, "Resistance mechanisms of cancer cells to the novel vacuolar H⁺-ATPase inhibitor archazolid B," submitted at *Invest New Drugs*, accepted 7 July 2014.
- R. Hamm, Y.-R. Chen, E.-J. Seo, M. Zeino, C.-F. Wu, R. Müller, N.-S. Yang, T. Efferth, "Induction of cholesterol biosynthesis by archazolid B in T24 bladder cancer cells," *Biochem Pharm*, vol. 91, pp. 18-30, 2014.

Original publications as co-author

- A. Panossian, R. Hamm, G. Wikman, T. Efferth, "Mechanism of action of Rhodiola, salidroside, tyrosol and triandrin in isolated neuroglial cells: An interactive pathway analysis of the downstream effects using RNA microarray data," *Phytomedicine*, vol. 21, pp. 1325-1348, 2014.
- B. Wiench, Y. R. Chen, M. Paulsen, R. Hamm, S. Schröder, N. S. Yang, T. Efferth, "Integration of Different "-omics" Technologies Identifies Inhibition of the IGF1R-Akt-mTOR Signaling Cascade Involved in the Cytotoxic Effect of Shikonin against Leukemia Cells," *Evid Based Complement Alternat Med*, vol. 2013, 2013.
- A. Panossian, R. Hamm, O. Kadioglu, G. Wikman, T. Efferth, "Synergy and Antagonism of Active Constituents of ADAPT-232 on Transcriptional Level of Metabolic Regulation of Isolated Neuroglial Cells," *Front Neurosci*, vol. 7, 2013.

Submitted manuscripts

- E.-J. Seo, B. Wiench, R. Hamm, M. Paulsen, R. Müller, Y. Zu, Y. Fu, T. Efferth, "Cytotoxicity of natural products and derivatives towards MCF-7 monolayer cells and cancer stem-like mammospheres," 2014.

Poster

- R. Hamm, Y.-R. Chen, E.-J. Seo, M. Zeino, C.-F. Wu, R. Müller, N.-S. Yang, T. Efferth, “Induction of cholesterol biosynthesis by archazolid B in T24 bladder cancer cells” [Poster], 128th meeting of the Gesellschaft Deutscher Naturforscher und Ärzte (GDNÄ) “Vorbild Natur: Faszination Mensch und Technologie”, Mainz, 2014.
- R. Hamm, Y. Sugimoto, H. Steinmetz, T. Efferth, “Resistance mechanisms of cancer cells to the novel vacuolar H⁺-ATPase inhibitor archazolid B” [Poster], 128th meeting of the Gesellschaft Deutscher Naturforscher und Ärzte (GDNÄ) “Vorbild Natur: Faszination Mensch und Technologie”, Mainz, 2014.
- R. Hamm, M. Zeino, R. Müller, T. Efferth, “Up-regulation of cholesterol associated genes as novel resistance mechanism in glioblastoma cells in response to archazolid B” [Poster], 128th meeting of the Gesellschaft Deutscher Naturforscher und Ärzte (GDNÄ) “Vorbild Natur: Faszination Mensch und Technologie”, Mainz, 2014.
- R. Hamm, T. Eichhorn, R. Wiedmann, K. von Schwarzenberg, A. Vollmar, T. Efferth, “Functional and transcriptome-wide analysis of archazolid B as therapeutics for highly invasive cancer“ [Poster], 12th Young Scientist Meeting of the German Society for Cell Biology (DGZ) “RNA & Disease”, Jena, 2011.

Erklärung

Hiermit erkläre ich an Eides statt, dass ich diese Arbeit selbständig verfasst und keine anderen als die angegebenen Quellen und Hilfsmittel verwendet habe.

Mainz, 15.09.2014

Ort, Datum

Rebecca Hamm

Rebecca Hamm

Acknowledgement

First of all, I would like to express my deepest gratitude to Prof. [REDACTED] for the continuous support and motivation during my challenging research projects. He gave me the opportunity to work in his laboratories and be part of his excellent international group.

I thank Prof. [REDACTED] for reading and reviewing my thesis. In addition, I would like to thank Prof. [REDACTED] for taking part in my defense.

I also want to thank Dr. [REDACTED] for his support in flow cytometry and Dr. [REDACTED] for her patience in answering my questions concerning confocal microscopy.

Thanks to all team members of the Department of Pharmaceutical Biology. In particular, Dr. [REDACTED] for their experimental help and expertise. Special thanks also go to [REDACTED] for being the “good souls” of the group. I am really thankful for the experience of working in such an international team. Beside scientific discussions I always appreciated exploring different cultures.

I wish to thank my colleague [REDACTED] for our inspiring discussions as well as for his experimental help and careful proofreading of my manuscripts and thesis. Beside this, he became a really good friend I could always count on.

I owe special thanks to my parents [REDACTED]. Thank you for your endless support and trust in me.

Last but not least, I would like to thank my better half [REDACTED] for his steady encouragement and his patience in helping me with computer problems.

Abstract

Resistance of cancer cells towards chemotherapy is the major cause of therapy failure. Hence, the evaluation of cellular defense mechanisms is essential in the establishment of new chemotherapeutics. In this study, classical intrinsic and acquired as well as new resistance mechanisms relevant in the cellular response to the novel vacuolar H⁺-ATPase inhibitor archazolid B were investigated. Archazolid B, originally produced by the myxobacterium *Archangium gephyra*, displayed cytotoxicity in the low nanomolar range on a panel of cancer cell lines. The drug showed enhanced cytotoxic activity against nearly all cancerous cells compared to their non-cancerous pendants. With regards to ABC transporters, archazolid B was identified as a moderate substrate of ABCB1 (P-glycoprotein) and a weak substrate of ABCG2 (BCRP), whereas hypersensitivity was observed in ABCB5-expressing cells. The cytotoxic effect of archazolid B was shown to be independent of the cellular p53 status. However, cells expressing constitutively active EGFR displayed significantly increased resistance. Acquired drug resistance was studied by establishing an archazolid B-resistant MCF-7 cell line. Experiments showed that this secondary resistance was not conferred by aberrant expression or DNA mutations of the gene encoding vacuolar H⁺-ATPase subunit c, the direct target of archazolid B. Instead, a slight increase of *ABCB1* and a significant overexpression of *EGFR* as well as reduced proliferation may contribute to acquired archazolid B resistance. For identification of new resistance strategies upon archazolid B treatment, *omics* data from bladder cancer and glioblastoma cells were analyzed, revealing drastic disturbances in cholesterol homeostasis, affecting cholesterol biosynthesis, uptake and transport. As shown by filipin staining, archazolid B led to accumulation of free cholesterol in lysosomes, which triggered sterol responses, mediated by SREBP-2 and LXR, including up-regulation of *HMGCR*, the key enzyme of cholesterol biosynthesis. Furthermore, inhibition of LDL uptake as well as impaired LDLR surface expression were observed, indicating newly synthesized cholesterol to be the main source of cholesterol in archazolid B-treated cells. This was proven by the fact that under archazolid B treatment, total free cholesterol levels as well as cell survival were significantly reduced by inhibiting HMGCR with fluvastatin. The combination of archazolid B with statins may therefore be an attractive strategy to circumvent cholesterol-mediated cell survival and in turn potentiate the promising anticancer effects of archazolid B.

Zusammenfassung

Resistenz von Krebszellen gegenüber Chemotherapeutika ist der Hauptgrund für Therapieversagen. Im Hinblick darauf stellt die Evaluierung von zellulären Verteidigungsmechanismen einen essentiellen Schritt bei der Etablierung neuer Krebsmedikamente dar. In der vorliegenden Arbeit wurden daher klassische (intrinsische und erworbene) sowie neue Resistenzmechanismen untersucht, die bei der zellulären Antwort auf den neuen vakuolären H⁺-ATPase Inhibitor Archazolid B eine Rolle spielen. Archazolid B, welches ursprünglich aus dem Myxobakterium *Archangium gephyra* stammt, zeigte toxische Wirkung auf eine Auswahl verschiedener Krebszell-Linien bei Konzentrationen im unteren nanomolaren Bereich. Die abtötende Wirkung der Substanz war bei fast allen Tumorzellen im Vergleich zu den zugehörigen Normalzellen stärker ausgeprägt. Bei der Untersuchung von ABC-Transportern wurde Archazolid B als mäßiges Substrat von ABCB1 (P-Glykoprotein) und schwaches Substrat von ABCG2 (BCRP) identifiziert, wohingegen Hypersensitivität in ABCB5-exprimierenden Zellen beobachtet wurde. Der zytotoxische Effekt von Archazolid B stellte sich als unabhängig vom zellulären p53 Status heraus, jedoch zeigten Zellen mit konstitutiv aktivem EGFR eine deutlich gesteigerte Resistenz gegenüber der Substanz. Erworbene Resistenzmechanismen wurden anhand einer eigens etablierten Archazolid B-resistenten MCF-7 Zell-Linie untersucht. Eine abnorme Expression oder DNA-Mutation des Gens, welches für die vakuoläre H⁺-ATPase Untereinheit c (die direkte Zielstruktur von Archazolid B) kodiert, wurde nicht gefunden. Stattdessen scheinen ein leichter Anstieg von *ABCB1*, eine signifikante Überexpression von *EGFR* sowie eine reduzierte Proliferationsrate zu der erworbenen Resistenz beizutragen. Zur Identifizierung neuer Resistenzstrategien wurden *omics*-Daten von Blasenkrebs und Glioblastoma-Zellen analysiert. Diese wiesen auf deutliche Störungen der Cholesterolumhomöostase, welche Biosynthese, Aufnahme und Transport umfassten, hin. Durch Filipin-Färbung konnte die Ansammlung von freiem Cholesterol in Lysosomen nachgewiesen werden. Vermittelt durch SREBP-2 und LXR führte dies unter anderem zum Anstieg von *HMGCR*, dem Schlüsselenzym der Cholesterolsynthese. Aufgrund zusätzlicher Störung der LDL Aufnahme sowie Beeinträchtigung der LDLR-Oberflächenexpression wurde neu-synthetisiertes Cholesterol als die Hauptquelle von Cholesterol unter Archazolid B-Behandlung identifiziert. Tatsächlich konnte die Menge an freiem Cholesterol sowie lebensfähigen Zellen durch zusätzliche Inhibierung der *HMGCR* mit Fluvastatin signifikant reduziert werden. Die Kombination von Archazolid B mit Statinen könnte daher eine attraktive Strategie darstellen, um Cholesterol-bedingtes Zellüberleben zu vermeiden und im Gegenzug das vielversprechende Antikrebspotential von Archazolid B zu potenzieren.

Table of contents

Acknowledgement	VI
Abstract	VII
Zusammenfassung.....	VIII
Table of contents.....	IX
List of Abbreviations.....	XIV
1 Introduction.....	1
1.1 Cancer in general.....	1
1.2 Cancer treatment.....	2
1.2.1 Classical chemotherapy.....	2
1.2.2 Targeted cancer therapy	3
1.2.3 Natural products for cancer therapy	3
1.2.4 Myxobacterial substances for cancer treatment.....	4
1.3 V-ATPase as a drug target.....	5
1.3.1 V-ATPase function.....	5
1.3.2 V-ATPase structure	6
1.3.3 V-ATPase and cancer.....	7
1.3.4 V-ATPase inhibitor archazolid B	8
1.4 Drug resistance	9
1.4.1 ABC transporters.....	9
1.4.2 Tumor suppressor p53	11
1.4.3 Oncogene EGFR	12
1.4.4 V-ATPase.....	13
1.4.5 Proliferation.....	14
1.5 Cholesterol and cancer.....	14
2 Aim of the thesis	16

3	Results	17
3.1	Role of established resistance mechanisms	17
3.1.1	Cytotoxicity of archazolid B towards tumor and non-tumor cells	17
3.1.2	Archazolid B and ABC transporters	18
3.1.2.1	Archazolid B and ABCB1 (P-glycoprotein)	18
3.1.2.2	Archazolid B and ABCG2 (BCRP)	22
3.1.2.3	Archazolid B and ABCB5	22
3.1.3	Archazolid B and p53	23
3.1.4	Archazolid B and EGFR	24
3.1.5	MCF-7ArchB cells and acquired drug resistance	24
3.1.5.1	Resistance of MCF-7ArchB cells towards archazolid B	25
3.1.5.2	Gene expression of <i>ATP6V0C</i> , <i>EGFR</i> and <i>ABCB1</i> in MCF-7ArchB cells	25
3.1.5.3	Sequence analysis of <i>ATP6V0C</i> in MCF-7 and MCF-7ArchB cells	26
3.1.5.4	Growth kinetic studies with MCF-7 and MCF-7ArchB cells	28
3.1.6	Summary: Role of established resistance mechanisms	29
3.2	Cholesterol synthesis as a new resistance mechanism	30
3.2.1	Archazolid B affects cholesterol homeostasis and endocytosis in T24 cells	30
3.2.1.1	Archazolid B versus doxorubicin	30
3.2.1.2	<i>Omics</i> analysis	31
3.2.1.3	Validation of cholesterol genes by real-time RT-PCR	43
3.2.1.4	Nuclear expression of SREBPs	43
3.2.1.5	Staining of free cholesterol with filipin	44
3.2.1.6	Inhibition of LDL uptake by archazolid B	47
3.2.1.7	LDLR surface expression	47
3.2.1.8	Combination of archazolid B with fluvastatin	48

3.2.2	ArchB affects cholesterol homeostasis in U87MG/ Δ EGFR glioblastoma cells.....	51
3.2.2.1	Gene expression profiling.....	51
3.2.2.2	Validation of cholesterol genes by real-time RT-PCR	60
3.2.2.3	Staining of free cholesterol with filipin	61
3.2.3	Summary: Cholesterol synthesis as a new resistance mechanism	63
4	Discussion.....	64
4.1	Role of established resistance mechanisms	64
4.1.1	Cytotoxicity of archazolid B towards tumor and non-tumor cells.....	64
4.1.2	Archazolid B and ABC transporters.....	65
4.1.3	Role of tumor suppressor p53 and oncogene EGFR	66
4.1.4	MCF-7ArchB cells and acquired resistance mechanisms	67
4.2	Cholesterol synthesis as a new resistance mechanism.....	68
4.2.1	Accumulation of free cholesterol	68
4.2.2	Up-regulation of cholesterol-associated genes	68
4.2.3	LDL uptake and LDLR surface expression.....	70
4.2.4	Free cholesterol levels under archazolid B treatment.....	71
4.2.5	Combination of archazolid B with fluvastatin.....	72
4.3	Side effects of archazolid B on normal tissue.....	72
5	Summary and Conclusion	74
6	Material and Methods	76
6.1	Chemicals and equipment.....	76
6.2	Cell culture.....	80
6.2.1	Multidrug-resistant cell lines.....	81
6.2.2	P53 knockout cells	81
6.2.3	EGFR transfected cells.....	81

6.2.4	Further tumor cell lines	82
6.2.5	Non-tumor cell lines.....	82
6.2.6	Human peripheral mononuclear cells (PMNC).....	82
6.3	Generation of archazolid B-resistant MCF-7 cells (MCF-7ArchB).....	83
6.4	Growth kinetic studies	83
6.5	Cytotoxicity assay	83
6.6	<i>Omics</i> assays: transcriptomics and proteomics.....	84
6.6.1	mRNA microarray.....	84
6.6.1.1	RNA isolation.....	84
6.6.1.2	Probe labeling and hybridization.....	85
6.6.1.3	Scanning and data processing.....	86
6.6.2	miRNA microarray.....	86
6.6.2.1	RNA isolation.....	86
6.6.2.2	Probe labeling and hybridization.....	86
6.6.2.3	Scanning and data processing.....	87
6.6.3	Proteomics analysis.....	87
6.6.3.1	Protein extraction.....	87
6.6.3.2	Stable isotope dimethyl labeling.....	87
6.6.3.3	Data processing	89
6.6.4	<i>Omics</i> data analysis	89
6.6.4.1	Chipster analysis.....	89
6.6.4.2	Ingenuity Pathway Analysis.....	89
6.7	Real-time RT-PCR	90
6.7.1	mRNA microarray validation.....	91
6.7.2	Gene expression: <i>ABCBI</i> , <i>EGFR</i> , <i>ATP6V0C</i>	92

6.8	Sequencing	93
6.9	Molecular docking.....	93
6.10	Nuclear expression of SREBPs (Western blot).....	94
6.10.1	Sample preparation	94
6.10.2	SDS-PAGE	95
6.10.3	Tank blotting.....	96
6.10.4	Antibody staining and detection	96
6.11	Staining of free cholesterol with filipin.....	97
6.11.1	Cell seeding and treatment.....	97
6.11.2	Staining	97
6.11.3	Flow cytometry	97
6.11.4	Fluorescence microscopy.....	98
6.12	LDL uptake (Confocal microscopy).....	98
6.13	LDLR surface expression (Flow cytometry)	99
6.14	Statistical analysis.....	99
7	References	100

List of Abbreviations

Table 1: Abbreviations

Abbreviation	Connotation
ABC	ATP-binding cassette
ABCA1	ATP-binding cassette sub-family A member 1
ABCB1	ATP-binding cassette sub-family B member 1/P-glycoprotein
ABCB5	ATP-binding cassette sub-family B member 5
ABCG2	ATP-binding cassette sub-family G member 2/BCRP
ACN	Acetonitrile
APS	Ammonium persulfate
ArchB	Archazolid B
ATP6V0C	V-ATPase subunit c
BCRP	Breast cancer resistance protein
BSA	Bovine serum albumin
CHO	Chinese hamster ovary
C _t	Cycle threshold
DHCR24	24-dehydrocholesterol reductase
DMSO	Dimethyl sulfoxide
EGF(R)	Epidermal growth factor (receptor)
EMS	Ethyl methanesulfonate
FA	Formic acid
FACS	Fluorescence-activated cell sorting
FBS	Fetal bovine serum
FC	Fold change
FDA	Food and Drug Administration
FDFT1	Farnesyl-diphosphate farnesyltransferase 1
Fluva	Fluvastatin
GBM	Glioblastoma multiforme
HEPES	4-(2-hydroxyethyl)-1-piperazineethanesulfonic acid
HF	High fluorescence
HMGCR	3-hydroxy-3-methylglutaryl-CoA reductase
HMGCS1	3-hydroxy-3-methylglutaryl-Coenzyme A synthase 1, soluble
IC ₅₀	Half maximal inhibitory concentration
INSIG1	Insulin induced gene 1
IPA	Ingenuity Pathway Analysis
LC-MS/MS	Liquid chromatography-mass spectrometry/mass spectrometry
LDL(R)	Low density lipoprotein (receptor)
LF	Low fluorescence
LXR	Liver X receptor
MAP	Mitogen-activated protein
MDR	Multidrug resistance

MFI	Mean fluorescence intensity
MMTS	S-methyl methanethiosulfonate
MPR	Mannose-6-phosphate receptor
MSMO1	Methylsterol monooxygenase 1
MYLIP	Myosin regulatory light chain interacting protein/inducible degrader of LDL receptor
N/A	Not available
NBD	Nucleotide-binding domain
NPC	Niemann-Pick disease, type C
NPC1	Niemann-Pick disease, type C1
NPC2	Niemann-Pick disease, type C2
P/S	Penicillin/streptomycin
PFA	Paraformaldehyde
P-gp	P-glycoprotein
PI3K	phosphatidylinositol 3-kinase
PMNC	Human peripheral mononuclear cells
PMS	Phenazine methosulfate
Q-TOF-MS	Quadrupole time-of-flight mass spectrometer
RT-PCR	Reverse transcription PCR
RXR	Retinoid X receptor
SCX	Strong cation exchange
SD	Standard deviation
SDS	Sodium dodecyl sulfate
SQLE	Squalene monooxygenase
SREBF1	Sterol regulatory element binding transcription factor 1
SREBP	Sterol regulatory element binding protein
SREBP-1	Sterol regulatory element binding protein-1
SREBP-2	Sterol regulatory element binding protein-2
nSREBP-2	Nuclear sterol regulatory element binding protein-2
STAT	Signal transducer and activator of transcription
TBST-T	Tris-buffered saline-Tween20
TCEP	Tris (2-carboxyethyl) phosphine hydrochloride
TCM	Traditional Chinese Medicine
TEABC	Triethylammonium bicarbonate
TEMED	Tetramethylenediamine
TFA	Trifluoroacetic acid
TGN	Trans-Golgi network
TM(D)	Transmembrane domain
Tris	Tris (hydroxymethyl) aminomethane
V-ATPase	Vacuolar H ⁺ -ATPase
VEGFR	Vascular endothelial growth factor receptor
WHO	World Health Organization
XTT	2,3-Bis-(2-methoxy-4-nitro-5-sulfophenyl)-2H-tetrazolium-5-carboxanilide

1 Introduction

1.1 Cancer in general

Cancer is a major cause of mortality accounting for about 7.6 million deaths worldwide in 2008 [1]. By 2030, the global burden of cancer is believed to increase drastically to about 26 million new cancer cases and 17 million cancer deaths per year, mainly due to continuing growth and aging of the world's population [2]. Cancer, which is also termed malignant neoplasm, describes a vast group of diseases caused by unregulated proliferation of cells. The resulting malignant tumor, in contrast to a benign tumors, is able to metastasize, meaning that it can enter the blood and/or the lymphatic system, thus spreading to other parts of the body and causing secondary tumors [3]. Despite their complexity, malignant tumors display a set of common characteristics. In 2000, Hanahan and Weinberg suggested six hallmarks of cancer that enable malignant tumor growth (Figure 1): Resistance to cell death, maintenance of proliferative signals, avoidance of growth suppressors, stimulation of angiogenesis, limitless replication as well as tissue invasion and metastasis [4]. Eleven years later, two further hallmarks of cancer were proposed: deregulation of cellular energetics and avoidance of immune destruction [5].

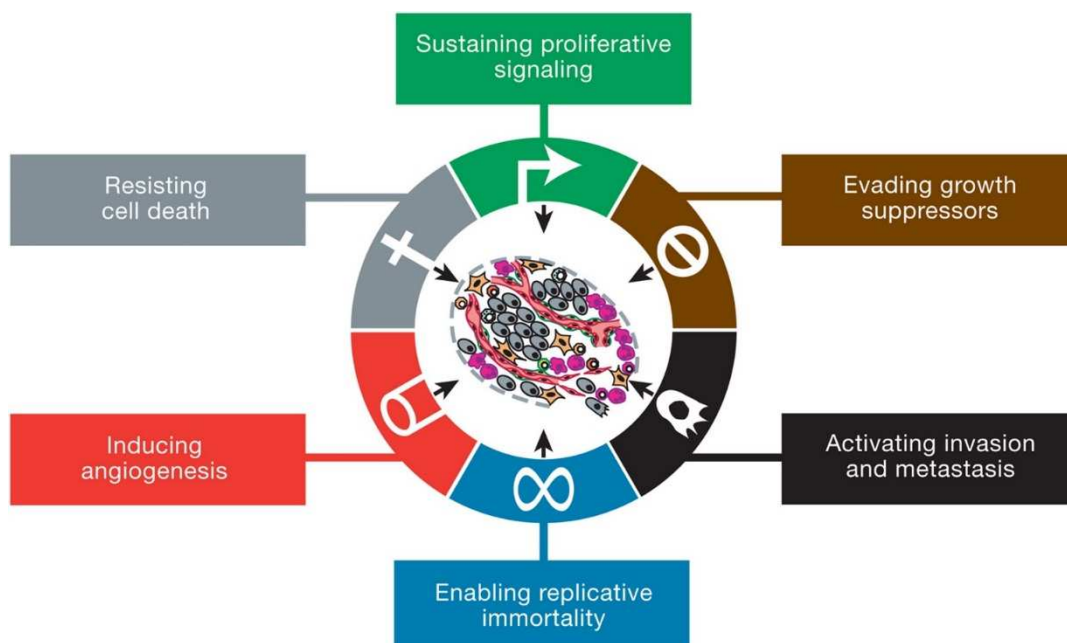


Figure 1: The hallmarks of cancer. Cancer cells display a common set of characteristics that enable malignant tumor growth. Image taken from Hanahan and Weinberg [5].

Tumorigenesis is a multistep process requiring several mutations of the genetic material [6]. Although germline mutations may contribute by increasing cancer risk, the essential mutations are usually somatic events that accumulate over a person's lifespan [7]. In addition to that, gene expression in cancer cells can also be altered by epigenetic mechanisms e.g. chromosomal modifications [8]. Interestingly, only 5-10% of all cancer cases are linked to inherited genetic defects whereas the remaining 90-95% are due to environment and lifestyle [9]. Diet, tobacco, infections, obesity, alcohol but also stress and physical inactivity are factors that negatively influence cancer formation [9].

1.2 Cancer treatment

The treatment of cancer as a complex disease is a great challenge. Current treatment strategies include surgery, radiotherapy and chemotherapy. Out of these three, only chemotherapy is effective against metastatic cancer by reaching all parts of the body and therefore became the focus of current cancer research [10].

1.2.1 Classical chemotherapy

Cancer chemotherapy describes the treatment of cancer with one or more cytotoxic drugs. In the early 20th century, the investigation of arsenicals constituted an early step in the use of drugs against cancer [11]. The modern era of chemotherapy, however, is closely linked to World War II. Due to enhanced research on chemical warfare, nitrogen mustard was identified as an effective therapeutic for lymphoid tumors [10, 12]. Classical chemotherapy targets fast proliferating cells and includes alkylating drugs (e.g. carmustin and cyclophosphamide), platinum derivatives (e.g. cisplatin and carboplatin), antimetabolites (e.g. methotrexate and gemcitabine), DNA-topoisomerase inhibitors (e.g. topotecan and doxorubicin) and microtubule inhibitors (e.g. vinblastine and paclitaxel) [13]. Although these drugs are effective against cancer cells, they also compromise non-malignant cells (especially cells with high proliferation rate) thereby leading to severe side effects. These side effects include e.g. myelosuppression, immunosuppression, specific organ damage (lung, liver, kidney, heart), nausea, vomiting, fever, diarrhea, hair loss and bleeding problems [14].

1.2.2 Targeted cancer therapy

Within the last two decades, targeted therapy emerged as a new promising strategy in the fight against cancer. In contrast to classical chemotherapy, affecting all rapidly proliferating cells by interfering with DNA or microtubule function, the focus of targeted therapy lies on cancer-specific molecular abnormalities (e.g. overexpression, mutation) which are targeted by monoclonal antibodies or small molecules [15]. Until now, more than 30 drugs for targeted therapy have been approved in clinical use. Most of these drugs target kinases in growth promoting pathways, like epidermal growth factor receptor (EGFR) and vascular endothelial growth factor receptor (VEGFR) pathways, which can be inhibited on multiple signaling levels [16]. However, though targeted drugs constitute a new era of personalized medicine for cancer treatment, there are some limitations and obstacles. Targeted therapy also displays side effects and is often related to immense costs, especially when monoclonal antibodies are involved [15]. Furthermore, like classical cancer treatment, targeted therapy can be hindered by drug resistance e.g. via outgrowth of a resistant subpopulation [17]. The vacuolar H⁺-ATPase (V-ATPase) as a potential drug target for cancer therapy is introduced in the following chapter.

1.2.3 Natural products for cancer therapy

Natural products, mainly derived from plants and microorganisms, are small molecules and substances playing a significant role in cancer treatment. With respect to cancer therapy, over the period from 1940s up to 2010, 41% of the worldwide-approved anticancer drugs were natural products or directly derived from them [18]. The use of traditional medicine is documented in cultures all around the world and dates back to about 5000 years ago [19]. According to the World Health Organization (WHO), about 80% of the world population depend on plant derived traditional medicine for primary health care [20]. The medicinal effect of plants is based on the expression of pharmacological active secondary metabolites [21]. Examples of Traditional Chinese Medicine (TCM)-derived herbal drugs in cancer therapy are the microtubule inhibitors vinblastine from *Catharanthus roseus* and paclitaxel from *Taxus brevifolia* [22]. Beside medicinal plants, the microbial world provides a vast source of structurally diverse bioactive metabolites [23]. Since the discovery of penicillin by Alexander Fleming in 1928, secondary metabolites from microorganisms have been contributing immensely to health and well-being of people [24]. In cancer treatment, antibiotics constitute one of the most important groups of chemotherapeutics [25]. Antitumor antibiotics produced

by microbes include e.g. doxorubicin, daunomycin, bleomycin, actinomycin D and pentostatin [25].

1.2.4 Myxobacterial substances for cancer treatment

Belonging to the gram-negative eubacteria, myxobacteria are spread all over the world and typically found in soil but also in rotting plant material, decaying insects and dung [26]. Myxobacteria display two important features: 1) Cells form characteristic swarms and move by gliding 2) Under starvation, cells aggregate and fruiting bodies are formed, in which cells are converted to myxospores as a guarantee of survival [27]. Myxobacteria represent a vast source of secondary metabolites. Up to now, about 7500 myxobacterial strains have been identified, bearing not less than 100 core structures and 500 derivatives [28]. The anticancer potential of distinct myxobacterial substances is due to their interaction with three main targets: 1) tubulin 2) actin and 3) V-ATPase [29]. The most prominent myxobacterial substance is the tubulin stabilizer epothilone. In 2007, a semisynthetic analogue of the naturally occurring epothilone B (from *Sorangium cellulosum*), ixabepilone (Ixempra[®]), was approved by the Food and Drug Administration (FDA) for the treatment of breast cancer [30, 31]. Currently, five epothilone or epothilone derived drugs are in clinical trials [31]. In contrast to epothilone, tubulysin and disorazol are potent tubulin destabilizers, displaying high toxicity against mammalian cancer cells [32, 33]. A folic acid-tubulysin conjugate (EC1456) is in phase I trial against advanced solid tumors [34]. Furthermore, chondramides and rhizopodin, exerting their cytostatic effect by interfering with actin, are important myxobacterial compounds produced by *Chondromyces crocatus* and *Myxococcus stipitatus* [35, 36]. Targeting the V-ATPase, apicularens and the even more potent archazolids have come into the focus of anticancer research [37]. The archazolid family comprises six members (A, B, C, D, E and F). Archazolid A, B and F are originally produced by *Archangium gephyra* whereas the myxobacterial strain *Cystobacter violaceus* represents the source of the archazolid glycosides – archazolid C, D and E [38-41]. Comparing all archazolids, the non-glycosylated forms – A, B and F – revealed the highest effect displaying V-ATPase inhibition and cytotoxicity in the low nanomolar range [41].

The compound of our interest was archazolid B which is explained together with its target – the V-ATPase – in the following chapter.

1.3 V-ATPase as a drug target

1.3.1 V-ATPase function

V-ATPases are heteromultimeric proton pumps that can be found in every eukaryotic cell from yeast to human [42]. These ATP-dependent proton pumps are located in the membrane of intracellular compartments including endosomes, lysosomes and secretory vesicles as well as in the plasma membrane of specialized cells (e.g. renal intercalated cells, osteoclasts, macrophages), playing a fundamental role in pH regulation [43]. Acidification by V-ATPases has been reported to be essential for various processes including receptor-mediated endocytosis, ligand-receptor dissociation, receptor recycling as well as protein processing [44]. Figure 2 displays the role of V-ATPase in membrane transport.

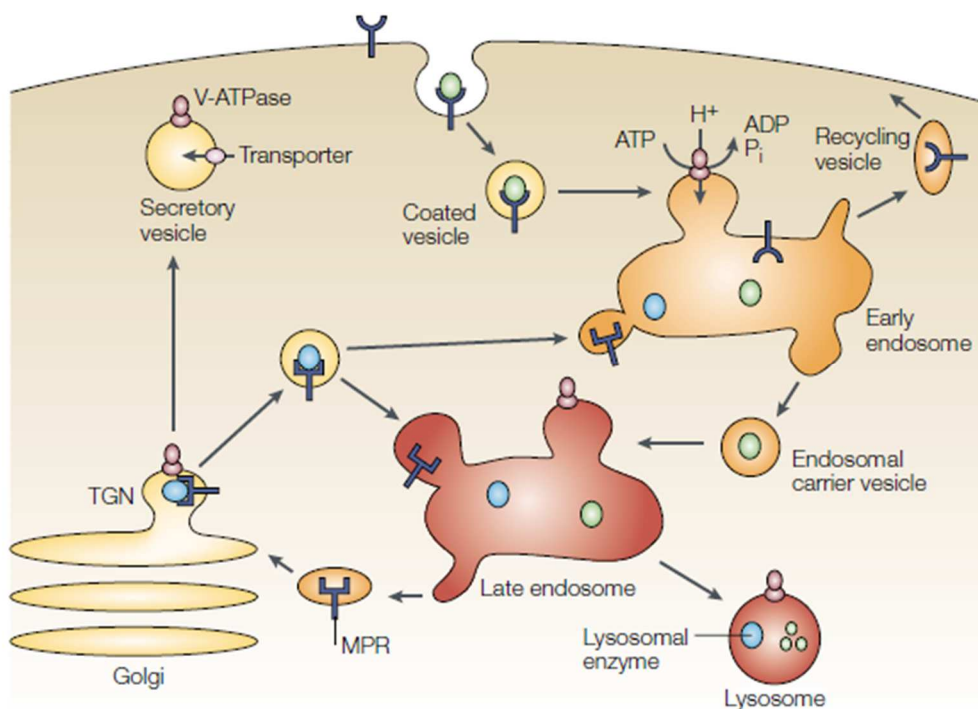


Figure 2: V-ATPase and membrane transport. Acidification of endosomes, lysosomes and vesicles by V-ATPases is important for receptor-mediated endocytosis and intracellular targeting. Optimal pH values (yellow: neutral pH, red: acidic pH) are crucial for ligand-receptor dissociation, receptor recycling, carrier vesicle formation and release of lysosomal enzymes from mannose-6-phosphate receptor (MPR) to the trans-Golgi network (TGN). Image taken from Nishi and Forgac [43].

1.3.2 V-ATPase structure

The V-ATPase is a multisubunit complex composed of two domains: V_1 domain mediating ATP hydrolysis and V_0 domain being responsible for proton transport across the membrane. The V_1 complex with a molecular mass of 650 kDa is localized on the cytoplasmic side of the membrane. It is formed by eight different subunits: A, B, C, D, E, F, G and H. ATP hydrolysis occurs at the interface of the A and B subunits, with three altering copies of each forming a hexameric ring. A central stalk is composed of subunits D and F, whereas subunits C, E, G and H form peripheral stalks. Both types of stalks connect the V_1 domain and the integral V_0 domain. The V_0 domain, mediating proton transport, has a molecular weight of 260 kDa and consists of subunits a, d, e and the ring of proteolipids [45]. In the mammalian V-ATPase, this ring is formed by two different proteolipid subunits (c and c'), whereas in yeast, an additional proteolipid subunit c' can be found [46].

The V-ATPase displays structural and functional similarities to the mitochondrial F-ATPase [43, 47]. However, they operate in opposite directions: In contrast to the V-ATPase that hydrolyzes ATP for translocation of protons, the F-ATPase is an ATP synthase, thus generating ATP by utilization of the proton gradient [48]. Based on models proposed for F-ATPases and V-ATPases, the following mechanism of proton transport by V-ATPases across the membrane has been hypothesized: Cytoplasmic H^+ enters the inner half channel of subunit a and binds to one subunit of the c-ring. Hydrolysis of ATP, at a coupling ratio of $1ATP/2H^+$, leads to clockwise rotation of the c-ring and after nearly 360° , H^+ leaves the membrane through the outer half channel of subunit a [49].

Structure and function of the V-ATPase are shown in Figure 3.

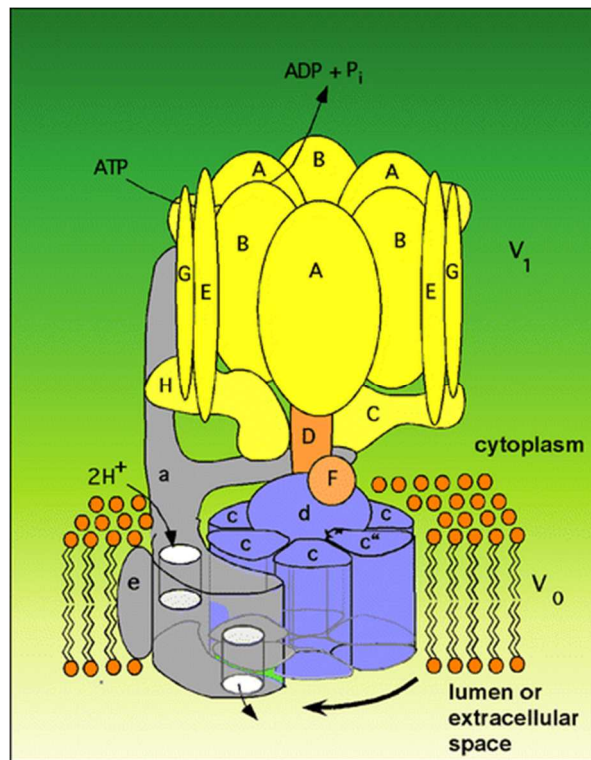


Figure 3: Structure and function of the V-ATPase. The V-ATPase consists of two different domains, V₁ and V₀. V₁ is composed of subunits A-H and V₀ of subunits a, d, e and the proteolipid ring [45]. In the mammalian V-ATPase, this ring is formed by two different proteolipid subunits (c and c'), whereas in yeast an additional proteolipid subunit c' can be found [46]. Subunit a of the V₀ domain provides two H⁺ half channels. Upon entering the inner half channel, H⁺ binds to one subunit of the c-ring. ATP hydrolysis (coupling ratio: 1ATP/2H⁺) mediated by subunit V₁ leads to rotation of the H⁺-transporting c-ring of subunit V₀ resulting in release of H⁺ through the outer half channel [49]. Image taken from Hinton et al. [46].

1.3.3 V-ATPase and cancer

V-ATPases are presumed to be involved in a large number of diseases including diabetes, osteoporosis, Alzheimer's, Parkinson's, cardiovascular disorders and cancer [50]. Due to metabolic changes, tumor cells display enhanced cytosolic pH, whereas the tumor environment is more acidic compared to normal cells [51]. Maintaining this gradient is essential for tumor function and mediated by acid extruders [51]. One of these extruders is the V-ATPase which is often overexpressed in tumor cells, especially in the plasma membrane [52, 53]. Maintenance of the pH gradient by V-ATPases in cancer cells has been related to tumor progression and malignancy leading to metastasis and increased proliferation [54]. Acidification of the tumor environment by V-ATPase enhances invasion and metastasis due to activation of proteolytic enzymes at low pH and degradation of the extracellular matrix, whereas maintenance of high cytosolic pH is critical for tumor cell survival, since acidosis is known to trigger apoptosis [54, 55].

Due to its important role in tumor pH homeostasis, the V-ATPase is considered as an attractive target for cancer therapy [54, 56]. The first V-ATPase inhibitors, bafilomycins and concanamycins, were already discovered in the 1980's [57]. The present thesis deals with the novel V-ATPase inhibitor archazolid B, which is introduced in the following section.

1.3.4 V-ATPase inhibitor archazolid B

Archazolid B (Figure 4) is a macrolide antibiotic originally produced by the myxobacterium *Archangium gephyra*, but meanwhile also accessible by chemical synthesis [38, 58, 59]. With a molecular weight of 725 Da (PubChem database; <http://pubchem.ncbi.nlm.nih.gov>), it still belongs to small molecules. Archazolid B prevents lysosomal acidification by specific inhibition of V-ATPase at nanomolar concentrations, without targeting any of F- and P-ATPases [37]. The drug interacts with the equatorial region of the V_0 subunit c surface, thus preventing the rotation of the c-ring. In addition to that, binding of archazolid B may also directly impair proton exchange between a-subunit and c-ring through interaction with the essential glutamate [60, 61]. Displaying cytotoxicity in the nanomolar range, archazolid B induces cell death by activating the intrinsic mitochondrial apoptotic pathway and causes energy stress responses such as activation of autophagy or glycolysis [62]. Furthermore, it has also been reported to affect endocytotic processes. So, the drug inhibited transferrin/transferrin receptor uptake and led to impaired EGFR internalization and localization thus influencing EGFR signaling and cell migration [63, 64].

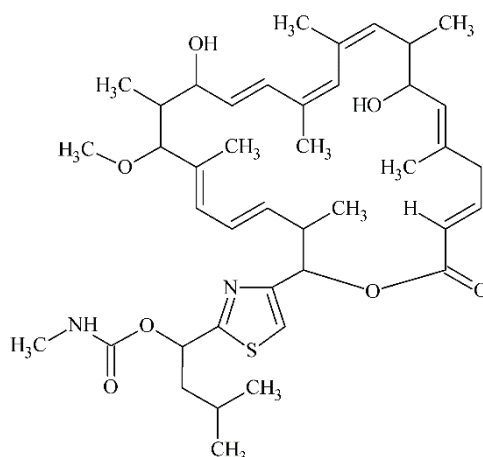


Figure 4: Chemical structure of archazolid B.

1.4 Drug resistance

The primary cause of failure in cancer treatment is the development of resistance towards chemotherapeutics. Tumors can either be intrinsically resistant or acquire resistance upon treatment with chemotherapeutics [65]. The mechanisms by which cancer cells diminish the effectiveness of chemotherapy are various, including changes in drug availability within the cell, DNA damage repair, target expression as well as altered apoptosis and survival signaling [66]. The different mechanisms of drug resistance investigated in this study are explained in the following section.

1.4.1 ABC transporters

One of the main mechanisms by which drug resistance is conferred in cancer cells, is the overexpression of distinct ATP binding cassette (ABC) transporters. These are able to mediate drug efflux and thus reduce intracellular drug levels [67]. With 48 human ABC genes, the ABC transporter superfamily constitutes the largest family of transporter genes. According to domain organization and amino acid homology, 7 subfamilies can be distinguished, labelled A-G [68]. The functional unit of an ABC transporter comprises two transmembrane domains (TMDs) as well as two nucleotide-binding domains (NBDs). It is either formed by a full transporter or by dimerization of two half-transporters [68]. The ABC transporters studied in this thesis are ABCB1, ABCG2 and ABCB5 and will be explained in more detail in the following.

Drug resistance of tumors is not only limited to a single drug, but often occurs against a broad spectrum of agents. The involvement of ABC transporters in this so called multidrug resistance (MDR) has been discovered in the early 1970s and resulted in the identification of P-glycoprotein (P-gp/ABCB1) as a central mediator of multidrug efflux [69]. Displaying a molecular weight of 170 kDa, P-gp is encoded by the *ABCB1* gene (or human *MDR1*) [70]. The x-ray structure of human P-gp has not been revealed yet. However, an x-ray structure of mouse P-gp is available, displaying 87% sequence identity to human P-gp [71]. The following information refers to the findings of this x-ray structure. P-gp is a full transporter with an intracellular-facing conformation in the absence of nucleotides, consisting of two bundles of six transmembrane helices each. The cavity formed by these bundles is open to the cytoplasm as well as to the inner leaflet, thus allowing direct access of hydrophobic substances from the membrane. The presumptive drug-binding pocket is mainly composed of hydrophobic and aromatic residues [71]. The structure of mouse P-gp is shown in Figure 5.

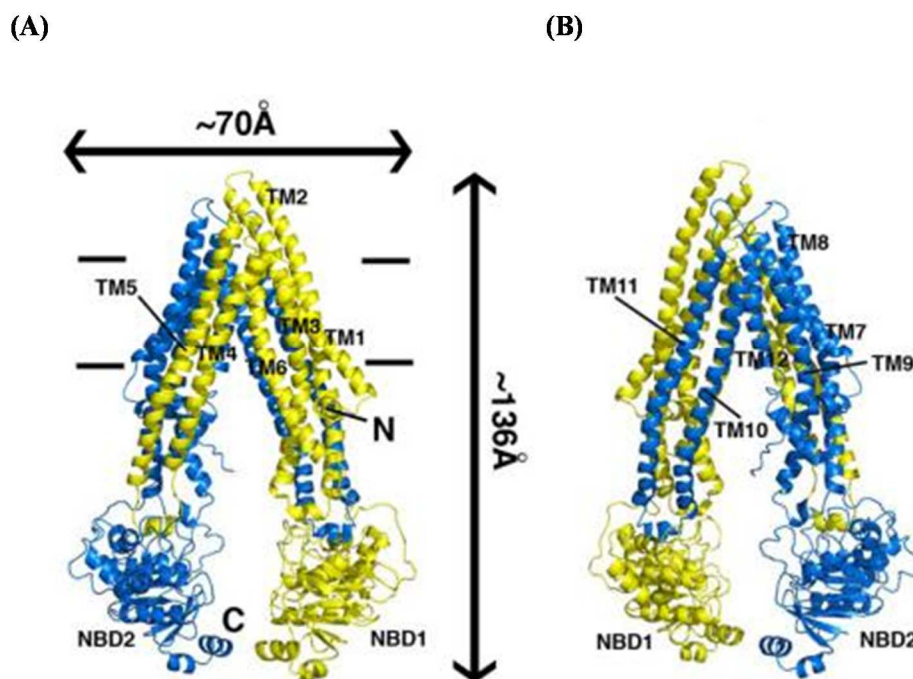


Figure 5: Structure of mouse P-gp as front (A) and back (B) view. Transmembrane domains (TM1-12), N- and C-terminus as well as nucleotide binding domains (NBD1 and NBD2) are labelled. The N-terminal half is colored yellow, whereas the C-terminal half is colored blue. Image taken from Aller et al. [71] and slightly modified.

Amongst ABC transporters, P-gp mediates the strongest resistance to the broadest range of compounds, which are mainly hydrophobic, amphiphatic natural products [69, 72]. Transport by P-gp is known for a large variety of chemotherapeutics that are functionally and chemically different. These include basic anticancer drugs, e.g. anthracyclines (doxorubicin, daunomycin), the *Vinca* alkaloids (vincristine, vinblastine and vindesine), etoposide, colchicine and others [73]. The exact mechanism of P-gp mediated drug transport is not clarified. Currently, there are two different models for drug export: Hydrophobic vacuum cleaner and flippase model [74]. In the hydrophobic vacuum-cleaner model, drugs enter the drug-binding pocket from the cytoplasmic leaflet and are effluxed directly to the extracellular space. The flippase model is based on the assumption that a substrate is transported (flipped) from the inner leaflet to the outer leaflet of the membrane from where the drug either reaches the extracellular space by passive diffusion or moves back to the inner leaflet by flip-flop [74]. ATP binding to P-gp is essential for drug transport and two ATP molecules are needed for one catalytic cycle. According to the ATP switch model, ligand binding to the transmembrane domain facilitates loading of NBDs with ATP molecules which form a closed dimer. The closed dimer induces a conformational change in the TMDs leading to release of the substrate into extracellular space. Sequential hydrolysis of bound ATPs restores the transporter to the nucleotide-free open state and completes the cycle [75]. Drug resistance mediated by P-gp has been shown to be reversible

by multiple agents (e.g. verapamil, quinidine, tamoxifen). However, due to unwanted side-effects or lack of efficiency in clinical trials, these so called “inhibitors” are, so far, not involved in oncologic practice [76].

Another well-known ABC transporter mediating MDR is the breast cancer resistance protein (BCRP/ABCG2) which has been discovered in 1998 [77]. In contrast to P-gp, BCRP represents a half-transporter which forms a 140 kDa homo-dimer connected by disulfide bonds [78]. Substrate specificities of BCRP and P-gp are considerably overlapping, however, differences in efficiencies are observable [79].

The third ABC transporter studied in this thesis, ABCB5, is a rather novel member of the P-gp subfamily [80]. Two major mRNA species of *ABCB5* are known: *ABCB5 β* encoding a half-transporter and *ABCB5* encoding a full transporter. HEK293 cells transfected with cDNA encoding full-sized ABCB5 showed expression of a 150-160 kDa transporter and displayed resistance towards taxanes and anthracyclines [81]. The same cells were also used for the experiments presented in this thesis.

1.4.2 Tumor suppressor p53

Loss of tumor suppressor function has been reported to contribute effectively to drug resistance [66]. A central role in mediating drug resistance is ascribed to p53, which was discovered in 1979 and later identified as a tumor suppressor in 1989 [82, 83]. Being one of the key players in the regulation of cell cycle arrest, DNA repair and apoptosis, p53 guards the genome stability and prevents aberrant cell growth [84]. Normally expressed at low levels with a short half-life, p53 is stabilized in response to various stress events including DNA damage, hypoxia, viral infection or oncogene activation [85]. Activation of the stable p53 requires posttranslational modifications including phosphorylation, acetylation, ubiquitylation, leading to conformational changes of the protein [83]. Depending on its activation, p53 may function as a transcription factor causing an induction of specific genes after DNA binding or mediating gene repression. P53 induced expression of p21 (WAF1), GADD45 and 14-3-3- σ leads to cell cycle arrest, whereas apoptosis is related to expression of death receptors (e.g. Fas/APO1, KILLER/DR5) and mitochondrial proteins (e.g. Bax, NOXA) [83, 85]. Repression of c-myc, Bcl2, Survivin, MDR1 and Cyclin B by activated p53, also affects cell cycle, cell growth and apoptosis [86]. The central role of the tumor suppressor p53 is underlined by the fact that the encoding gene TP53 is mutated in about 50% of all human cancers and that TP53 mutations

can cause resistance to chemo- and radiotherapy [86, 87]. Most of these mutations are loss-of-function mutations leading to impaired DNA binding of the tumor suppressor under stress stimuli (e.g. chemotherapeutics, radiation), which results in failure of growth inhibition and apoptosis [87]. Gain-of-function mutations, however, have also been reported to compromise chemotherapeutic outcome [88, 89]. In the present study, experiments were performed on human colon cancer HCT116 WT p53 wild-type and p53 knockout HCT116 p53^{-/-} cells.

1.4.3 Oncogene EGFR

The epidermal growth factor receptor (EGFR), also known as HER1 or c-erbB-1, is a 170 kDa transmembrane protein belonging to the erB family of tyrosine kinase receptors. The EGFR receptor can be activated by a variety of ligands including epidermal growth factor (EGF) [90]. Upon extracellular ligand binding, the erB family members form homo- or hetero-dimers leading to activation of downstream cascades through auto-phosphorylation of tyrosine residues [90]. As shown in Figure 6, EGFR signaling activates the Ras–Raf–MAP (mitogen-activated protein) kinase pathway, the PI3K (phosphatidylinositol 3 kinase)-Akt pathway and the STAT (signal transducer and activator of transcription) signaling pathway, thus promoting proliferation, cell growth, migration, cell cycle progression, cell survival and differentiation [91]. Aberrant EGFR signaling has been related to chemoresistance and can be induced by cytotoxic drugs as a defense mechanism [92]. In contrast to normal cells, carcinomas often display EGFR overexpression or amplification or mutation of the EGFR gene [93]. Furthermore, enhanced expression of EGFR in head and neck, ovarian, bladder and oesophageal cancers strongly correlates with a bad prognosis [94]. EGFR mediated signaling plays a crucial role in glioblastoma multiforme (GBM), the most common and aggressive lethal brain tumor. Amplification of EGFR has been found in 40-50% of GBMs and is often accompanied by mutations [95]. The most common variant (EGFRvIII), leads to the expression of a constitutively active truncated EGFR protein and is observed in 20-50% of GBMs [96-98]. Considering these facts, targeting EGFR in glioblastoma seems to be promising. However, detailed studies showed that the outcome of targeting EGFR in glioblastoma therapy is rather poor due to complex molecular mechanisms in EGFR/EGFRvIII signaling, including aberrant downstream pathways or receptor crosstalk with oncogenic transcription factors or other receptor tyrosine kinases, leading to drug resistance of the tumor [99]. Harboring this EGFRvIII mutation, glioblastoma cells show a weaker response to the EGFR tyrosine kinase inhibitor gefitinib compared to cells expressing normal EGFR [100]. However, drug resistance conferred

by EGFRvIII mutation is not only limited to kinase inhibitors, but has also been reported for drugs with a completely different mode of action (e.g. cisplatin, taxol and vincristine) through suppression of apoptosis [101]. In the present thesis, resistance of the glioblastoma cell lines U87MG and U87MG. Δ EGFR, harboring EGFRvIII mutation, towards archazolid B is evaluated.

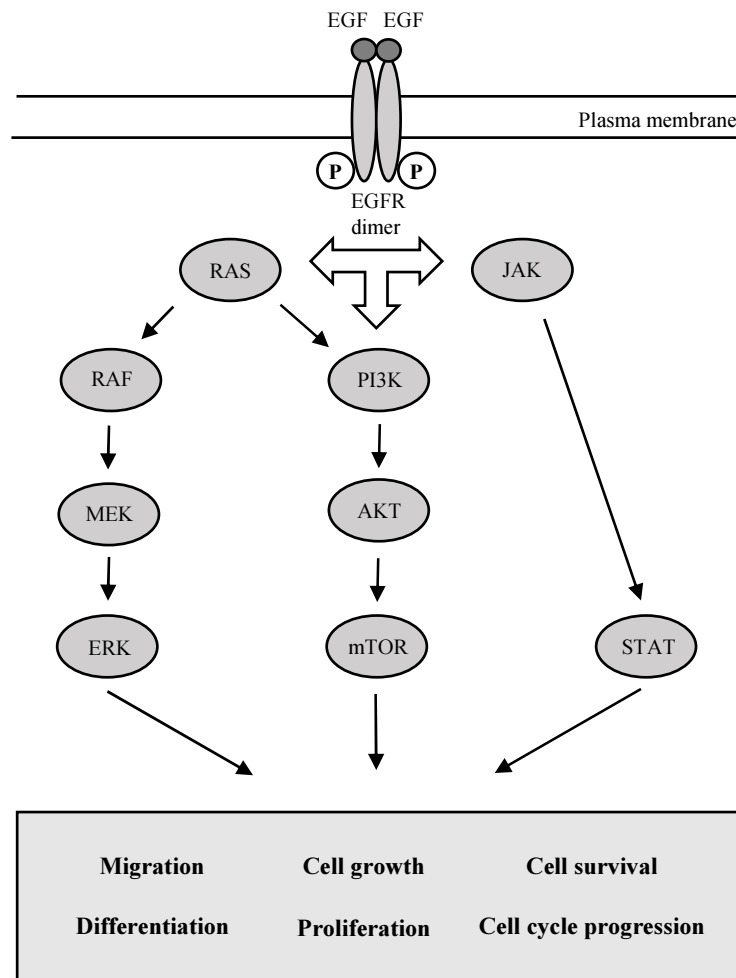


Figure 6: EGFR signaling pathway.

1.4.4 V-ATPase

Due to their important role in pH regulation, V-ATPases are also involved in chemoresistance. Multidrug resistant cells often show enhanced expression of V-ATPase and contain more acidic compartments than drug-sensitive parental cells [102, 103]. This leads to abnormal protonation and sequestration of basic drugs (e.g. doxorubicin) in endo-lysosomes, drastically reducing the efficacy of the chemotherapeutic since it is not delivered to the nucleus [104]. Deregulation of extracellular and cytoplasmic pH, as mediated by V-ATPases, has also been related to impaired chemotherapeutic uptake and modulation of drug cytotoxicity [104, 105].

1.4.5 Proliferation

Maintenance of proliferation signaling has been defined as a hallmark of cancer dictating malignant growth [4]. The dependency of drug cytotoxicity on proliferation is known for more than 40 years now [106]. Classical chemotherapeutics, e.g. doxorubicin, cisplatin or vinblastine, work by interfering with DNA or microtubules, thus targeting fast proliferating cells [13]. Considering this fact, drug resistance as a result of impaired or inhibited proliferation is evident. It has been demonstrated that in cancer cells, cell growth and proliferation are enhanced due to metabolic reprogramming [107]. In this context, decreased cell proliferation may also be seen as an adaptive mechanism of the tumor which guarantees survival under unfavorable metabolic conditions.

1.5 Cholesterol and cancer

In the early 1920s, Otto Warburg observed that cancer cells convert high amounts of glucose using less efficient glycolysis even when oxygen supply is not restricted. This phenomenon called “Warburg effect” displayed the first link between aberrant cell metabolism and cancer [108]. However, due to lack of evidence and shifted focus of research on genes and chromosomes, this “metabolic” model was more or less disregarded in the following decades until new technologies paved the way for precise *in vivo* studies resulting in renewed interest in metabolic changes [107]. Nowadays, altered tumor metabolism is generally accepted as a hallmark of cancer [109]. During the last years, lipid metabolism of cancer cells came into the center of attention, displaying influence on various cellular functions like cell growth, proliferation or differentiation and motility [110]. The crucial role of cholesterol and its synthesis, constituting an important process in cancer lipid metabolism, is evaluated in the following.

In mammalian cells, there are two main sources of cholesterol: 1) Endogenous cholesterol through biosynthesis from acetyl-CoA through mevalonate and 2) uptake of extracellular low density lipoprotein (LDL) particles by receptor-mediated endocytosis, followed by lysosomal degradation and release of free cholesterol [111, 112]. Cholesterol homeostasis is tightly controlled by the action of SREBPs (sterol regulatory element binding proteins) and liver X receptor (LXR) transcription factor [113]. At low cholesterol levels, SREBPs, localized in the endoplasmic reticulum, are activated and translocate to the nucleus, where they induce the expression of genes involved in fatty acid synthesis as well as cholesterol synthesis and uptake

[114]. LXR receptor, a nuclear receptor transcription factor is activated by cellular oxysterol derivatives of cholesterol [115]. This leads to ABCA1- and ABCG1-mediated cholesterol efflux and expression of myosin regulatory light chain interacting protein (MYLIP) [115]. MYLIP, an E3 ubiquitin ligase, reduces LDLR protein levels by targeting the receptor for degradation [116]. Cholesterol is a central molecule for proper cellular functions. Cancer cells are known to have an increased demand of it and often display elevated LDL metabolism or increased levels of 3-hydroxy-3-methylglutaryl-CoA reductase (HMGCR), the key enzyme of cholesterol biosynthesis [117, 118]. High dietary cholesterol intake significantly correlates with the risk of several cancer types, including colon, lung, breast, kidney and bladder cancer [119]. Furthermore, increased cholesterol levels have been linked to drug resistance [120]. Rapidly proliferating cells, like cancer cells, depend on cholesterol since it is essential for cell membrane biosynthesis and a main component of lipid rafts. Lipid rafts constitute signaling platforms for various proteins e.g. EGFR, Ras and Src, thereby modulating migration and proliferation as well as apoptosis and cell survival [121]. In return, enhanced growth factor signaling, which often occurs in tumors, may activate sterol regulatory binding protein-1 (SREBP-1), leading to enhanced expression of cholesterol-associated genes [122]. Cholesterol is also essential for vesicular transport including clathrin-mediated endocytosis of LDL, EGF and transferrin [123]. Its depletion from the plasma membrane has been shown to severely inhibit formation of clathrin-coated vesicles [124, 125]. New-synthesis of cholesterol occurs via the mevalonate pathway which additionally provides compounds important for various cellular functions, e.g. isoprenoids for posttranslational protein modification [111]. Amongst the prenylated proteins associated with the plasma membrane are small G proteins such as Ras (farnesylation), Rho and Rac (geranyl geranylation), which are known to display significant roles in cancer [126]. Recently, HMGCR, being the regulating enzyme of the mevalonate pathway, was suggested as a candidate metabolic oncogene cooperating with RAS and increasing cell growth and transformation [127]. Point mutations have been shown to disrupt sterol-stimulated degradation of HMGCR thus increasing activity of the enzyme [128]. Considering cancer prognosis, high mRNA levels of HMGCR and further genes of the mevalonate pathway correlated with poor survival of breast cancer patients [127]. HMGCR is directly targeted by statins, originally developed for the treatment of hypercholesterolemia [129]. Identification of HMGCR as an important molecule in cell transformation has further fueled the interest in statins, whose anticancer activity was already discovered about 20 years ago [129]. Clinical trials performed in the last years, yielded valuable results displaying a great benefit of statins in combination with classical chemotherapy [130].

2 Aim of the thesis

Treatment of cancer is a long-term issue. Frequent chemotherapy sessions are generally necessary and recurrence of the tumor after months or years often requires further treatment. The success of chemotherapy is determined on the one hand by the detrimental potential of the anticancer drug and on the other hand by the responsiveness of the tumor. Resistance of cancer cells towards chemotherapeutics, whether intrinsic or acquired, is still the major cause of therapy failure. Hence, the evaluation of cellular defense mechanisms is essential in the establishment of new chemotherapeutics.

The myxobacterial antibiotic archazolid B is an inhibitor of the vacuolar H⁺-ATPase (V-ATPase) [37]. The V-ATPase has turned out to be an attractive target for cancer therapy within the last decade [54, 56]. Research on archazolid B has been mainly focused on its mode of action and how detrimental effects are exerted in cancer cells. However, up to now, only little is known about resistance mechanisms in response to archazolid B treatment.

Thus, the aim of this thesis was

- 1. to investigate classical intrinsic as well as acquired resistance mechanisms exerted by cells under archazolid B treatment**
- 2. to elucidate new resistance mechanisms in cells in response to archazolid B**

3 Results

3.1 Role of established resistance mechanisms

Considering the problem of drug resistance, the identification of resistance mechanisms is essential in the establishment of new chemotherapeutics. The aim of the thesis was to shed light on defense mechanisms that are relevant in the cellular response to archazolid B. By this, the potential of archazolid B for its use in cancer therapy can be further evaluated. In the first part of the work, archazolid B was investigated in the context of established resistance strategies. At first, the effectiveness of archazolid B in tumor and non-tumor cells of different cancer types was evaluated. The classical resistance mechanisms investigated were ABC transporters, the tumor suppressor p53 and the oncogene EGFR. Acquired resistance mechanisms were studied by establishing an archazolid B-resistant MCF-7 cell line.¹

3.1.1 Cytotoxicity of archazolid B towards tumor and non-tumor cells

To evaluate the effectiveness and specificity of archazolid B, cytotoxicity assays using XTT (2,3-Bis-(2-methoxy-4-nitro-5-sulphophenyl)-2H-tetrazolium-5-carboxanilide) sodium salt were performed on tumor and non-tumor cells of different cancer types, including breast, blood, colon and liver (Figure 7). Non-tumor MCF-10a breast, CCD-18Co colon and AML12 liver cells displayed a 2- to 20-fold higher resistance towards archazolid B compared to their tumorous pendants. The sensitivity of human peripheral mononuclear cells (PMNC), however, was in the same range as the leukemic cell lines, indicating certain toxicity of the drug towards blood cells. The half-maximal inhibitory concentration (IC_{50}) of archazolid B in the different cancer types varied from 0.23 nM to 1.39 nM. Interestingly, archazolid B showed the most drastic cytotoxic effect in HCT116 wild-type colon carcinoma cells displaying cell viability below 5%. In the other cell lines, cell survival between 20% and 40% was observable even at

¹ The results presented in this part of the work were recently accepted for publication in a peer-reviewed scientific journal:

R. Hamm, Y. Sugimoto, H. Steinmetz, T. Efferth, "Resistance mechanisms of cancer cells to the novel vacuolar H⁺-ATPase inhibitor archazolid B," submitted at *Invest New Drugs*, accepted 7 July 2014.

All figures, tables and text passages of this publication used in a modified form in this dissertation were prepared or written by myself.

high concentrations of archazolid B. The lowest cytotoxic effect was accomplished in liver cells, where a prolonged incubation time of 96 h was required to obtain IC_{50} values.

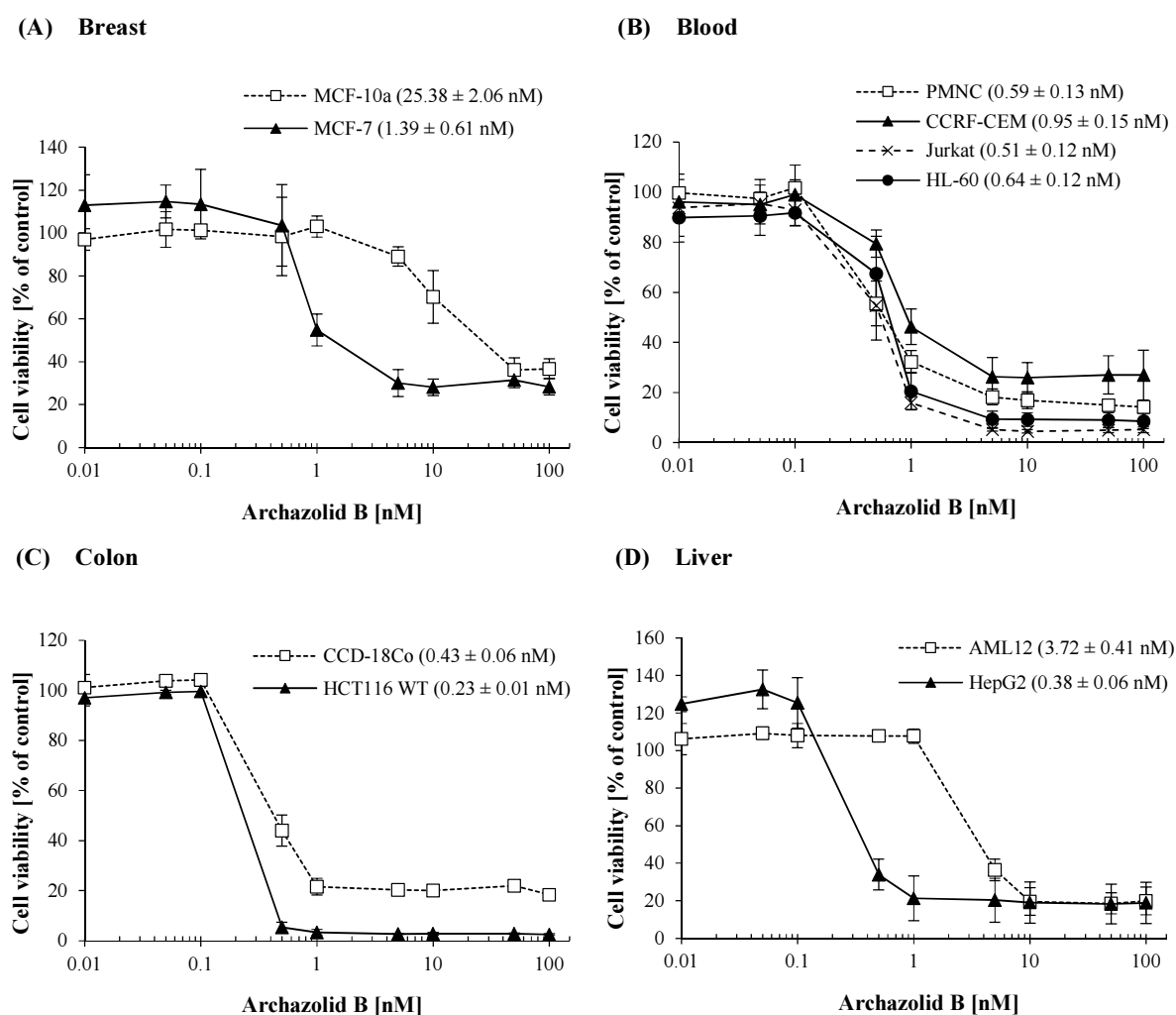


Figure 7: Cytotoxic effect of archazolid B against tumor and non-tumor cells of different cancer types. Archazolid B was tested on breast (A), blood (B), colon (C) and liver cells (D). Breast, blood and colon cells were incubated for 72 h, liver cells were incubated for 96 h in order to obtain IC_{50} values. XTT assays were performed to determine dose-response curves. IC_{50} concentrations are parenthesized. Viability of cells is represented by mean \pm SD of three independent experiments including three parallel measurements each and it is expressed as percentage survival of control.

3.1.2 Archazolid B and ABC transporters

3.1.2.1 Archazolid B and ABCB1 (P-glycoprotein)

Cytotoxicity assay

In order to see if archazolid B is a potential substrate of ABCB1 (P-gp), cytotoxicity assays were performed on CCRF-CEM as well as on P-gp-expressing CEM/ADR5000 cells. Cells were treated for 72 h with archazolid B. As shown in Figure 8, the IC_{50} values were 36.51 nM

for CEM/ADR5000 cells and 0.95 nM for parental CCRF-CEM cells. The degree of resistance was 38.4 thus indicating an interaction of archazolid B with P-gp, which was further analyzed in the following.

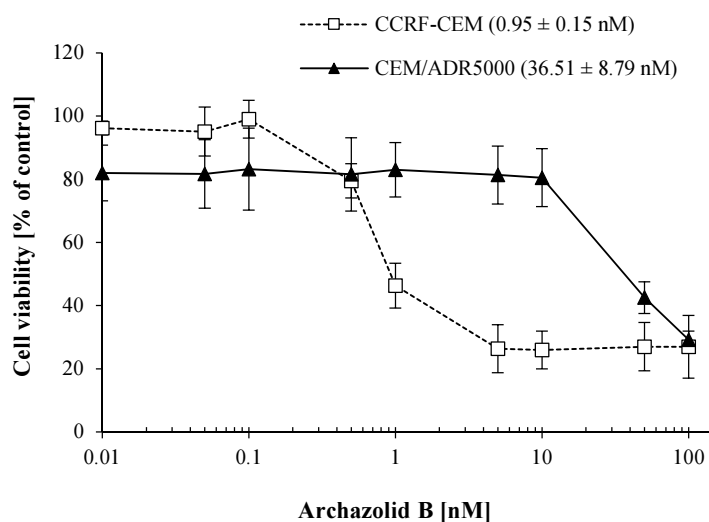


Figure 8: Cytotoxic effect of archazolid B against ABCB1 (P-gp)-expressing cells. CCRF-CEM and P-gp-expressing CEM/ADR5000 cells were incubated for 72 h with archazolid B. XTT assays were performed to determine dose-response curves. IC_{50} concentrations are parenthesized. Viability of cells is represented by mean \pm SD of three independent experiments including three parallel measurements each and it is expressed as percentage survival of control.

Molecular docking

The cytotoxicity assay (Figure 8) showed that ABCB1 (P-gp)-expressing cells displayed cross-resistance to archazolid B. Therefore, it can be hypothesized that archazolid B may interact with P-gp in the same manner as other drugs affected by P-gp-mediated MDR phenotype. For this reason, an *in silico* molecular docking of archazolid B to human P-gp, obtained by homology modelling, was performed. For comparison, doxorubicin and R-/S-verapamil were included in the docking as well. The anthracycline doxorubicin is a known substrate of P-gp, whereas verapamil, a calcium channel blocker, acts as a chemosensitizer reversing MDR [131]. Interestingly, the binding energy displayed by archazolid B (-12.1 kcal/mol) was significantly higher than those obtained for doxorubicin (-8.0 kcal/mol), R-verapamil (-8.0 kcal/mol) and S-verapamil (-8.1 kcal/mol). As shown in Figure 9, archazolid B was docked to the same binding site of P-gp as R- and S-verapamil, whereas doxorubicin bound to a closely neighboring side. Archazolid B displayed eight amino-acids in common with R-verapamil (L65, M68, F72, I868, M949, Y953, F978 and V981) and six amino-acids with S-verapamil (F72, F336, Y953,

F957, F978 and V981), as shown in Figure 10A. In contrast to that, doxorubicin exhibited no amino-acids in common with archazolid B (Figure 10B).

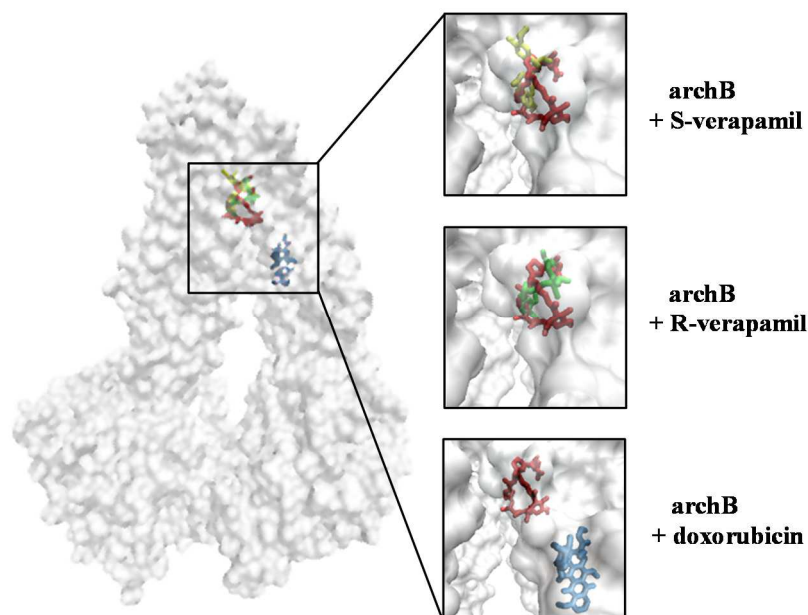


Figure 9: Molecular docking of archazolid B, R/S-verapamil and doxorubicin to P-gp. On the left side, the homology-modelled P-gp is shown in grey (transparent). The ligands are represented in licorice as follows: archazolid B (red), S-verapamil (yellow), R-verapamil (green), doxorubicin (blue). Close-ups of the binding region can be found on the right side.

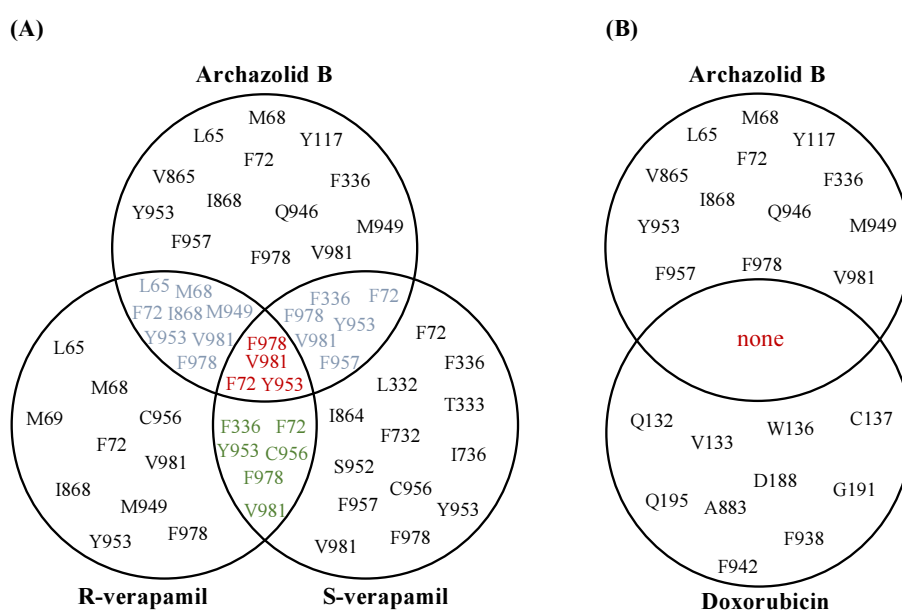


Figure 10: Venn diagrams: Amino-acids of P-glycoprotein mediating ligand binding. Residues were obtained performing molecular docking. **(A)** Intersection sets of archazolid B and R/S-verapamil. **(B)** Intersection set of archazolid B and doxorubicin.

Drug combination assays

The docking analyses indicated a possible binding of archazolid B to P-gp at the same site as verapamil. In order to evaluate whether verapamil is able to reverse resistance towards archazolid B, cytotoxicity assays were performed. As shown in Figure 11A, a combination of archazolid B and 10 μM verapamil led to a sensitization of CEM/ADR5000 cells as displayed by a 12-fold reduction of the IC_{50} concentration of archazolid B.

The calcium channel blocker verapamil has been shown to efficiently reverse doxorubicin resistance [132]. In accordance to that, combination of doxorubicin with 20 μM verapamil led to a 10-fold reduction of the IC_{50} value in CEM/ADR5000 cells (Figure 11B). Since the docking experiments suggested a common binding site for archazolid B and verapamil, archazolid B was tested for MDR reversing qualities as well. However, in contrast to verapamil, archazolid B was not able to re-sensitize CEM/ADR5000 cells to doxorubicin (Figure 11B), indicating that archazolid B is not an inhibitor of P-gp-mediated transport.

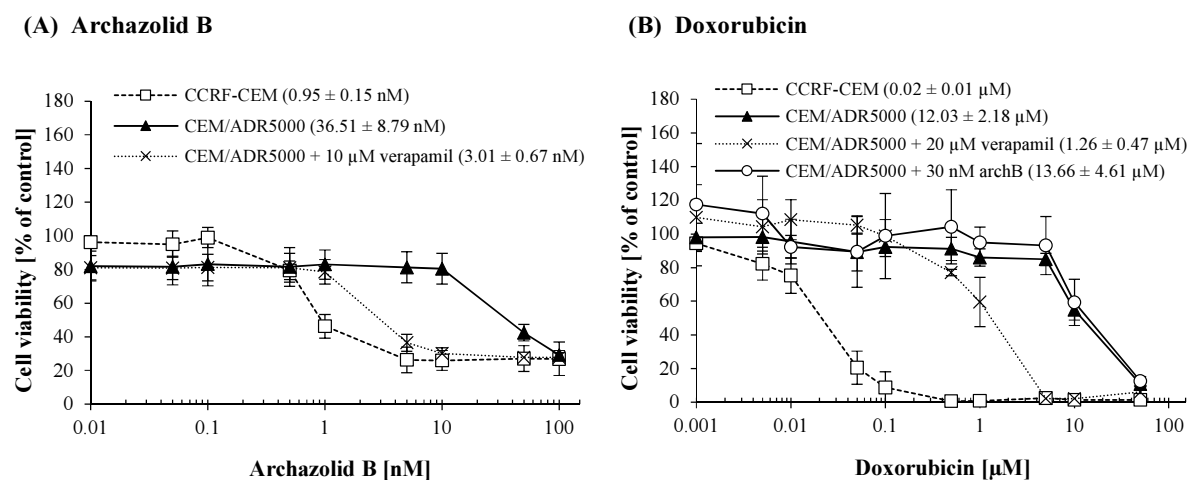


Figure 11: Cytotoxicity of archazolid B (A) and doxorubicin (B) combinations. Cells were incubated with drug combinations for 72 h. Then, XTT assays were performed to determine dose response curves. IC_{50} concentrations are parenthesized. Viability of cells is represented by mean \pm SD of three independent experiments including three parallel measurements each and it is expressed as percentage survival of control.

3.1.2.2 Archazolid B and ABCG2 (BCRP)

To determine whether cytotoxicity of archazolid B is influenced by this transporter, XTT assays were performed on MDA-MB-231-pcDNA3 cell line and the BCRP-expressing pendant. Since cell viability was still high after 72 h treatment, a prolongation of the incubation time up to 96 h was necessary in order to obtain IC_{50} values. As Figure 12 shows, the impact of BCRP on the cytotoxic effect of archazolid B was rather low compared to P-gp. The degree of resistance was 1.9 and pointed to weak interaction of archazolid B with BCRP.

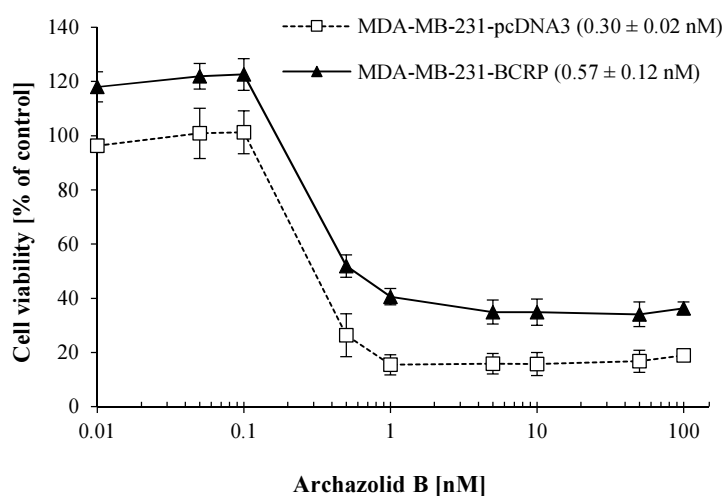


Figure 12: Cytotoxic effect of archazolid B against ABCG2 (BCRP)-expressing cells. MDA-MB-231-pcDNA3 and BCRP expressing MDA-MB-231-BCRP cells were incubated for 96 h with archazolid B. XTT assays were performed to determine dose-response curves. IC_{50} concentrations are parenthesized. Viability of cells is represented by mean \pm SD of three independent experiments including three parallel measurements each and it is expressed as percentage survival of control.

3.1.2.3 Archazolid B and ABCB5

The cytotoxic effect of archazolid B was also evaluated on ABCB5-expressing HEK293 cells and compared to the wild-type cell line. Although ABCB5 belongs to the same subfamily as P-gp (ABCB1), ABCB5 drug transporter expressing cells displayed hypersensitivity (collateral sensitivity) towards archazolid B. As shown in Figure 13, the IC_{50} values were 4.73 nM for HEK293 cells and 0.95 nM for HEK293-ABCB5 cells, resulting in a degree of resistance of 0.2.

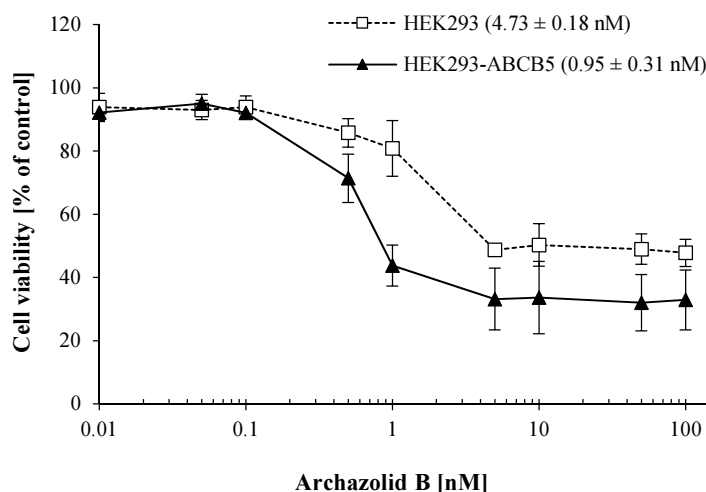


Figure 13: Cytotoxic effect of archazolid B against ABCB5-expressing cells. HEK293 and ABCB5-expressing HEK293-ABCB5 cells were incubated for 72 h with archazolid B. XTT assays were performed to determine dose-response curves. IC_{50} concentrations are parenthesized. Viability of cells is represented by mean \pm SD of three independent experiments including three parallel measurements each and it is expressed as percentage survival of control.

3.1.3 Archazolid B and p53

Performing cytotoxicity assays, the influence of the tumor suppressor p53 was evaluated. HCT116 and HCT116 p53^{-/-} cells were treated for 72 h with archazolid B. As displayed in Figure 14, wild-type and p53 knockout cells did not show a difference in IC_{50} values (degree of resistance: 1.0). Hence, it can be assumed that cytotoxicity conferred by archazolid B is independent of the p53 status of the cell.

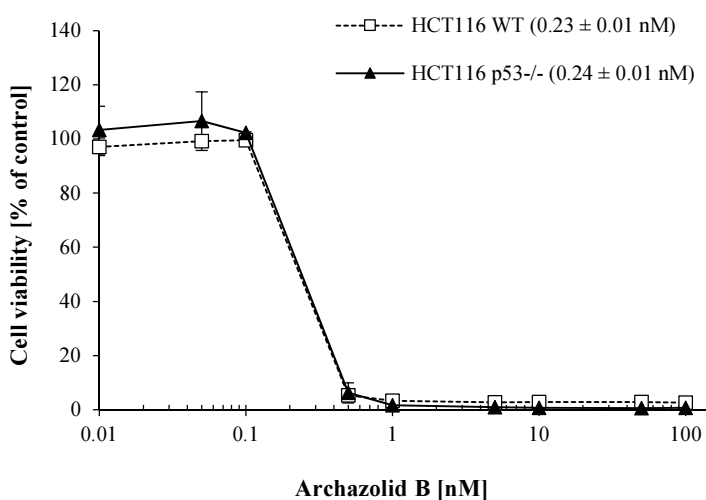


Figure 14: Cytotoxic effect of archazolid B against p53 knockout cells. HCT116 WT and p53 knockout HCT116 p53^{-/-} cells were incubated for 72 h with archazolid B. XTT assays were performed to determine dose-response curves. IC_{50} concentrations are parenthesized. Viability of cells is represented by mean \pm SD of three independent experiments including three parallel measurements each and it is expressed as percentage survival of control.

3.1.4 Archazolid B and EGFR

Cytotoxicity of archazolid B on U87MG and U87MG. Δ EGFR cells was analyzed using XTT assay. Dose-response curves were calculated after 72 h incubation with the drug (Figure 15). The cell line with constitutively active EGFR (U87MG. Δ EGFR) showed a nearly 10-fold higher resistance towards archazolid B compared to the wild-type cells. This result indicates a certain role of EGFR signaling in cell survival after archazolid B exposure, which was further investigated later in this work.

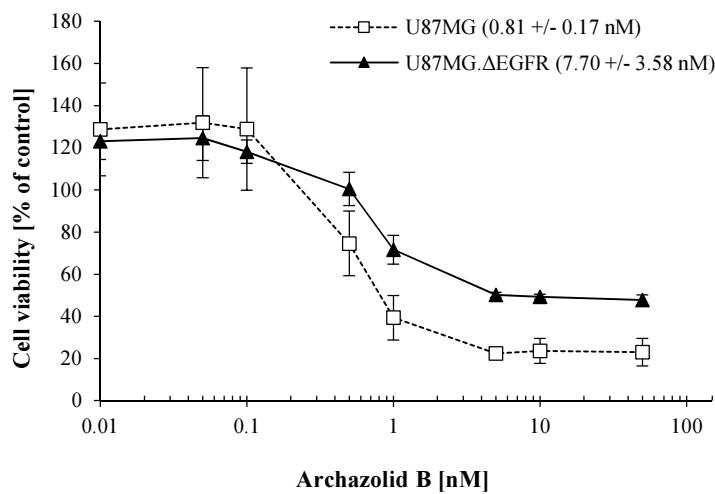


Figure 15: Cytotoxic effect of archazolid B against EGFR mutant cells. U87MG and U87MG. Δ EGFR cells, expressing constitutively active EGFR, were incubated for 72 h with archazolid B. XTT assays were performed to determine dose-response curves. IC_{50} concentrations are parenthesized. Viability of cells is represented by mean \pm SD of three independent experiments including three parallel measurements each and it is expressed as percentage survival of control.

3.1.5 MCF-7ArchB cells and acquired drug resistance

After studying archazolid B in the context of intrinsic resistance mechanisms, it was of interest whether cells can acquire resistance to archazolid B and which are the underlying mechanisms. For this reason, an archazolid B-resistant MCF-7-derived subline (MCF-7ArchB) was established.

3.1.5.1 Resistance of MCF-7ArchB cells towards archazolid B

Archazolid B-resistant MCF-7ArchB cells were generated by repeated treatment of MCF-7 cells with archazolid B. MCF-7 breast cancer cells have been frequently used in the past for the generation of sublines resistant to diverse anticancer drugs [133, 134]. The degree of resistance of MCF7ArchB cells to archazolid B was compared to that of normal MCF-7 cells performing cytotoxicity assays. As shown in Figure 16, MCF-7ArchB cells displayed a 2.7-fold higher resistance towards the drug, which remained constant from passage 6 to passage 26. In order to further enhance resistance towards archazolid B, treatment with ethylmethane sulfonate (EMS) was performed in addition. EMS is a well-known mutagen causing point mutations and chromosomal breakage by DNA alkylation [135]. However, it was not possible to further increase resistance of the cells towards archazolid B by this method.

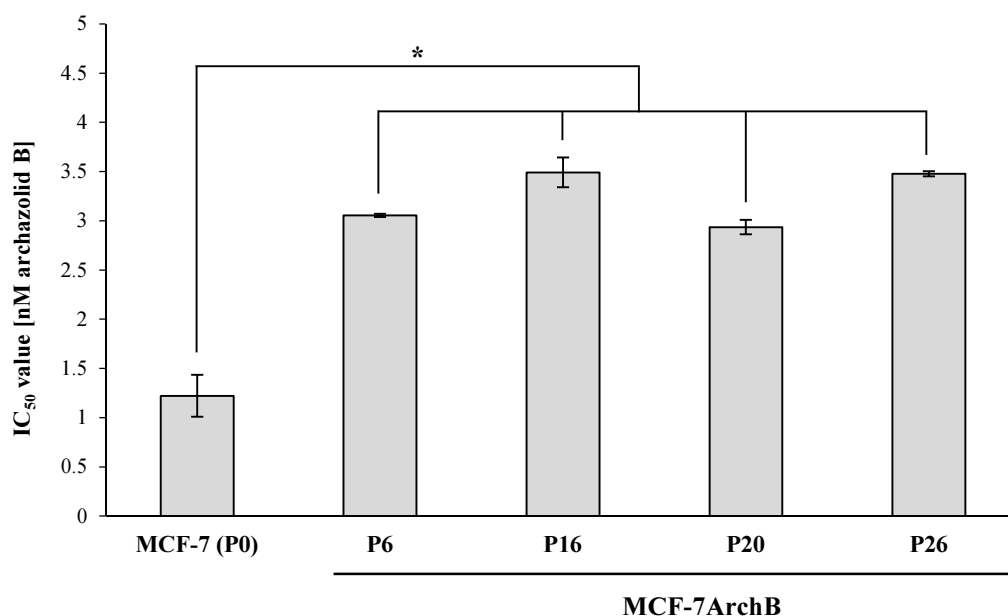


Figure 16: Cytotoxicity of archazolid B on MCF-7ArchB cells. Cells pretreated for 0, 6, 16, 20 or 26 passages with archazolid B were treated for 72h with archazolid B. XTT assays were performed to determine dose-response curves. Bars represent IC₅₀ concentrations evaluated by linear regression. (*Significantly different to MCF-7 control (P0) according to Student's t-test, P < 0.05)

3.1.5.2 Gene expression of *ATP6V0C*, *EGFR* and *ABCB1* in MCF-7ArchB cells

To evaluate which mechanisms may confer acquired resistance towards archazolid B in MCF-7ArchB cells, gene expression was analyzed using real-time reverse transcription PCR (RT-PCR). Besides *ABCB1*, encoding P-gp as a well-known resistance mechanism to established anticancer drugs, mRNA expression of *EGFR* and V-ATPase subunit c (*ATP6V0C*) was investigated in MCF-7ArchB cells. *EGFR* has been chosen, since glioblastoma cells, expressing

constitutively active EGFR displayed a 10-fold higher resistance towards archazolid B compared to EGFR wild-type cells (3.1.4). *ATP6V0C* has been selected as candidate gene, since *ATP6V0C* is a part of the integral V0 domain of the V-ATPase which has been identified as the binding site of archazolids [60, 61]. As displayed in Figure 17, there was no change in *ATP6V0C* expression. However, up-regulation of *ABCB1* (about 140%) and *EGFR* (about 160%) was observed in MCF-7ArchB cells compared to MCF-7 control cells, indicating that these two genes may contribute to increased resistance of MCF-7ArchB cells towards archazolid B.

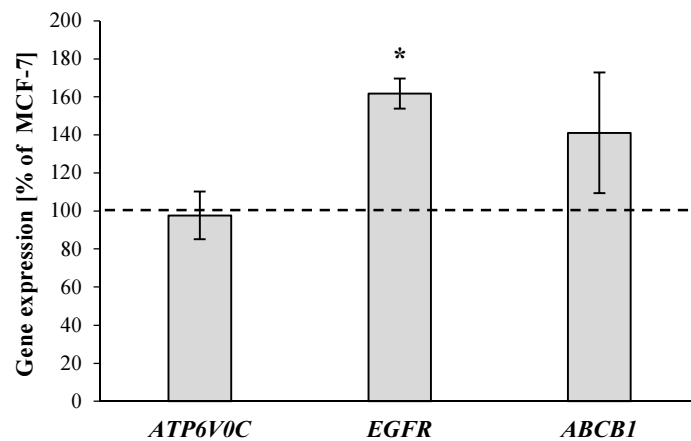


Figure 17: Gene expression in MCF-7ArchB cells. Total cellular RNA was extracted and *ATP6V0C*, *EGFR* and *ABCB1* gene expression was quantified using real-time RT-PCR. Bars represent gene expression (mean \pm SD) in MCF-7ArchB cells relative to MCF-7 control cells. Two independent experiments were performed including four measurements each. (*Significantly different to MCF-7 control according to Student's t-test, $P < 0.05$)

3.1.5.3 Sequence analysis of *ATP6V0C* in MCF-7 and MCF-7ArchB cells

Since real-time RT-PCR showed that *ATP6V0C* expression was not altered in MCF-7ArchB cells (3.1.5.2), we wanted to investigate if a possible acquired point mutation might account for the resistance against archazolid B. The coding region of *ATP6V0C* as well as the corresponding protein sequence are shown in Figure 18A and B. Amino-acids of V-ATPase subunit c that interact with archazolids have been evaluated for *Saccharomyces cerevisiae* using molecular docking and mutation experiments [60, 61]. To confirm that the same amino-acids may also be involved in binding to human V-ATPase subunit c, a sequence alignment with human and yeast V-ATPase subunit c was performed using Standard Protein BLAST. As displayed in Figure 18C, all amino-acids of the identified archazolid binding region turned out to be conserved and the alignment resulted in 72% sequence identity. Based on this results, total RNA from MCF-7 and MCF-7ArchB cells (P6, P16, P20, P26) was isolated, converted to cDNA and amplified

using a high-fidelity polymerase. Sequencing of the PCR product, however, revealed no mutation in the coding region of the gene in any MCF-7ArchB passage, indicating that drug resistance of MCF-7ArchB cells is not conferred by impaired drug-target interaction.

(A)

Gene sequence of human *ATP6V0C* (gi|310832380|ref|NM_001694.3); coding region:

```
ATGTCCGAGTCCAAGAGCGGCCCGAGTATGCTTCGTTTTTCGCCGTCATGGGCGCCTCGGCCGCCA
TGGTCTTCAGCGCCCTGGGCGCTGCCTATGGCACAGCCAAGAGCGGTACCGGCATTGCGGCCATGTC
TGTCATGCGGCCGAGCAGATCATGAAGTCCATCATCCCAGTGGTCATGGCTGGCATCATCGCCATC
TACGGCCTGGTGGTGGCAGTCCTCATCGCCAACCTCCCTGAATGACGACATCAGCCTCTACAAGAGCT
TCCTCCAGCTGGGCGCCGGCCTGAGCGTGGGCGCTGAGCGGCCCTGGCAGCCGGCTTTGCCATCGGCAT
CGTGGGGGACGCTGGCGTGCGGGGCACCGCCAGCAGCCCCGACTATTCGTGGGCATGATCCTGATT
CTCATCTTCGCCGAGGTGCTCGGCCTCTACGGTCTCATCGTCGCCCTCATCCTCTCCACAAAGTAG
```

(B)

Protein sequence of human *V-ATPase subunit c* (gi|14424534|gb|AAH09290.1):

```
M S E S K S G P E Y A S F F A V M G A S A A M V F S A L G A A Y G
T A K S G T G I A A M S V M R P E Q I M K S I I P V V M A G I I A I
Y G L V V A V L I A N S L N D D I S L Y K S F L Q L G A G L S V G
L S G L A A G F A I G I V G D A G V R G T A Q Q P R L F V G M I L
I L I F A E V L G L Y G L I V A L I L S T K
```

(C)

Protein sequence alignment of *V-ATPase subunit c* (yeast/human):

```
Yeast (Saccharomyces cerevisiae; gi|398364261|ref|NP_010887.3)
Human (gi|14424534|gb|AAH09290.1)

Yeast   6   PVYAPFFGAIGCASAIIFTSLGAAYGTAKSGVGICATCVLRPDLDFKNIVPVMAGIIAI 65
        P YA FF  +G ++A++F++LGAAAYGTAKSG GI A  V+RP+ + K+I+PV+MAGIIAI
Human   8   PEYASFFAVMGASAAMVFSALGAAYGTAKSGTGIAAMSVMRPEQIMKSIIPVVMAGIIAI 67

Yeast   66   YGLVSVLVCYSLGQKQALYTGFIQLGAGLSVGLSGLAAGFAIGIVGDAGVRGSSQQPRL 125
        YGLVV+VL+ SL  +LY  F+QLGAGLSVGLSGLAAGFAIGIVGDAGVRG++QQPRL
Human   68   YGLVVAVLIANSLNDDISLYKSFLQLGAGLSVGLSGLAAGFAIGIVGDAGVRGTAQQPRL 127

Yeast   126  FVGMILILIFAEVLGLYGLIVALLNSR 153
        FVGMILILIFAEVLGLYGLIVAL+L+++
Human   128  FVGMILILIFAEVLGLYGLIVALILSTK 155
```

Figure 18: Gene sequencing (*ATP6V0C*). (A) Sequence of *ATP6V0C* (coding region). No difference was observed between MCF-7 and MCF-7ArchB cells performing gene sequencing. (B) Protein sequence encoded by *ATP6V0C*. (C) Protein sequence alignment of *V-ATPase subunit c* from *Saccharomyces cerevisiae* (yeast) and *Homo sapiens*. The alignment was performed using Standard Protein BLAST. Amino-acids of the equatorial region where archazolids bind are highlighted and displayed in magenta [61]. The alignment shows 72% sequence identity. Mismatches are indicated by a gap, similar (but not identical) amino-acids are indicated by “+”.

3.1.5.4 Growth kinetic studies with MCF-7 and MCF-7ArchB cells

Real-time RT-PCR experiments revealed enhanced expression of *EGFR* in MCF-7ArchB cells (3.1.5.2). Due to this fact, it is quite likely that differences in proliferation may also account for archazolid B resistance. For this reason, cell growth of MCF-7 and MCF-7ArchB cells was monitored over a period of 9 days. Growth kinetics curves are shown in Figure 19. Compared to MCF-7 control, MCF-7ArchB cells displayed a general tendency to grow slower. A significant decrease of proliferation was observed for MCF-7ArchB (P26) cells.

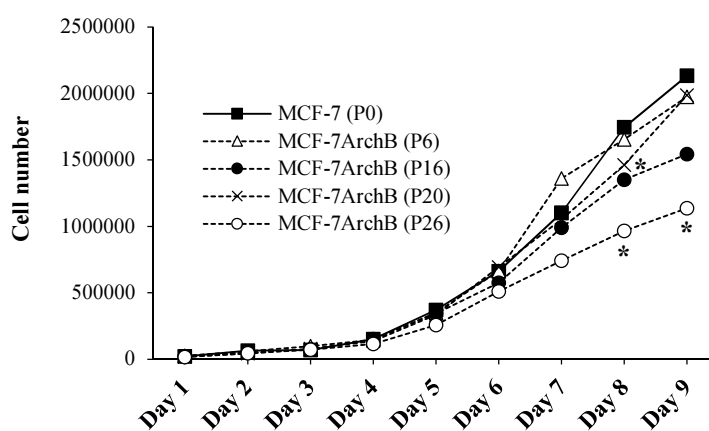


Figure 19: Growth kinetics curves. MCF-7 control (P0) and MCF-7ArchB cells (P6, P16, P20, P26) were seeded at day 0 at the number of 25,000 cells. Cells were counted over a period of 9 days with a Neubauer chamber. The number of cells for each day is represented by mean of three independent experiments. (*Significantly different from MCF-7 control (P0) according to Student's t-test, $P < 0.05$)

3.1.6 Summary: Role of established resistance mechanisms

In this part of the work, classical intrinsic as well as acquired resistance mechanisms exerted by cells in response to archazolid B treatment were investigated.

Archazolid B displayed cytotoxicity in the low nanomolar range towards a panel of different cancer types (breast, blood, colon, liver). Except for peripheral mononuclear blood cells, resistance towards the drug was 2 to 18-fold higher in corresponding non-tumorous cell lines.

Investigating the role of ABC transporters, ABCB1 (P-gp) and ABCG2 (BCRP) expression increased resistance towards archazolid B, whereas *ABCB5*-transfected cells displayed collateral sensitivity. Molecular docking to human P-gp revealed binding of archazolid B to the same site as verapamil. However, in contrast to verapamil, archazolid B was not able to re-sensitize cells to doxorubicin thus classifying archazolid B as a substrate and not a modulator of P-gp-mediated transport.

The cytotoxic effect of archazolid B was shown to be independent of the tumor suppressor p53, whereas cells overexpressing constitutively active EGFR (EGFRvIII mutant) displayed significantly increased resistance towards archazolid B.

Acquired drug resistance was studied by establishing an archazolid B-resistant MCF-7 cell line. The resulting resistance index was about 2.7 compared to untreated cells. Gene expression analysis indicated that archazolid B resistance may result from slight *ABCB1* and significant *EGFR* overexpression, whereas aberrant expression or mutation of *ATP6V0C*, the gene encoding V-ATPase subunit c, was not observed. Furthermore, growth kinetic curves revealed that decreased proliferation may also contribute to enhanced archazolid B resistance in MCF-7ArchB cells.

3.2 Cholesterol synthesis as a new resistance mechanism

In the first part of the work archazolid B was investigated in the context of established resistance mechanisms. However, the reasons for drug resistance are multifactorial and classical mechanisms are not able to explain archazolid B resistance of cells to a full extent. Hence, the second part of the work deals with the identification of new resistance mechanisms in response to archazolid B treatment. Experiments were performed on T24 urinary bladder cancer cells as well as on U87MG and U87MG. Δ EGFR glioblastoma cells.

3.2.1 Archazolid B affects cholesterol homeostasis and endocytosis in T24 cells

For identification of new resistance strategies in T24 cells in response to archazolid B treatment, *omics* data (mRNA microarray, miRNA microarray and protein quantification) were analyzed. Validation experiments were performed using real-time RT-PCR, flow cytometry, fluorescence microscopy, confocal microscopy, western blotting and drug combination assays.²

3.2.1.1 Archazolid B versus doxorubicin

Cytotoxicity of archazolid B against T24 urinary bladder cancer cells was evaluated for different incubation times using XTT assay. Dose-response curves were calculated after 24 h, 48 h, 72 h, 96 h and 120 h treatment with the drug. As shown in Figure 20A, archazolid B exerted cytotoxic activity within the low nanomolar range. However, the effect on cell viability was time-dependent. Within the first 48 h, the cell number hardly decreased below 80%, whereas after 72 h treatment, a dramatic drop in viability down to about 40% was observed. Even an incubation time of 120 h could not achieve complete cytotoxicity (with 5% of cells still surviving). Interestingly, for each incubation time, cell viability always remained constant even when high concentrations of archazolid B were used. For comparison, the experiment was also performed with the conventional anticancer drug doxorubicin. In contrast to archazolid B,

² The results presented in this part of the work were recently published in a peer-reviewed scientific journal:

R. Hamm, Y.-R. Chen, E.-J. Seo, M. Zeino, C.-F. Wu, R. Müller, N.-S. Yang, "Induction of cholesterol biosynthesis by archazolid B in T24 bladder cancer cells," *Biochem Pharm*, vol. 91, pp. 18-30, 2014.

All figures, tables and text passages of this publication used in a modified form in this dissertation were prepared or written by myself.

the cytotoxic effect of doxorubicin was more instant (Figure 20B). After 48 h, cell viability was already down to about 30% and below 5% after 72 h incubation with the drug.

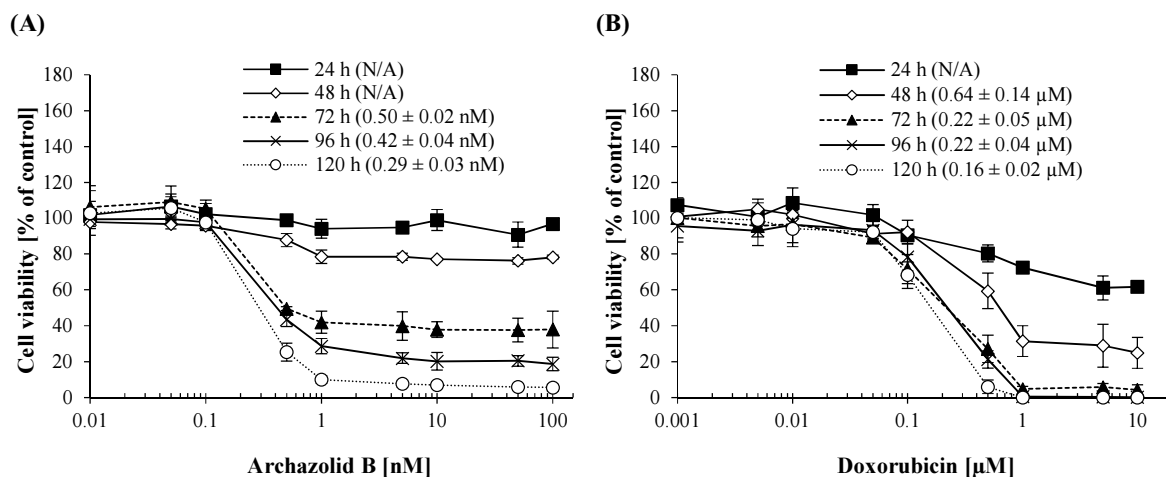


Figure 20: Cytotoxicity of archazolid B (A) and doxorubicin (B) against T24 urinary bladder cancer cells. Cells were incubated for 24 h, 48 h, 72 h, 96 h and 120 h with archazolid B or doxorubicin. XTT assays were performed to determine dose-response curves. IC₅₀ concentrations are parenthesized. Viability of cells is represented by mean ± SD of three independent experiments including three parallel measurements each and it is expressed as percentage survival of control.

3.2.1.2 Omics analysis

Transcriptomics – mRNA microarray

In order to identify new resistance mechanisms evoked by archazolid B, gene expression profiling was performed. Results were obtained treating the cells with 10 nM archazolid B, which equals $20 \times \text{IC}_{50}$ (72 h) concentration. Dimethyl sulfoxide (DMSO) solvent control samples were prepared as well. After 24 h incubation time, total RNA was isolated for a whole human genome mRNA gene expression microarray. Expression data were analyzed using Chipster software. Genes were filtered by three times standard deviation and significance was assessed using empirical Bayes t-test ($P < 0.05$) with Benjamini-Hochberg correction. As a last step, a threshold of 1.5 (fold change, FC) was applied to the dataset and resulting 318 genes were further analyzed using the Core Analysis tool of Ingenuity Pathway Analysis (IPA) software. The most deregulated genes in consequence to archazolid B treatment are summarized in Table 2.

Table 2: Top up- and down-regulated genes in T24 cells after 24 h treatment with 10 nM archazolid B.

Gene	Description	Fold change
<i>Up-regulated genes</i>		
<i>INSIG1</i>	insulin induced gene 1	6.6
<i>BHLHE40</i>	basic helix-loop-helix family, member e40	6.5
<i>SCD</i>	stearoyl-CoA desaturase (delta-9-desaturase)	5.6
<i>PFKFB4</i>	6-phosphofructo-2-kinase/fructose-2,6-biphosphate 4	5.2
<i>TM4SF19</i>	transmembrane 4 L six family member 19, isoform 1	4.5
<i>HMGCS1</i>	3-hydroxy-3-methylglutaryl-Coenzyme A synthase 1 (sol.)	4.2
<i>AK4</i>	adenylate kinase 4	4.0
<i>EGR1</i>	early growth response 1	4.0
<i>ANKRD37</i>	ankyrin repeat domain 37	3.9
<i>TM4SF19</i>	transmembrane 4 L six family member 19, isoform 2	3.8
<i>Down-regulated genes</i>		
<i>IGFBP5</i>	insulin-like growth factor binding protein 5, isoform 1	-3.6
<i>IGFBP5</i>	insulin-like growth factor binding protein 5, isoform 2	-3.0
<i>CTGF</i>	connective tissue growth factor, isoform 2	-2.7
<i>CTGF</i>	connective tissue growth factor, isoform 1	-2.7
<i>UCP2</i>	uncoupling protein 2 (mitochondrial, proton carrier)	-2.6
<i>EDN1</i>	endothelin 1	-2.4
<i>COL8A1</i>	collagen, type VIII, alpha 1	-2.4
<i>PCK2</i>	phosphoenolpyruvate carboxykinase 2 (mitochondrial)	-2.3
<i>OSCAR</i>	osteoclast associated, immunoglobulin-like receptor	-2.3
<i>TAGLN</i>	transgelin	-2.3

Deregulated genes were correlated with cellular functions including cell death and survival, cellular growth and proliferation, lipid metabolism, molecular transport, small molecule biochemistry and cell signaling (Figure 21).

Furthermore, several genetic networks were found to be significantly deregulated in T24 cells after archazolid B treatment. These networks were correlated to lipid metabolism, small molecule biochemistry, cellular development and cell growth and proliferation. Figure 22 displays one of the most affected networks upon archazolid B treatment.

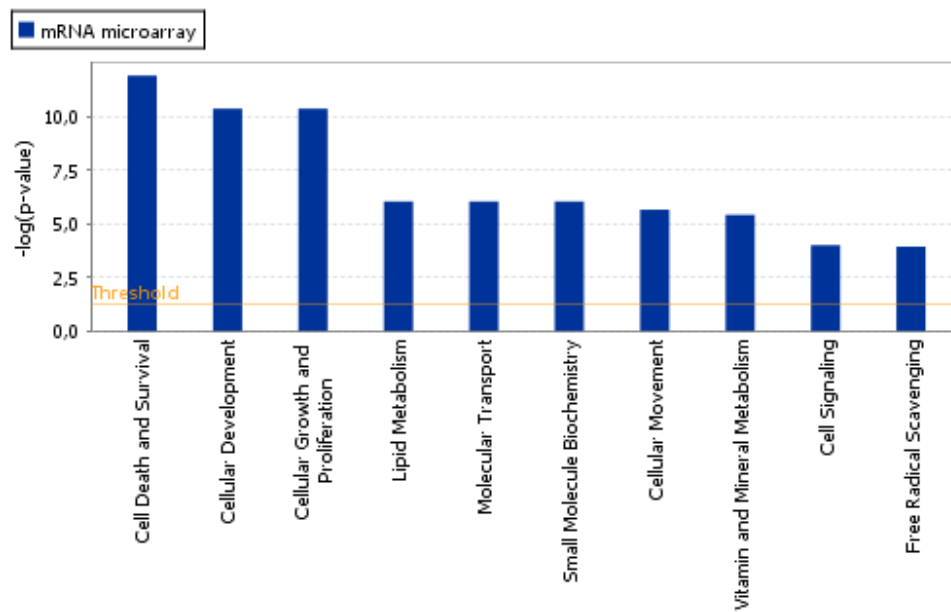


Figure 21: Top cellular functions affected in T24 cells after 24 h treatment with 10 nM archazolid B. Gene expression data were obtained using microarray technology. P-values were calculated using right-tailed Fisher's exact test.

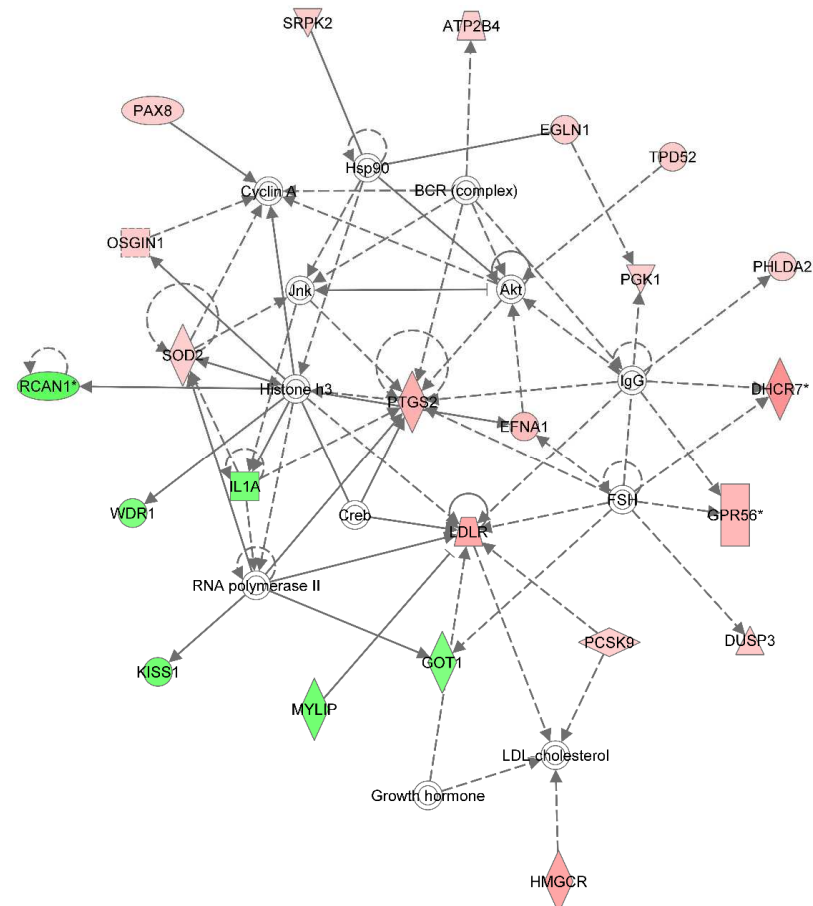


Figure 22: Deregulated network correlated to lipid metabolism, small molecule biochemistry and vitamin and mineral metabolism. T24 cells were treated for 24 h with 10 nM archazolid B. Red colored genes were up-regulated, green colored ones were down-regulated after treatment. Continuous lines show a direct interaction, dotted lines an indirect interaction.

The IPA Core Analysis tool also assigns genes to canonical pathways. Interestingly, the top-deregulated pathways upon archazolid B treatment were all correlated to cholesterol biosynthesis (Figure 23). Ratios of the top-five pathways were between 0.5 and 0.7, indicating that 50-70% of all genes in these pathways were deregulated by archazolid B.

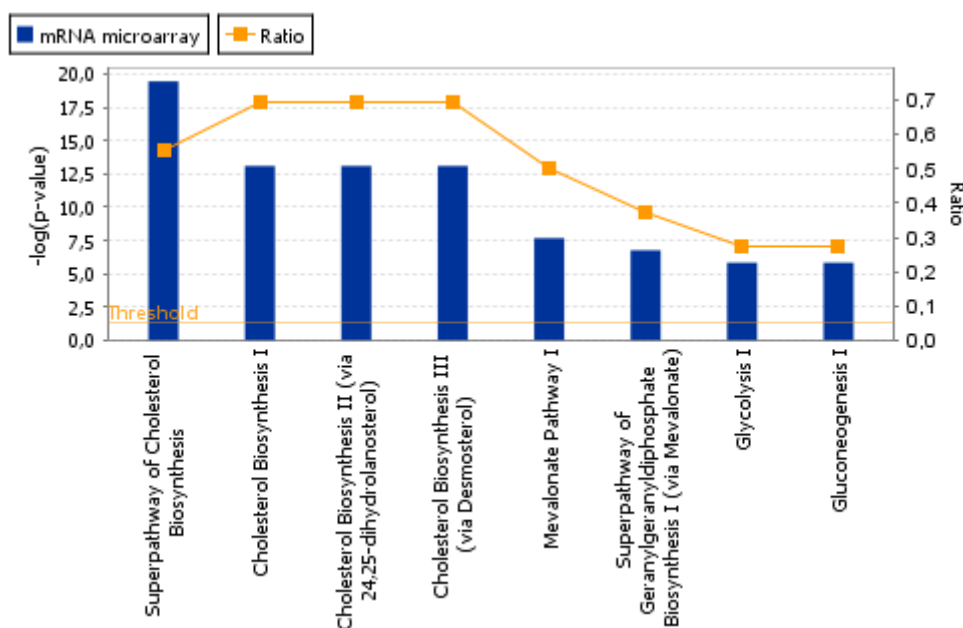


Figure 23: Top pathways significantly enriched in deregulated genes after 24 h treatment of T24 cells with 10 nM archazolid B. P-values were calculated using right-tailed Fisher's exact test. Ratios indicate the number of genes in a given pathway divided by the total number of genes that make up that pathway.

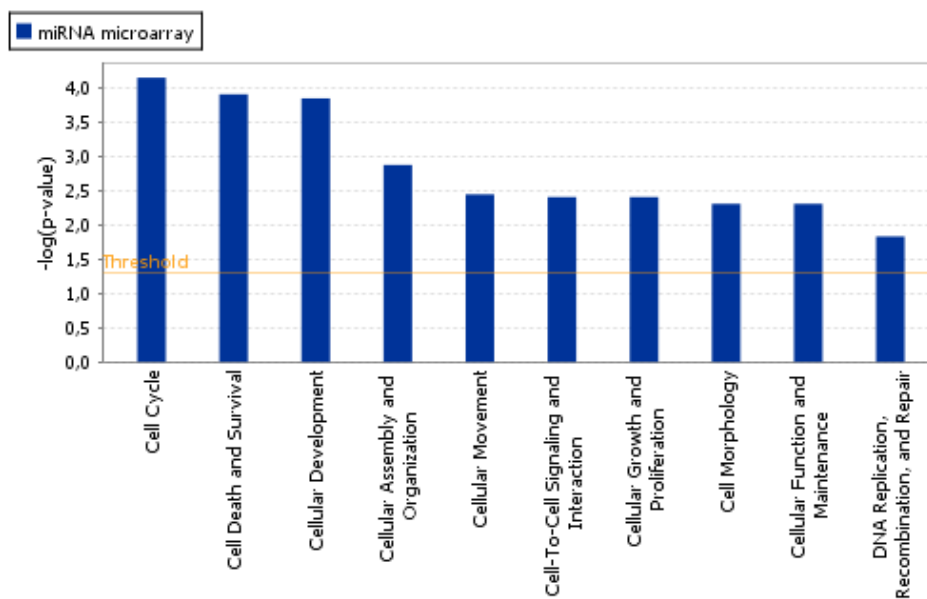
Transcriptomics – miRNA microarray

In order to identify the whole effect of archazolid B on transcription in T24 cells, changes in miRNA expression were analyzed as well. MiRNAs are endogenous, non-coding RNA sequences that influence gene expression by post-transcriptional modulation [136]. Cells were treated with 10 nM archazolid B or DMSO solvent control for 24 h before miRNA was isolated for a miRNA microarray. A threshold of 1.5 (fold change) was applied to the dataset and resulting 184 miRNAs were further analyzed using the Core Analysis tool of IPA software. The most deregulated miRNAs in response to archazolid B treatment are summarized in Table 3.

As shown in Figure 24, distinct cellular functions including cell death and survival, cellular growth and proliferation, cell morphology as well as cellular function and maintenance were correlated to deregulated miRNAs.

Table 3: Top up- and down-regulated miRNAs in T24 cells after 24 h treatment with 10 nM archazolid B.

Up-regulated miRNAs	Fold change	Down-regulated miRNAs	Fold change
hsa-miR-376a	15.0	hsa-miR-891a	-5.4
hsa-miR-374b	10.4	hsa-miR-1271	-4.2
hsa-miR-568	8.2	hsa-miR-935	-4.1
hsa-miR-802	7.9	hsa-miR-1304	-4.0
hsa-miR-496	7.6	hsa-miR-526b:9.1	-4.0
hsa-miR-520e	7.5	hsa-miR-128b:9.1	-3.5
hsa-miR-623	7.3	hsa-miR-202	-3.5
hsa-miR-299-3p	6.6	hsa-miR-629	-3.4
hsa-miR-1225-5p	6.5	hsa-miR-542-5p	-3.1
hsa-miR-208a	6.2	hsa-miR-139-3p	-3.1

**Figure 24: Top cellular functions affected in T24 cells after 24 h treatment with 10 nM archazolid B.** MiRNA data were obtained using microarray technology. P-values were calculated using right-tailed Fisher's exact test.

Target Filter analysis showed that the deregulated miRNAs target 13,479 mRNAs. 252 of these targets were also deregulated in the mRNA microarray, corresponding to an overlap of 79% with regards to all deregulated genes. This result indicates a functional relationship between mRNA and miRNA after archazolid B treatment. Table 4 shows cholesterol-associated molecules deregulated on gene level and targeted by miRNA after 24 h treatment with 10 nM archazolid B. Only miRNAs with appropriate deregulation, which means opposite direction with regards to mRNA, were considered.

Table 4: Cholesterol-associated molecules deregulated on gene level and targeted by miRNA after 24 h treatment with 10 nM archazolid B.

Gene	Description	FC	Targeting	FC
		mRNA	miRNA	miRNA
<i>ACAT2</i>	acetyl-CoA acetyltransferase 2	1.9	-	-
<i>DHCR24</i>	24-dehydrocholesterol reductase	2.0	hsa-miR-1254	-1.6
			hsa-miR-664*	-1.7
			hsa-miR-671-5p	-2.8
<i>DHCR7</i>	7-dehydrocholesterol reductase	3.5	-	-
<i>EBP</i>	emopamil binding protein (sterol isomerase)	1.7	-	-
<i>FDFT1</i>	farnesyl-diphosphate farnesyltransferase 1	2.1	-	-
<i>HMGCR</i>	3-hydroxy-3-methylglutaryl-CoA reductase	2.8	hsa-miR-664*	-1.7
<i>HMGCS1</i>	3-hydroxy-3-methylglutaryl-CoA synthase 1 (sol.)	4.2	hsa-miR-129-3p	-2.3
			hsa-miR-34c-5p	-2.8
			hsa-miR-767-5p	-2.7
<i>ID11</i>	isopentenyl-diphosphate delta isomerase 1	2.2	-	-
<i>INSIG1</i>	insulin induced gene 1	6.6	hsa-miR-767-5p	-2.7
<i>INSIG2</i>	insulin induced gene 2	1.7	hsa-miR-767-3p	-2.7
<i>LDLR</i>	low-density lipoprotein receptor	2.7	hsa-miR-193a-5p	-1.6
<i>LSS</i>	lanosterol synthase	3.2	hsa-miR-767-3p	-2.7
<i>MSMO1</i>	methylsterol monooxygenase 1	2.9	hsa-miR-654-5p	-2.4
			hsa-miR-671-5p	-2.8
<i>MVD</i>	mevalonate (diphospho) decarboxylase	1.8	hsa-miR-663	-2.1
<i>MVK</i>	mevalonate kinase	1.7	hsa-miR-663	-2.1
<i>MYLIP</i>	myosin regulatory light chain interacting protein	-1.7	hsa-miR-490-5p	2.2
			hsa-miR-512-5p	1.7
			hsa-miR-542-3p	2.0
			hsa-miR-654-3p	1.8
<i>NPC1</i>	Niemann-Pick disease, type C1	2.8	hsa-miR-628-3p	-1.5
<i>NSDHL</i>	NAD(P) dependent steroid dehydrogenase-like	1.7	-	-
<i>SC5D</i>	sterol-C5-desaturase	1.9	-	-
<i>SQLE</i>	squalene monooxygenase	2.7	-	-

Taken together, transcriptomic data indicated disturbances in cholesterol homeostasis. Nearly all cholesterol biosynthesis genes were significantly up-regulated. Amongst them were HMGCR – the key enzyme of this pathway – and insulin induced gene 1 (INSIG1), the most up-regulated gene with a fold change of 6.6, playing an important role in the regulation of cholesterol biosynthesis [137]. In addition to that, the lysosomal cholesterol transporter Niemann-Pick disease, type C1 (NPC1) along with LDLR were clearly up-regulated, whereas the inducible degrader of the LDL receptor (MYLIP) displayed down-regulation.

Proteomics

After evaluation of deregulations on transcriptomic level, the effect of archazolid B on proteomics was analyzed in addition. T24 cells were treated with 10 nM archazolid B or DMSO solvent control. After 24 h incubation, proteins were isolated for stable-isotope dimethyl labeling followed by liquid chromatography-mass spectrometry/mass spectrometry (LC-MS/MS) analysis. A threshold of 1.5 (fold change) was applied to the dataset and resulting 198 proteins were further analyzed using the Core Analysis tool of IPA software. The most deregulated proteins in consequence to archazolid B treatment are summarized in Table 5.

Deregulated proteins were correlated with cellular functions including cell death and survival, cellular growth and proliferation, lipid metabolism, small molecule biochemistry and molecular transport (Figure 25). Furthermore, proteins were assigned to canonical pathways revealing that 3 out of the top 5 canonical pathways were related to endocytosis (Figure 26).

Table 5: Top up- and down-regulated proteins in T24 cells after 24 h treatment with 10 nM archazolid B.

Gene name	Protein name	Fold change
<i>Up-regulated proteins</i>		
APLP2	amyloid beta (A4) precursor-like protein 2	9.1
UBA2	ubiquitin-like modifier activating enzyme 2	6.7
RAP1B	RAP1B, member of RAS oncogene family	6.7
HIST1H4I...*	Histone cluster	6.7
CHMP7	charged multivesicular body protein 7	6.3
GSTK1	glutathione S-transferase kappa 1	6.3
APP	amyloid beta (A4) precursor protein	5.9
PEPD	peptidase D	5.3
PURA	purine-rich element binding protein A	5.3
VKORC1L1	vitamin K epoxide reductase complex, subunit 1-like 1	5.3
<i>Down-regulated proteins</i>		
ANXA6	annexin A6	-17.8
CMTM6	CKLF-like MARVEL transmembrane domain containing 6	-4.6
LETM1	leucine zipper-EF-hand containing transmembrane protein 1	-3.8
AIMP2	aminoacyl tRNA synthetase complex-interacting multif. protein 2	-3.6
CTSB	cathepsin B	-3.4
EIF5B	Eukaryotic translation initiation factor 5B	-2.7
TTC4	tetratricopeptide repeat domain 4	-2.4
TIMM8A	translocase of inner mitochondrial membrane 8 hom. A (yeast)	-2.2
SEC23B	Sec23 homolog B (<i>S. cerevisiae</i>)	-2.1
PPAT	phosphoribosyl pyrophosphate amidotransferase	-2.1
* HIST1H4I; HIST1H4A; HIST1H4D; HIST1H4F; HIST1H4K; HIST1H4J; HIST1H4C; HIST1H4H HIST1H4B; HIST1H4E; HIST1H4L; HIST2H4A; HIST4H4; HIST2H4B		

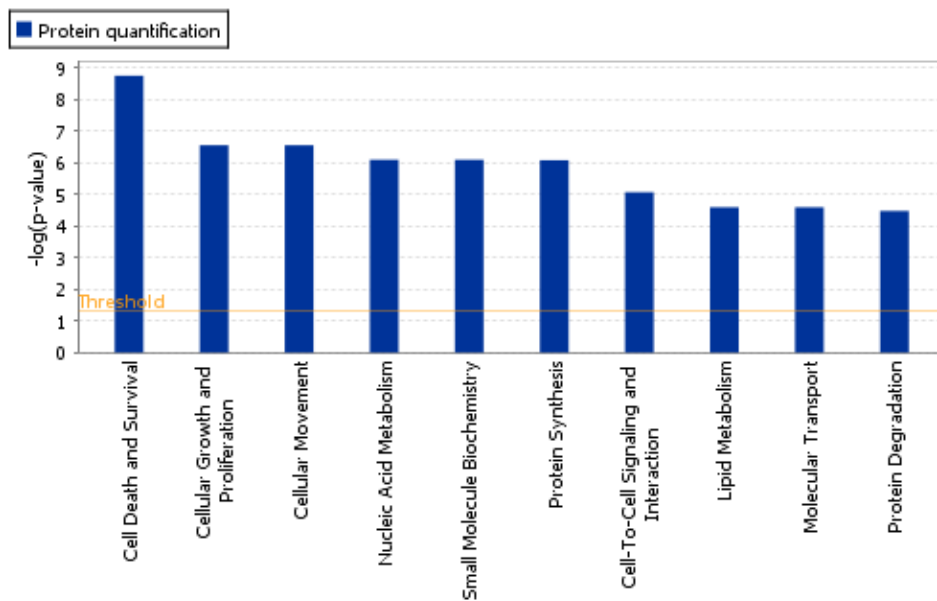


Figure 25: Top cellular functions affected in T24 cells after 24 h treatment with 10 nM archazolid B. Protein data were obtained using stable-isotope dimethyl labeling. P-values were calculated using right-tailed Fisher's exact test.

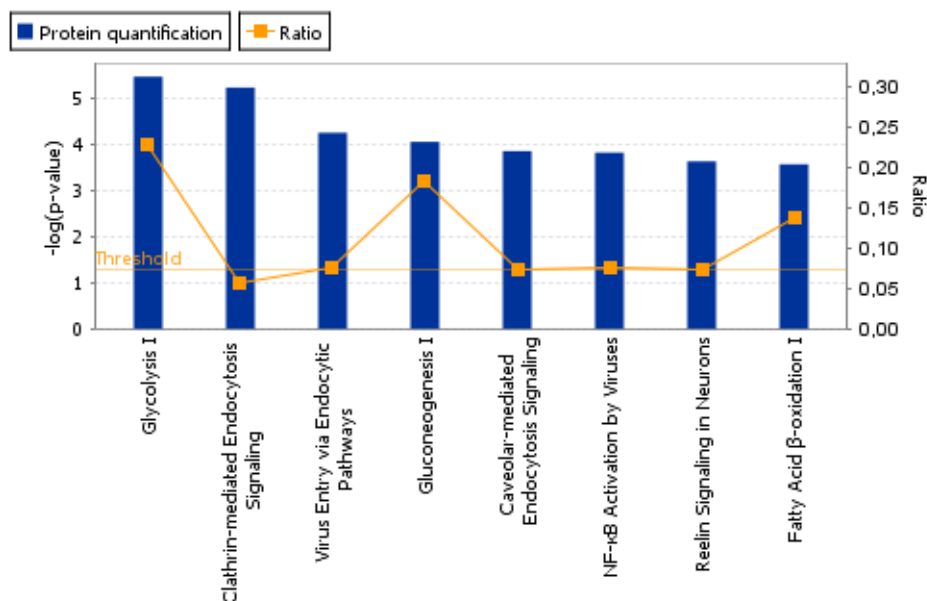


Figure 26: Top pathways significantly enriched in deregulated proteins after 24 h treatment of T24 cells with 10 nM archazolid B. P-values were calculated using right-tailed Fisher's exact test. Ratios indicate the number of proteins in a given pathway divided by the total number of proteins that make up that pathway.

Taken together, proteomics data indicated severe disturbances in endocytosis. Especially clathrin-mediated endocytosis, which is essential for LDLR internalization, turned out to be affected.

Merged analysis: transcriptomics and proteomics

In order to obtain a complete picture of archazolid B's effects on T24 cells, transcriptomics and proteomics data were compiled and reanalyzed. The number of deregulated molecules upon archazolid B treatment in each assay as well as the number of miRNA targets predicted by IPA Target Filter analysis are visualized in a Venn diagram (Figure 27). The intersection sets define the number of molecules in common among genes and proteins. Twenty-four molecules were present in all three datasets (12%). Amongst these molecules were 24-dehydrocholesterol reductase (DHCR24), farnesyl-diphosphate farnesyltransferase 1 (FDFT1) and 3-hydroxy-3-methylglutaryl-Coenzyme A synthase 1 soluble (HMGCS1), which play important roles in cholesterol biosynthesis.

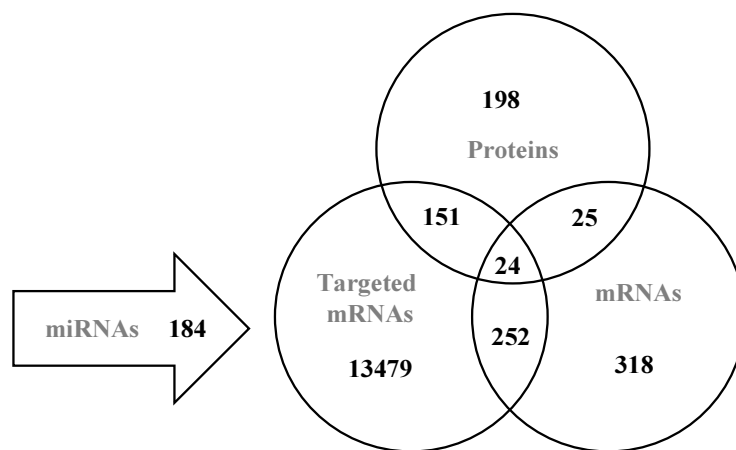


Figure 27: Venn diagram: results of mRNA microarray, miRNA microarray and stable-isotope dimethyl labeling for quantitative proteomics. Only molecules with a fold change $\geq \pm 1.5$ are presented in the diagram.

The data of the three *omics* assays were compiled to one data set and a Core Analysis was performed using IPA. Deregulated molecules were correlated to cellular functions. As shown in Figure 28, the results confirm previous findings that archazolid B displays a strong impact on cell death and survival, cellular growth and proliferation as well as on lipid metabolism.

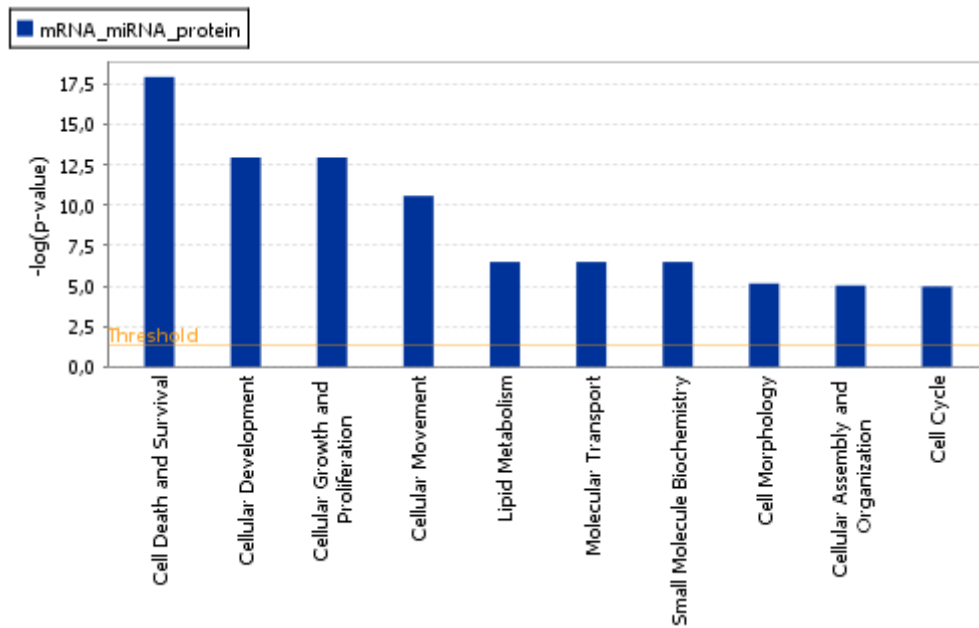


Figure 28: Top cellular functions affected in T24 cells after 24 h treatment with 10 nM archazolid B. Transcriptomic data were obtained performing mRNA and miRNA microarray, proteomic data were obtained using stable-isotope dimethyl labeling. P-values were calculated using right-tailed Fisher's exact test.

The top 20 deregulated pathways, ranked by significance (P-values), were displayed using the overlapping pathway mode. Thereby, two pathways are connected when they share at least one common molecule. As Figure 29 shows, cholesterol biosynthesis and clathrin-mediated endocytosis are linked via the liver X receptor/retinoid X receptor (LXR/RXR) pathway, more precisely via *LDLR*, *HMGCR* and *FDFT1*.

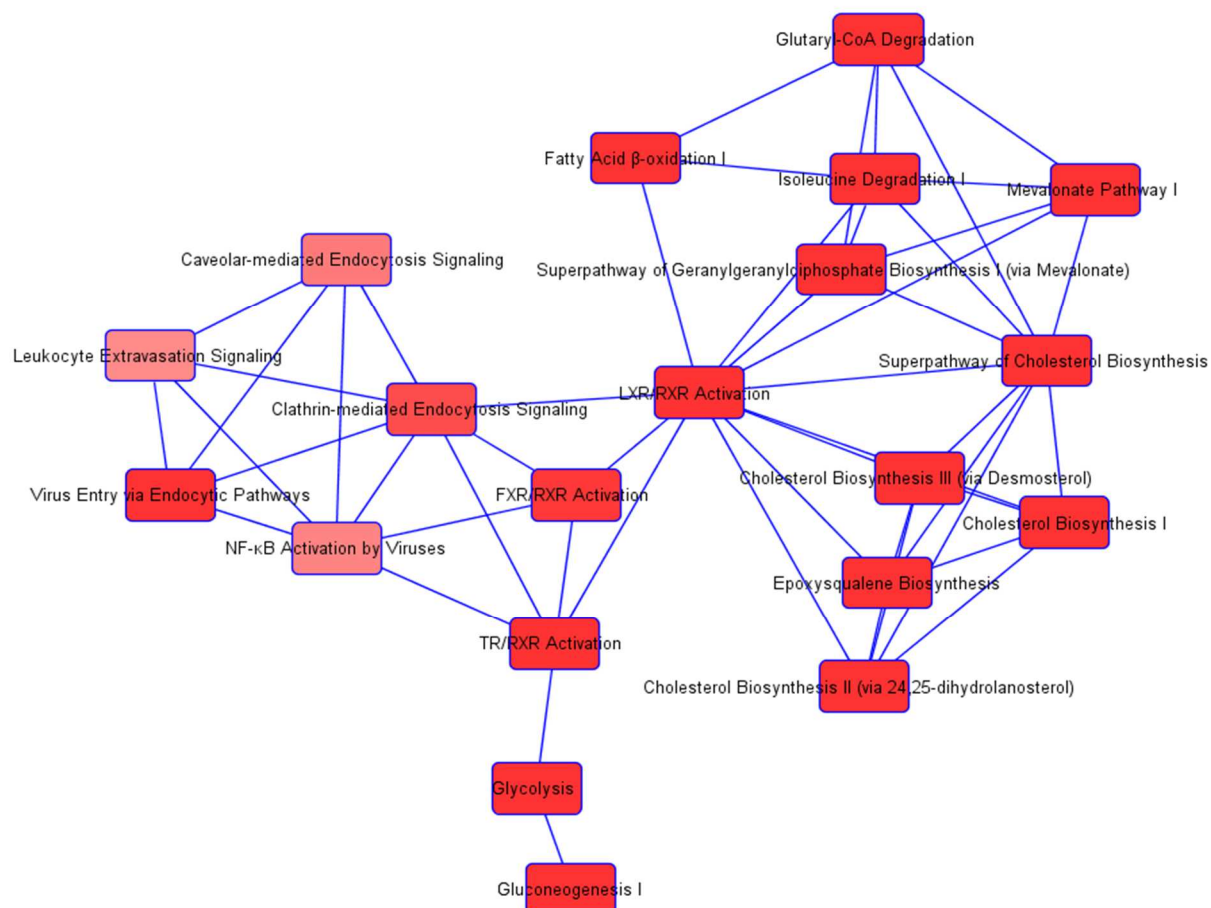


Figure 29: Overlapping pathways deregulated after 24 h treatment with 10 nM archazolid B. Transcriptomic data were obtained performing mRNA and miRNA microarray, proteomic data were obtained using stable-isotope dimethyl labeling. Color intensity is proportional to significance (P-value), assessed by right-tailed Fisher exact test.

Taken together, omics analysis strongly indicated that archazolid B causes disturbances in cholesterol homeostasis, affecting cholesterol biosynthesis and LDLR function (via clathrin-mediated endocytosis and LXR pathway).

3.2.1.3 Validation of cholesterol genes by real-time RT-PCR

For validation of the mRNA microarray data, real-time RT-PCR experiments were performed. To simultaneously verify the hypothesis that cholesterol homeostasis is affected by archazolid B, five cholesterol-related genes (*HMGCR*, *HMGCS1*, *LDLR*, *SQLE* and *INSIG1*) were selected and quantified. Results are shown in Table 6. The correlation coefficient between mRNA expression values determined by microarray and real-time RT-PCR was $R = 0.88$ (Pearson Correlation Test), indicating a high degree of concordance between the results obtained by the two different methods.

Table 6: Validation of microarray-based mRNA expression by real-time RT-PCR. Five cholesterol-associated genes were selected and quantified.

Gene	Description	Fold change	
		Microarray	Real-time RT-PCR
<i>HMGCR</i>	3-hydroxy-3-methylglutaryl-CoA reductase	2.8	4.6
<i>HMGCS1</i>	3-hydroxy-3-methylglutaryl-CoA synthase 1 (sol.)	4.2	5.5
<i>INSIG1</i>	insulin induced gene 1	6.6	19.9
<i>LDLR</i>	low-density lipoprotein receptor	2.7	6.2
<i>SQLE</i>	squalene monooxygenase	2.7	4.9

3.2.1.4 Nuclear expression of SREBPs

As detected by *omics* analysis and confirmed by real-time RT-PCR, the expression of cholesterol associated genes was enhanced in T24 cells after archazolid B treatment. In order to reveal if this was caused by SREBP activation and translocation, we performed Western Blot analysis with nuclear protein extracts from archazolid B and DMSO control treated cells using SREBP-1 and SREBP-2 antibodies. As shown in Figure 30A and B, the amount of activated SREBP-2 in the nucleus was increased after 2 h treatment with archazolid B. After 24 h and 72 h, however, there was a drastic decrease in nuclear SREBP-2. In case of SREBP-1, no nuclear expression was present and so no differences were observable comparing archazolid B to DMSO control (data not shown). These results indicated that SREBP-2, and not SREBP-1, mediates up-regulation of cholesterol-associated genes under archazolid B treatment.

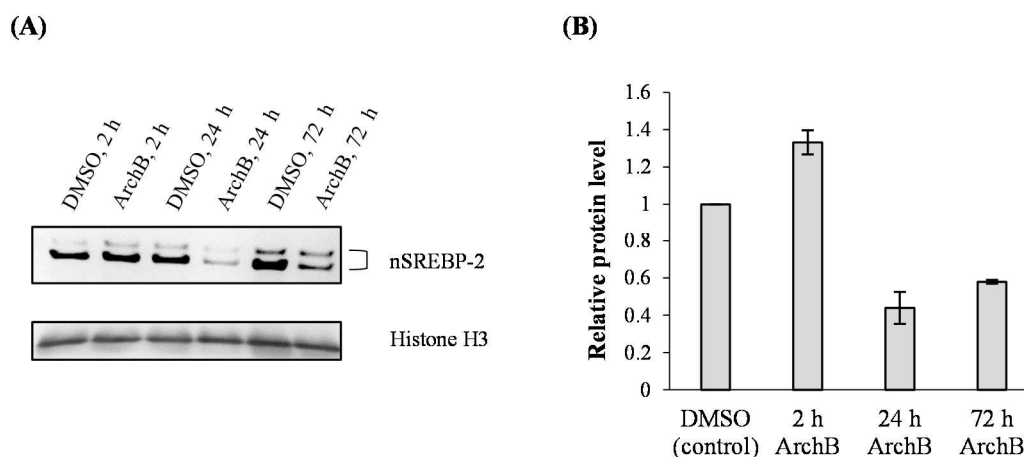


Figure 30: Expression of nuclear SREBP-2 (nSREBP-2). T24 cells were seeded one day before treatment. After 2 h, 24 h and 72 h incubation with 10 nM archazolid B or DMSO (control), cells were harvested and nuclear proteins were extracted. (A) Western blot analyses were performed with 12 μ g of nuclear extracts using anti-SREBP-2 antibody for primary antibody (1.5 h, RT). For secondary antibody, HRP-linked anti-rabbit IgG was used (1 h, RT). Histone H3 staining was performed in the same way. (B) Relative intensity of the bands was quantified using Histone H3-specific band as loading control. Two experiments were performed. Data are represented as mean \pm SD.

3.2.1.5 Staining of free cholesterol with filipin

Omics data analysis pointed to a disturbance of cholesterol homeostasis by archazolid B (3.2.1.2). Cholesterol homeostasis is sustained by cholesterol biosynthesis, LDL internalization and cholesterol esterification, which are sensitive to free cholesterol levels [138]. For this reason staining of free cholesterol was performed using filipin, a polyene antibiotic that forms complexes with 3β -hydroxysterols [139, 140].

Flow cytometry

To evaluate total levels of free cholesterol, T24 cells were stained with filipin and analyzed by flow cytometry. Measurements were performed after 12 h, 24 h, 48 h, 60 h, 72 h, 96 h and 120 h incubation with 10 nM archazolid B. As Figure 31 shows, a decrease of the filipin signal occurred within the first 24 h, indicating a lack of free cholesterol in the cells. However, the filipin signal was already overcompensated after 48 h treatment and then increased continuously up to 270% after 120 h treatment.

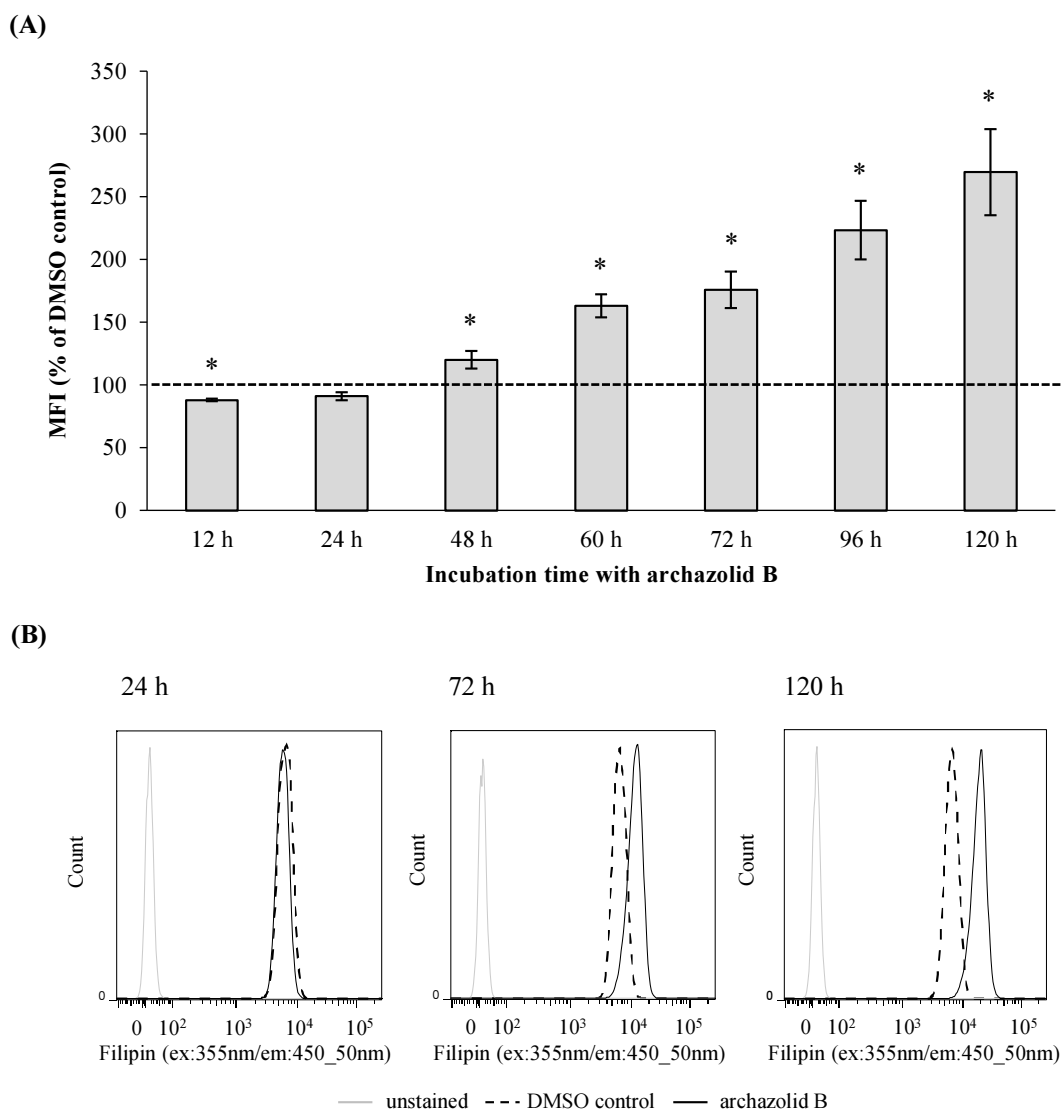


Figure 31: Levels of free cholesterol in T24 cells after treatment with archazolid B. T24 cells were seeded 20 h before, treated with archazolid B (10 nM), fixed and stained with filipin. (A) Mean fluorescence intensities (MFIs) of filipin were measured by flow cytometry. (B) Histograms show unstained cells for detection of auto-fluorescence (grey), DMSO control (black, dashed) and archazolid B treated cells (black). Experiments were performed three times in duplicates. (*Significantly different to DMSO control according to Student's t-test, $P < 0.05$)

Fluorescence microscopy

The previous analysis by flow cytometry revealed total levels of free cholesterol. To further examine its cellular distribution, cells were additionally analyzed by fluorescence microscopy after 24 h, 72 h and 120 h treatment with archazolid B. Compared to DMSO control, where filipin was distributed rather equally all over the cell, treatment with archazolid B led to a significant accumulation of fluorescent inclusions (Figure 32A). Quantification of the results was carried out by calculating the ratios of mean fluorescence intensity (MFI) of the area with

high fluorescence to the MFI of the area with low fluorescence (Figure 32B). The filipin intensity further increased after 72 h and 120 h treatment, indicating progressive sequestration of free cholesterol within these compartments which was accompanied by an enlargement of the entire cell.

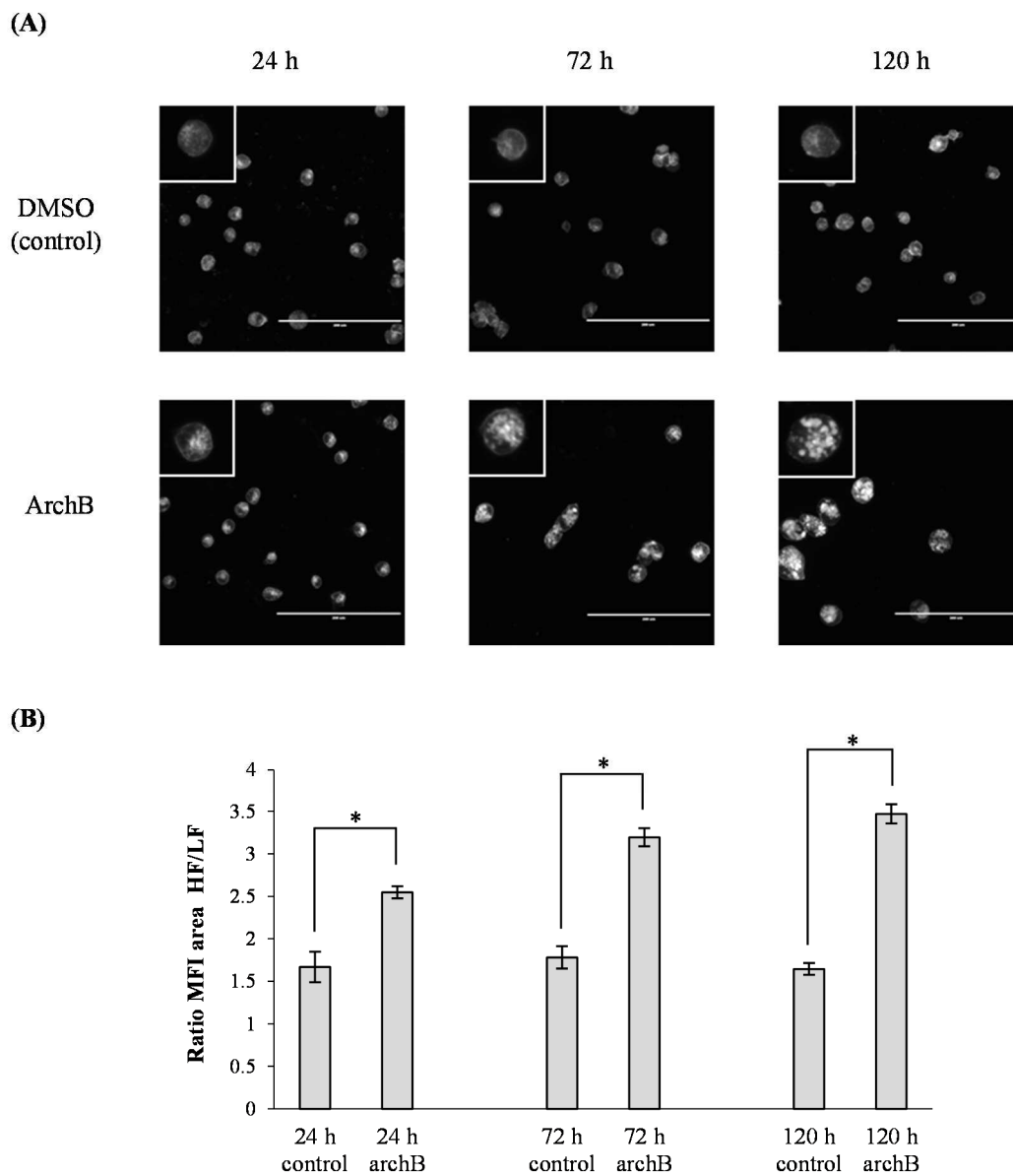


Figure 32: Distribution of free cholesterol in T24 cells after treatment with archazolid B (archB). T24 cells were seeded 20 h before, treated with archazolid B (10 nM), fixed and stained with filipin. (A) Distribution of filipin within the cells was visualized using fluorescence microscopy. Scale bar equals 200 μ m. (B) Accumulation of filipin within cellular compartments after treatment with archazolid B was quantified by calculating the ratio of mean fluorescence intensity (MFI) of the area with high fluorescence (HF) to MFI of the area with low fluorescence (LF). Ratios of 10 cells were calculated for each experiment and are represented by mean \pm SD of three independent experiments (*Significantly different to DMSO control according to Student's t-test, $P < 0.05$)

3.2.1.6 Inhibition of LDL uptake by archazolid B

Beside disturbances in cholesterol homeostasis, *omics* data analysis indicated deregulations in clathrin-mediated endocytosis after treatment with archazolid B (3.2.1.2). Endocytosis of LDL, a main source of cellular cholesterol, is a clathrin-mediated process [112]. For this reason, LDL uptake was visualized by confocal microscopy using BODIPY® FL-labeled LDL particles. Cell membranes were concomitantly stained with CellMask™ Orange for a better localization of the particles. As shown in Figure 33, upon treatment of T24 cells with 10 nM archazolid B for 24 h, LDL uptake was inhibited and the particles accumulated at the plasma membrane. In contrast to that, LDL was clearly internalized by DMSO control cells.

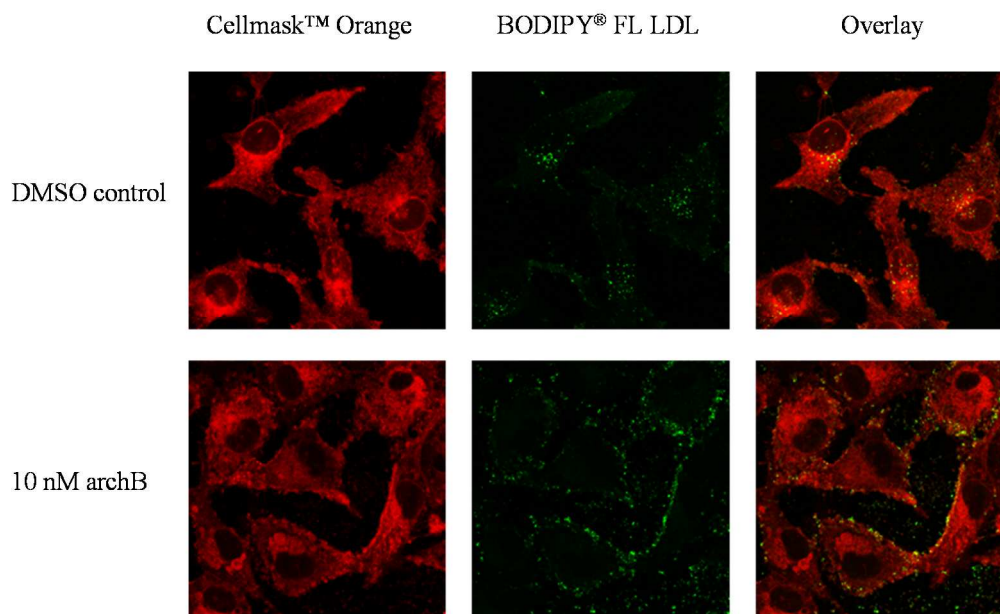


Figure 33: Inhibition of LDL uptake in T24 cells after 24 h treatment with 10 nM archazolid B (archB). T24 cells were seeded 24 h before and treated with 10 nM archazolid B or DMSO control for 24 h. After 15 min incubation with BODIPY® FL LDL and staining of the plasma membrane for 5 min, cells were fixed and analyzed using confocal microscopy. Three independent experiments were performed.

3.2.1.7 LDLR surface expression

Since LDL uptake was compromised in cells after archazolid B treatment, we wanted to know if LDLR expression on the cell surface is altered by the drug as well. Therefore antibody staining of LDLR and subsequent flow cytometry analysis was performed after 24 h incubation with 10 nM archazolid B. As shown in Figure 34, LDLR surface expression was significantly reduced (about 33%) in archazolid B-treated cells compared to DMSO control.

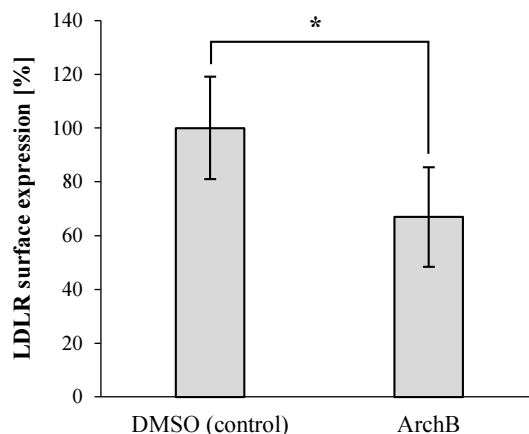


Figure 34: Cell surface expression of LDLR in T24 cells after 24 h treatment with 10 nM archazolid B. T24 cells were seeded 24 h before and treated with 10 nM archazolid B (archB) or DMSO control for 24 h. Cells were fixed and stained using mouse monoclonal anti-LDLR (C7) for primary antibody (1 h, 4°C) and anti-mouse conjugated with Alexa 488 for secondary antibody (40 min, 4°C). Then cells were analyzed by flow cytometry. Data are represented as mean \pm SD of two independent experiments including two parallel measurements. (*Significantly different according to Student's t-test, $P < 0.05$)

3.2.1.8 Combination of archazolid B with fluvastatin

Previous experiments showed a sequestration of free cholesterol upon archazolid B treatment (3.2.1.5). In addition to that, LDLR surface expression was reduced and LDL internalization turned out to be inhibited by archazolid B in T24 cells (3.2.1.6 and 3.2.1.7). Due to this fact, the cholesterol supply of the cell is likely compromised and needs to be compensated. Therefore, the contribution of cholesterol biosynthesis to cell survival after exposure to archazolid B was evaluated by performing cytotoxicity assays and filipin staining using combinations of archazolid B and fluvastatin. Fluvastatin is a member of the statin family inhibiting HMGCR, the key enzyme of cholesterol biosynthesis [141].

Cytotoxicity assay

Archazolid B was used in combination with a non-cytotoxic concentration of fluvastatin (0.5 μ M). As shown in Figure 35, the dose-response curve did not display additional cytotoxicity of fluvastatin at low concentrations of archazolid B. However, a decrease of about 20% in cell viability was observed at higher dose ranges compared to treatment with archazolid B alone.

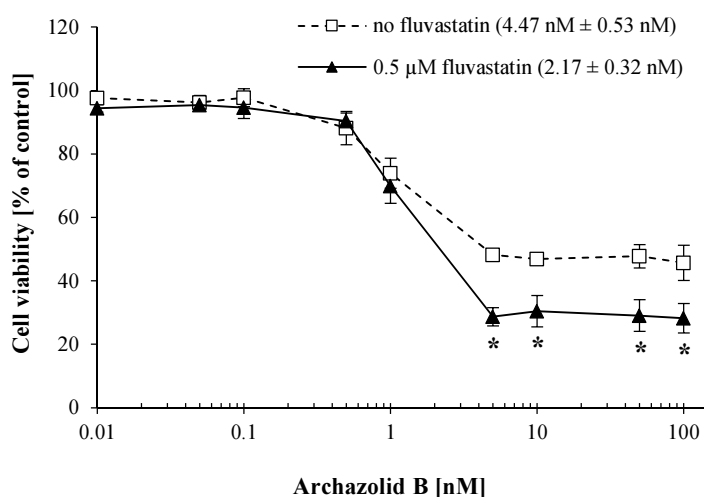


Figure 35: Cytotoxic effect of archazolid B in combination with fluvastatin after 72 h treatment of T24 cells. XTT assays were performed to determine dose response curves. IC_{50} concentrations are parenthesized. Viability of cells is represented by mean \pm SD of three independent experiments including three parallel measurements each and is expressed as percentage survival of control. (*Significantly different to archazolid B alone according to Student's t-test, $P < 0.05$)

Staining of free cholesterol with filipin

Filipin staining of free cholesterol was performed in order to prove that fluvastatin notably reduces cholesterol levels in archazolid B treated cells. Cells were treated with DMSO control, 0.5 μ M fluvastatin, 10 nM archazolid B or 0.5 μ M fluvastatin/10 nM archazolid B combination for 72 h and analyzed by flow cytometry (Figure 36A). Since the experiment was performed in medium containing fetal bovine serum (FBS), the effect of fluvastatin alone was expectedly low (6% decrease in MFI compared to DMSO control), due to uptake of LDL. The data obtained for archazolid B (167%) and archazolid B/fluvastatin combination (128%), however, clearly showed reduction of filipin intensity of about 39%. Even when excluding the effect of fluvastatin alone, the difference between MFIs of archazolid B and archazolid B/fluvastatin combination was highly significant (33%). To study the cellular distribution of free cholesterol, samples were also analyzed by fluorescence microscopy (Figure 36B). In DMSO- and fluvastatin-treated cells, filipin was equally distributed all over the cell. Compared to archazolid B alone, the archazolid B/fluvastatin combination showed a slightly reduced fluorescence in the sequestration area.

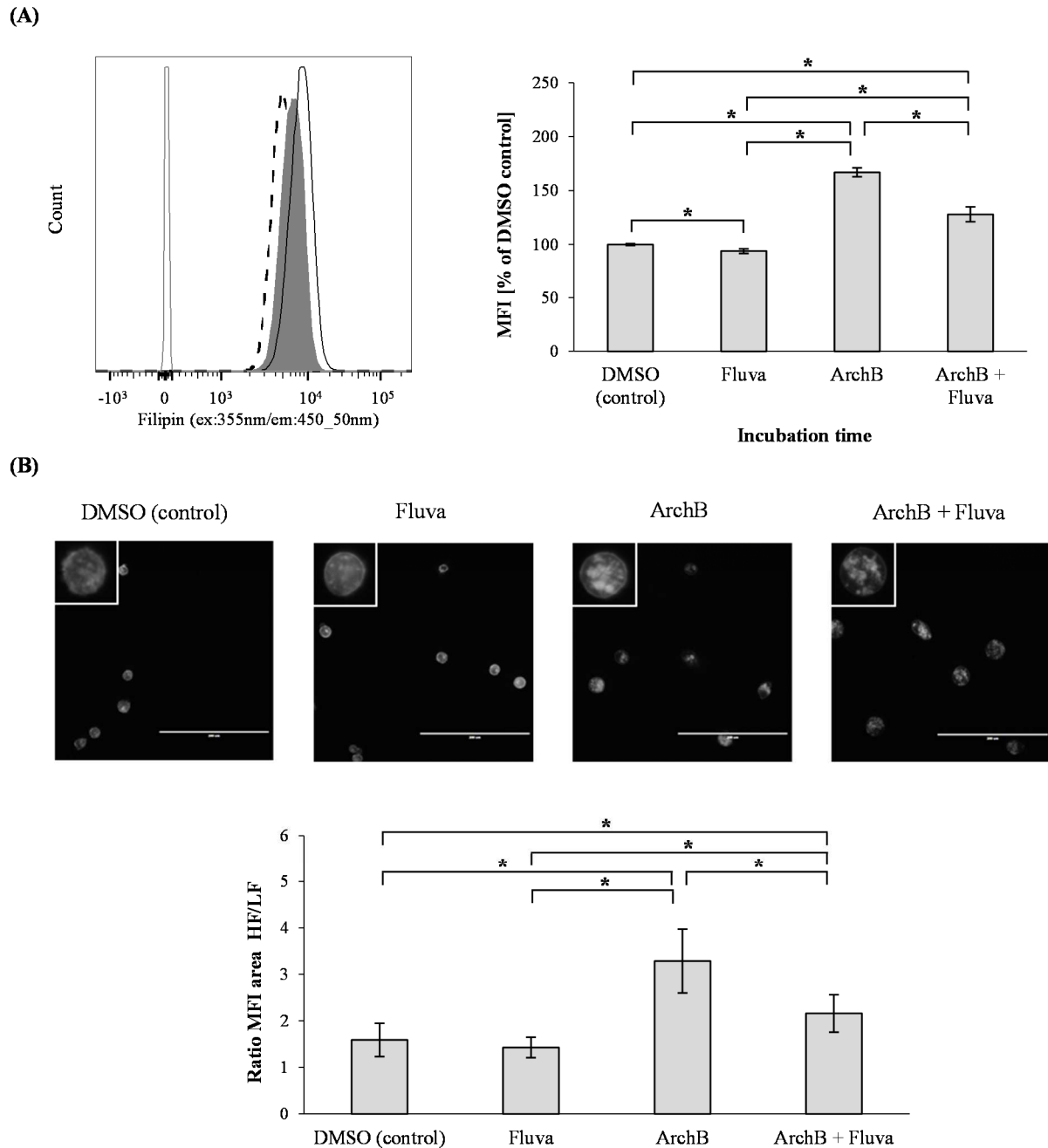


Figure 36: Effect of archazolid B/fluvastatin combination on free cholesterol level. T24 cells were seeded 24 h before treatment. Cells were incubated with DMSO (control), 0.5 μ M fluvastatin (fluva), 10 nM archazolid B (archB) or a combination of 10 nM archB and 0.5 μ M fluva for 72 h, fixed and stained with filipin. **(A)** Mean Fluorescence Intensities (MFIs) of filipin were measured by flow cytometry. Histograms show unstained cells for detection of auto-fluorescence (grey), DMSO control (black, dashed), archB-treated cells (black) and cells treated with a combination of archB and fluva (grey, tinted). MFI is represented by mean \pm SD of four parallel measurements derived from two independent experiments. **(B)** Distribution of filipin within the cells was visualized using fluorescence microscopy. Scale bar equals 200 μ m. Accumulation of filipin within cellular compartments after treatment with archB was quantified by calculating the ratio of MFI of the area with high fluorescence (HF) to MFI of the area with low fluorescence (LF). Ratios of 5 cells were calculated for each experiment and are represented by mean \pm SD of all ratios of two independent experiments. (*Significantly different according to Student's t-test, $P < 0.05$)

3.2.2 ArchB affects cholesterol homeostasis in U87MG/ Δ EGFR glioblastoma cells

Archazolid B remarkably disturbed cholesterol homeostasis in T24 cells. In order to evaluate whether these effects were cell line-independent, glioblastoma cells were used as a second test system. mRNA microarrays were performed on U87MG and U87MG. Δ EGFR cells, expressing constitutively active EGFR, after 24 h and 48 h treatment with archazolid B. In addition to that, gene expression profiles of untreated U87MG and U87MG. Δ EGFR cells were compared as well. Experiments were validated using real-time RT-PCR, flow cytometry and fluorescence microscopy.³

3.2.2.1 Gene expression profiling

Microarrays: 24 h/48 h archazolid B

U87MG and U87MG. Δ EGFR cells were treated with $20 \times IC_{50}$ (72h) concentration of archazolid B. DMSO solvent control samples were prepared as well. After 24 h and 48 h incubation, total RNA was isolated for a whole human genome mRNA gene expression microarray. Expression data were analyzed using Chipster software. Genes were filtered by two times standard deviation and significance was assessed using empirical Bayes t-test ($P < 0.05$) with Bonferroni correction. Datasets obtained for 24 h treatment with archazolid B were filtered to a fold change $\geq \pm 1.74$. In case of 48 h treatment, only genes with a fold change $\geq \pm 1.82$ were considered for analysis. The number of deregulated genes for each cell line and the number of genes in common are visualized in a Venn diagram (Figure 37). For both incubation times, more than 60% of the genes were present in both datasets. However, after 48 h treatment, U87MG. Δ EGFR cells exhibited a higher number of significantly deregulated genes (about 437 genes) compared to the wild-type cell line. Table 7 shows the top-deregulated genes in U87MG and U87MG. Δ EGFR cells after 24 h and 48 h exposure to archazolid B. It is to note that in both cell lines, three genes related to cholesterol biosynthesis and regulation, *HMGCS1*, *INSIG1* and

³ The results presented in this part of the work were recently accepted for publication in a peer-reviewed scientific journal:

R. Hamm, M. Zeino, R. Müller, T. Efferth, "Up-regulation of cholesterol associated genes as novel resistance mechanism in glioblastoma cells in response to archazolid B," submitted at *Toxicol Appl Pharmacol*, accepted 2 September 2014.

All figures, tables and text passages of this publication used in a modified form in this dissertation were prepared or written by myself.

MSMO1 (*methylsterol monoxygenase 1*), are amongst the top ten up-regulated genes after 24 h treatment with archazolid B.

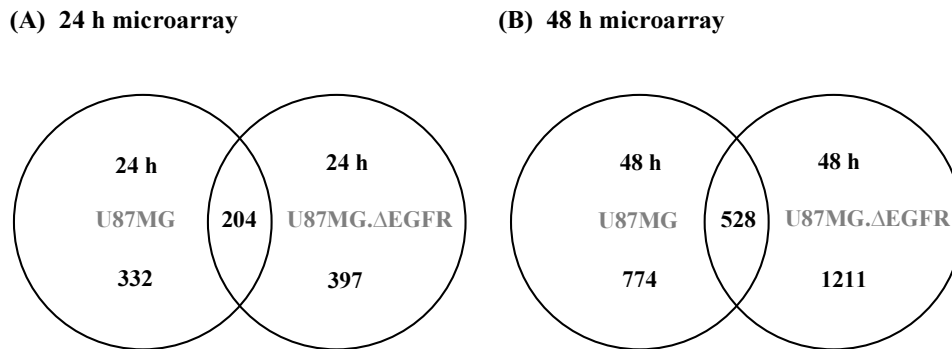


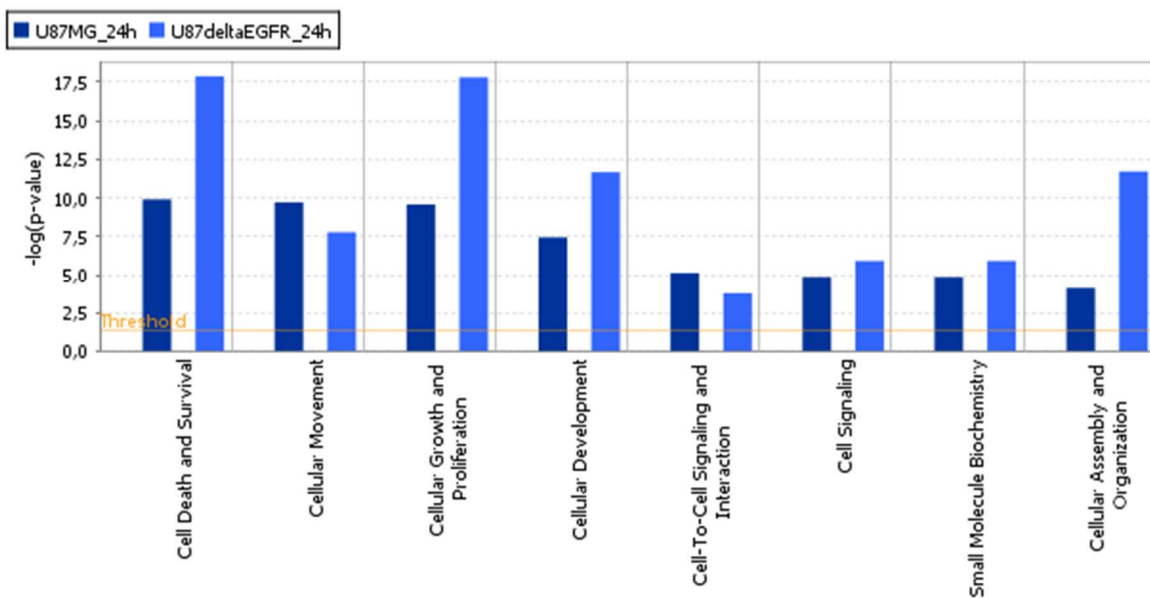
Figure 37: Venn diagrams: Number of genes deregulated in U87MG and U87MG.ΔEGFR cells after archazolid B treatment. Data were obtained using microarray technology. Genes were further analyzed using IPA. (A) For 24 h treatment only genes with a fold change $\geq \pm 1.74$ are presented in the diagram. (B) For 48 h treatment only genes with a fold change $\geq \pm 1.82$ are presented in the diagram.

Table 7: Top up- and down-regulated genes in U87MG/ΔEGFR cells upon treatment with archazolid B.

U87MG, 24 h		U87MG.ΔEGFR, 24 h		U87MG, 48 h		U87MG.ΔEGFR, 48 h	
Gene	FC	Gene	FC	Gene	FC	Gene	FC
<i>Up-regulated genes</i>							
<i>CPA4</i>	12.0	<i>HMGCS1</i>	12.4	<i>SPINK1</i>	38.1	<i>SPINK1</i>	42.8
<i>HMGCS1</i>	10.1	<i>CA9</i>	11.5	<i>PTGS2</i>	12.9	<i>PTGS2</i>	31.8
<i>IGFBP3</i>	9.3	<i>ANGPTL4</i>	9.7	<i>ATF3</i>	9.6	<i>IL6</i>	28.2
<i>IGFBP3</i>	8.6	<i>C10orf10</i>	8.3	<i>PTGS2</i>	9.5	<i>C11orf96</i>	19.2
<i>C10orf10</i>	6.5	<i>NDRG1</i>	8.1	<i>IL36B</i>	8.8	<i>TRIB3</i>	17.3
<i>INSIG1</i>	6.2	<i>INSIG1</i>	7.0	<i>C11orf96</i>	8.4	<i>DDIT3</i>	16.0
<i>CA9</i>	6.0	<i>MSMO1</i>	6.8	<i>IGFBP3</i>	8.1	<i>IGFBP1</i>	15.3
<i>SPINK1</i>	5.9	<i>ALDOC</i>	6.2	<i>IL36B</i>	7.3	<i>IGFBP1</i>	14.1
<i>MSMO1</i>	5.8	<i>SLC2A3</i>	6.2	<i>CRYM</i>	7.2	<i>CEMIP</i>	14.1
<i>ZP1</i>	5.5	<i>SPINK1</i>	6.0	<i>IL6</i>	6.8	<i>PTGS2</i>	13.6
<i>Down-regulated genes</i>							
<i>ID3</i>	-3.6	<i>CCL2</i>	-5.1	<i>NDP</i>	-8.4	<i>ID3</i>	-10.4
<i>TNFRSF21</i>	-3.2	<i>MYLIP</i>	-4.3	<i>ID3</i>	-6.5	<i>HOPX</i>	-9.0
<i>DIO2</i>	-3.1	<i>LYPD1</i>	-3.7	<i>COL1A2</i>	-5.8	<i>NDP</i>	-8.7
<i>KRT80</i>	-2.9	<i>CDC20</i>	-3.6	<i>CYR61</i>	-5.0	<i>CCL2</i>	-8.0
<i>CDC20</i>	-2.9	<i>FST</i>	-3.5	<i>ENC1</i>	-4.5	<i>CDC20</i>	-7.9
<i>FJX1</i>	-2.6	<i>KRT80</i>	-3.4	<i>TNFRSF21</i>	-4.3	<i>DIRAS3</i>	-7.8
<i>RRS1</i>	-2.6	<i>DDX10</i>	-3.3	<i>FJX1</i>	-3.9	<i>TMEM244</i>	-7.8
<i>TSC22D1</i>	-2.6	<i>DIRAS3</i>	-3.1	<i>CDC20</i>	-3.7	<i>DIO2</i>	-7.8
<i>NDP</i>	-2.5	<i>TNFRSF21</i>	-3.1	<i>COL1A1</i>	-3.7	<i>EFEMP1</i>	-7.8
<i>LRN3</i>	-2.4	<i>CCNB1</i>	-2.9	<i>DIO2</i>	-3.7	<i>ID1</i>	-7.6

Datasets were analyzed using the IPA Core Analysis tool. Core Analyses were further evaluated by Comparison Analyses of 24 h and 48 h datasets. Deregulated genes were correlated with cellular functions including cell death and survival, cellular growth and proliferation and cell signaling. Figure 38 shows the top functions affected by archazolid B treatment after 24 h and 48 h treatment, displayed as a Comparison Analysis of U87MG and U87MG.ΔEGFR. As indicated by P-values, U87MG.ΔEGFR were compromised more significantly.

(A)



(B)

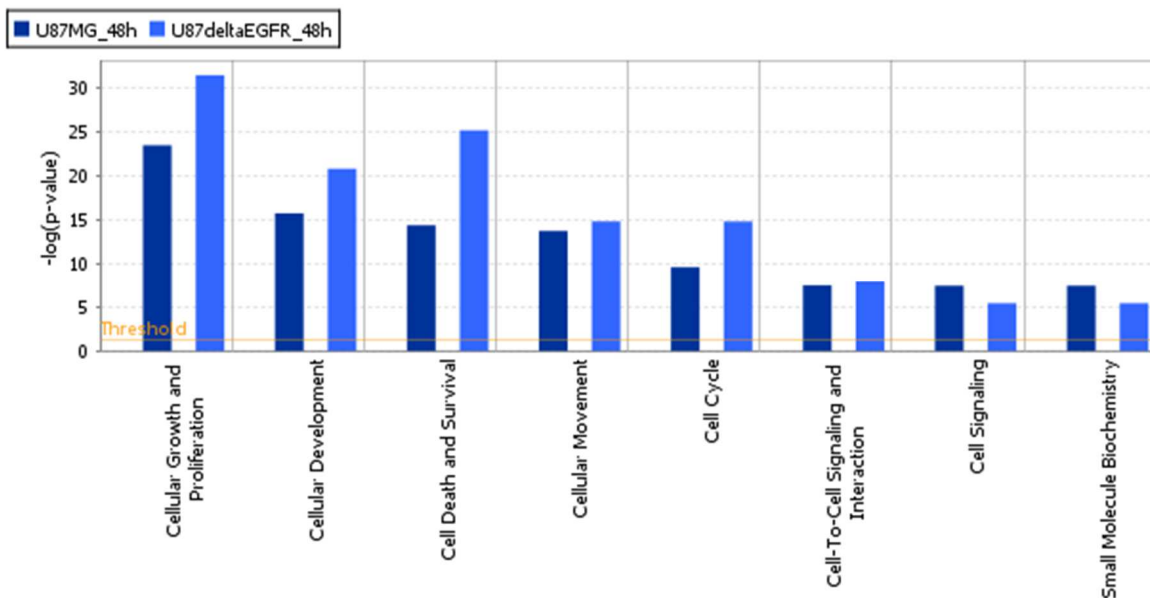


Figure 38: Ingenuity comparison analyses: Cellular functions affected after 24 h treatment (A) and 48 h treatment (B) of U87MG and U87MG.ΔEGFR cells with $20 \times IC_{50}$ archazolid B. Gene expression data were obtained using microarray technology. P-values were calculated using right-tailed Fisher's exact test.

Furthermore, several genetic networks were found to be significantly deregulated in glioblastoma cells after archazolid B treatment. These networks were correlated to lipid metabolism, small molecule biochemistry, molecular transport, cellular function and maintenance as well as cell death and survival. Figure 39 exemplarily displays one of the most affected networks in U87MG. Δ EGFR upon 24 h treatment with archazolid B.

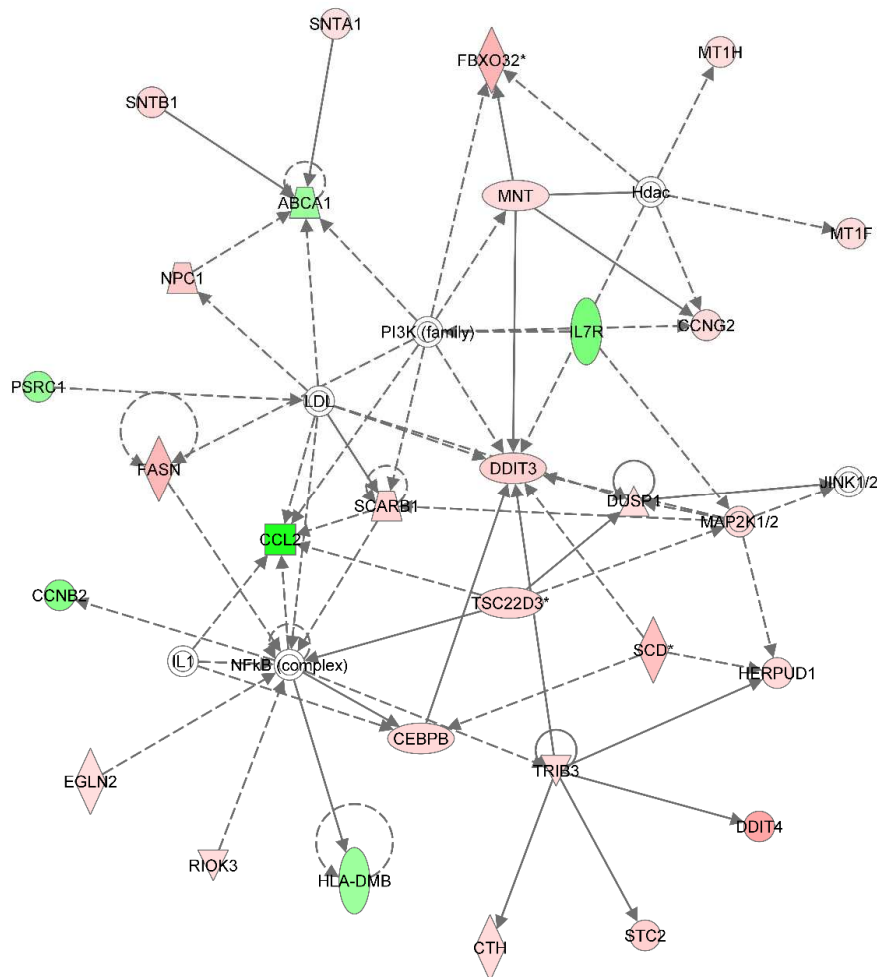


Figure 39: Deregulated network correlated to lipid metabolism, molecular transport and small molecule biochemistry. U87MG. Δ EGFR were treated for 24 h with 154 nM archazolid B. Red colored genes were up-regulated, green colored ones were down-regulated after treatment. Continuous lines show a direct interaction, dotted lines an indirect interaction.

Deregulated genes were assigned to canonical pathways. Similar to T24 cells, the top-deregulated pathways upon 24 h and 48 h archazolid B treatment were all correlated to cholesterol biosynthesis in U87MG as well as in U87MG. Δ EGFR cells (Figure 40). Furthermore, in cells treated for 48 h with archazolid B the LXR pathway also displayed strong deregulation. Variations in significance between datasets were likely due to different amounts of deregulated genes within the datasets.

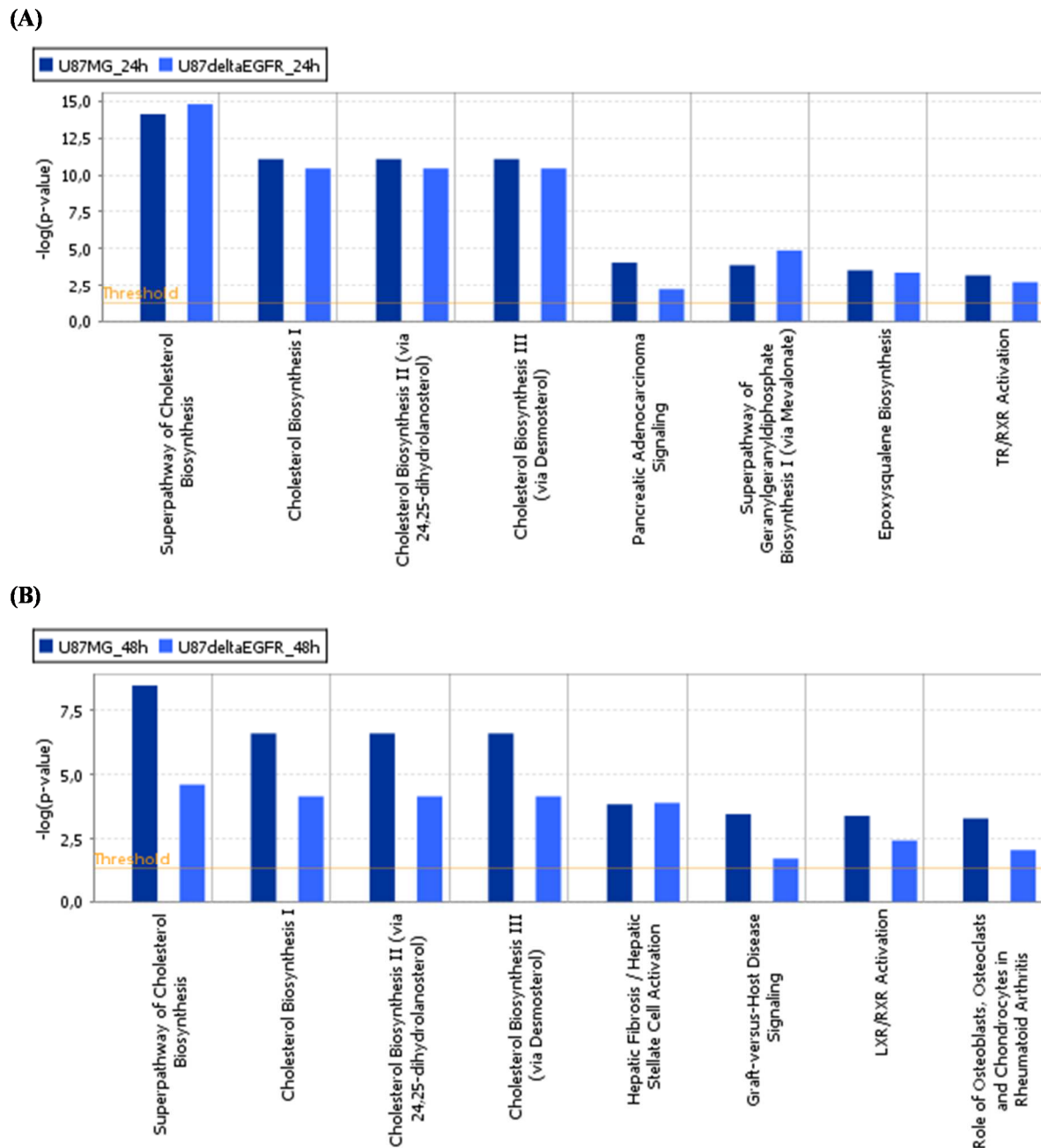


Figure 40: Ingenuity comparison analyses: Pathways significantly enriched in deregulated genes after 24 h treatment (A) and 48 h treatment (B) of U87MG and U87MG.ΔEGFR cells with $20 \times IC_{50}$ archazolid B. Gene expression data were obtained using microarray technology. P-values were calculated using right-tailed Fisher's exact test.

Further analysis of the datasets revealed significant deregulation of cholesterol-associated genes in U87MG and U87MG.ΔEGFR cells (Table 8). Amongst these genes were *HMGCR*, *NPC1*, *LDLR*, *ABCA1* and *MYLIP*. Genes were deregulated to about the same extent in both cell lines. Comparing 24 h to 48 h treatment, the fold changes of most genes slightly decreased. However, cholesterol-associated genes still remained clearly deregulated after 48 h.

Table 8: Cholesterol-associated genes deregulated in U87MG and U87MG.ΔEGFR upon treatment with $20 \times IC_{50}$ concentration of archazolid B. Changes in mRNA expression were detected performing microarrays after 24 h and 48 h treatment with archazolid B.

Gene	Description	Fold change			
		MG 24 h	ΔEGFR 24 h	MG 48 h	ΔEGFR 48 h
<i>ABCA1</i>	ATP-binding cassette, sub-family A (ABC1), member 1	-	-1.9	-2.0	-
<i>ACAT2</i>	acetyl-CoA acetyltransferase 2	2.5	2.3	1.9	-
<i>DHCR24</i>	24-dehydrocholesterol reductase	3.7	2.6	4.0	4.4
<i>EBP</i>	emopamil binding protein (sterol isomerase)	2.8	2.7	2.9	2.2
<i>FDFT1</i>	farnesyl-diphosphate farnesyltransferase 1	2.4	2.7	2.2	2.0
<i>FDPS</i>	farnesyl diphosphate synthase	2.0	2.1	2.7	2.8
<i>HMGCR</i>	3-hydroxy-3-methylglutaryl-CoA reductase	3.6	4.1	3.5	3.6
<i>HMGCS1</i>	3-hydroxy-3-methylglutaryl-CoA synthase 1, soluble	10.1	12.6	5.9	4.7
<i>INSIG1</i>	insulin induced gene 1	6.2	7.0	3.6	3.2
<i>INSIG2</i>	insulin induced gene 2	4.2	4.6	3.0	4.6
<i>LDLR</i>	low-density lipoprotein receptor	2.7	2.9	2.5	2.0
<i>LSS</i>	lanosterol synthase	3.9	4.5	5.5	4.5
<i>MSMO1</i>	methylsterol monooxygenase 1	5.8	6.8	4.0	4.2
<i>MVD</i>	mevalonate (diphospho) decarboxylase	2.9	4.0	3.5	3.5
<i>MVK</i>	mevalonate kinase	-	2.3	-	-
<i>MYLIP</i>	myosin regulatory light chain interacting protein	-	-4.3	-	-4.7
<i>NPC1</i>	Niemann-Pick disease, type C1	2.7	3.0	3.2	4.1
<i>NPC2</i>	Niemann-Pick disease, type C2	-	-	2.0	2.1
<i>NSDHL</i>	NAD(P) dependent steroid dehydrogenase-like	2.2	2.3	2.0	-
<i>SC5D</i>	sterol-C5-desaturase	2.1	2.5	-	-
<i>SQLE</i>	squalene monooxygenase	3.7	3.3	3.1	2.7

Similar to T24 cells, gene expression data of both glioblastoma cell lines treated with archazolid B for 24 h and 48 h strongly indicated disturbances in cholesterol homeostasis. Nearly all cholesterol biosynthesis genes were significantly up-regulated (e.g. HMGCR, HMGCS1). In addition to that, the lysosomal cholesterol transporters NPC1 and NPC2 along with LDLR were clearly up-regulated whereas the inducible degrader of the LDL receptor (MYLIP) as well as the cholesterol exporter ABCA1 displayed down-regulation.

Microarrays: 24 h/48 h controls

Cytotoxicity assays revealed that U87MG. Δ EGFR cells, expressing constitutively active EGFR, showed a nearly 10-fold higher resistance towards archazolid B compared to U87MG wild-type cells (3.1.4). Furthermore, gene expression profiling revealed a slightly higher expression of cholesterol-associated genes after 24 h treatment with archazolid B in the mutant cell line (3.2.2.1). For this reason, DMSO solvent control microarray datasets (24 h and 48 h) were reanalyzed in order to discover general differences between U87MG and U87MG. Δ EGFR cells with regards to cholesterol metabolism. Gene expression data were analyzed using Chipster software. U87MG. Δ EGFR datasets were always compared to corresponding U87MG datasets. Genes were filtered by three times standard deviation and significance was assessed using empirical Bayes t-test ($P < 0.05$) with Benjamini-Hochberg correction.

With the IPA Core Analysis tool, genes were assigned to canonical pathways. As shown in Figure 41, cholesterol biosynthesis, EGF signaling and PI3K/Akt signaling displayed significant deregulations in U87MG. Δ EGFR compared to wild-type cells. Ratios of cholesterol biosynthesis pathways were between 0.3 and 0.45, indicating that 30-45% of all genes in these pathways were deregulated in the mutant cell line. EGF signaling and PI3K/Akt signaling displayed 25-30% and 15-30% deregulated genes.

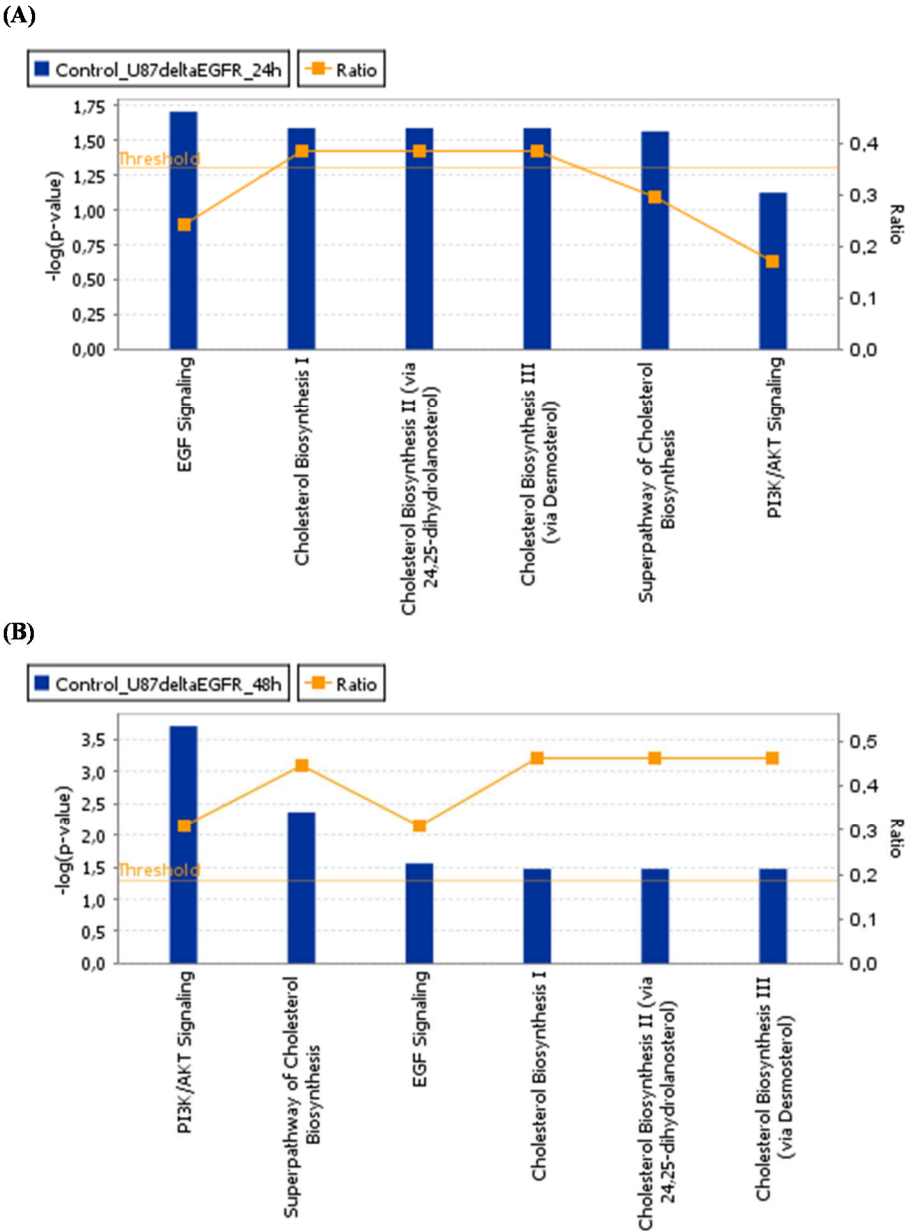


Figure 41: Selected pathways significantly enriched in deregulated genes in 24 h (A) and 48 h (B) U87MG.ΔEGFR control samples. Changes in gene expression were detected performing microarrays and comparing the results to U87MG samples. P-values were calculated using right-tailed Fisher’s exact test. Ratios indicate the number of genes in a given pathway divided by the total number of genes that make up that pathway.

Further analysis revealed significant deregulation of cholesterol-associated genes in U87MG.ΔEGFR cells as displayed in Table 9.

Table 9: Cholesterol-associated genes deregulated in U87MG.ΔEGFR control samples. Differences in gene expression were detected performing microarrays and comparing the results to U87MG samples.

Gene	Description	Fold change 24 h	Fold change 48 h
<i>ABCA1</i>	ATP-binding cassette, sub-family A (ABC1), member 1	-1.6	-1.7
<i>ACAT2</i>	acetyl-CoA acetyltransferase 2	1.5	1.7
<i>DHCR24</i>	24-dehydrocholesterol reductase	1.5	1.4
<i>FDFT1</i>	farnesyl-diphosphate farnesyltransferase 1	-	1.3
<i>FDPS</i>	farnesyl diphosphate synthase	1.3	-
<i>INSIG1</i>	insulin induced gene 1	-	1.6
<i>LDLR</i>	low-density lipoprotein receptor	1.3	1.6
<i>LSS</i>	lanosterol synthase (2,3-oxidosqualene-lanosterol cyclase)	1.4	2.2
<i>MVD</i>	mevalonate (diphospho) decarboxylase	-	1.3
<i>MVK</i>	mevalonate kinase	-	1.4
<i>PMVK</i>	phosphomevalonate kinase	1.4	-
<i>NSDHL</i>	NAD(P) dependent steroid dehydrogenase-like	1.4	-
<i>SC5D</i>	sterol-C5-desaturase	-	1.3
<i>SREBF1</i>	sterol regulatory element binding transcription factor 1	-	2.6
<i>TM7SF2</i>	transmembrane 7 superfamily member 2	4.1	2.1

Taken together, analysis of basic gene expression in U87MG.ΔEGFR cells revealed, beside deregulated EGF and PI3K signaling, an impact on cholesterol homeostasis. Compared to U87MG wild-type cells, the mutant cell line displayed up-regulation of cholesterol biosynthesis genes as well as SREBF1 (sterol regulatory element binding transcription factor 1), encoding SREBP1. In addition to that, the LDLR gene was clearly up-regulated whereas the cholesterol exporter ABCA1 displayed down-regulation.

3.2.2.2 Validation of cholesterol genes by real-time RT-PCR

Microarray results were validated by real-time RT-PCR experiments. Five genes related to cholesterol (*HMGCR*, *HMGCS1*, *LDLR*, *SQLE* and *INSIG1*) were selected and quantified. Results are displayed in Table 10. The correlation coefficients between mRNA expression values determined by microarray hybridization and real-time RT-PCR were $R = 0.82$ for 24 h treatment and $R = 0.77$ for 48 h treatment (Pearson Correlation Test). This indicated a high degree of concordance between the results obtained by the two different methods.

Table 10: Validation of microarray-based mRNA expression by real-time RT-PCR. Five cholesterol-associated genes were selected and quantified.

Cell line	Gene	Method	Fold change	
			24 h	48 h
U87MG	<i>HMGCR</i>	Microarray hybridization	3.6	3.5
		Real-time RT-PCR	4.8	4.2
U87MG	<i>HMGCS1</i>	Microarray hybridization	10.1	5.9
		Real-time RT-PCR	20.1	10.9
U87MG	<i>INSIG1</i>	Microarray hybridization	6.2	3.6
		Real-time RT-PCR	19.0	9.4
U87MG	<i>LDLR</i>	Microarray hybridization	2.7	2.5
		Real-time RT-PCR	4.8	3.7
U87MG	<i>SQLE</i>	Microarray hybridization	3.7	3.1
		Real-time RT-PCR	5.8	5.1
U87MG.ΔEGFR	<i>HMGCR</i>	Microarray hybridization	4.1	3.6
		Real-time RT-PCR	5.1	2.9
U87MG.ΔEGFR	<i>HMGCS1</i>	Microarray hybridization	12.6	4.7
		Real-time RT-PCR	17.2	6.3
U87MG.ΔEGFR	<i>INSIG1</i>	Microarray hybridization	7.0	3.2
		Real-time RT-PCR	20.8	5.1
U87MG.ΔEGFR	<i>LDLR</i>	Microarray hybridization	2.9	2.0
		Real-time RT-PCR	4.8	2.6
U87MG.ΔEGFR	<i>SQLE</i>	Microarray hybridization	3.3	2.7
		Real-time RT-PCR	5.6	3.9

3.2.2.3 Staining of free cholesterol with filipin

As previously performed on T24 cells (3.2.1.5), free cholesterol levels were determined using filipin. Gene expression data of U87MG and U87MG. Δ EGFR cells both pointed to disturbances in cholesterol homeostasis to about the same extent. However, the basic expression of cholesterol-associated genes was generally higher in U87MG. Δ EGFR cells. For this reason, filipin staining was exemplarily performed on U87MG. Δ EGFR cells.

Flow cytometry

U87MG. Δ EGFR cells were incubated with 154 nM archazolid B, which equals $20 \times IC_{50}$ concentration. Samples were stained with filipin and analyzed by flow cytometry. As displayed in Figure 42, the filipin signal was up to 118% after 24 h and further increased to 155% after 72 h.

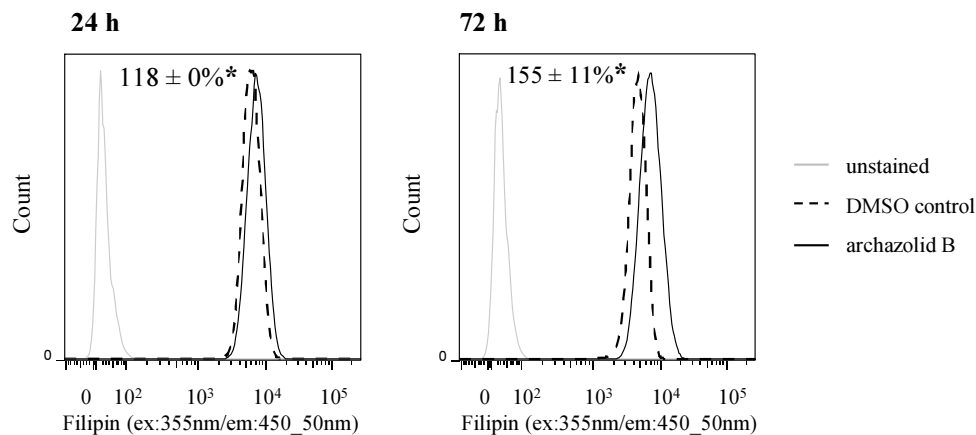


Figure 42: Levels of free cholesterol in U87MG. Δ EGFR cells after treatment with archazolid B. U87MG. Δ EGFR cells were seeded 20 h before, treated with 154 nM archazolid B for 24 h and 72 h, fixed and stained with filipin. Mean Fluorescence Intensities (MFIs) of filipin were measured by flow cytometry. Histograms show unstained cells for detection of auto-fluorescence (grey), DMSO control (back, dashed) and archazolid B-treated cells (black). MFI is expressed by mean \pm SD (as percentage of DMSO control) of three independent experiments including duplicates each. (*Significantly different to DMSO control according to Student's t-test, $P < 0.05$)

Fluorescence microscopy

Samples were further investigated by fluorescence microscopy in order to analyze the distribution of filipin within the cells (Figure 43). Compared to DMSO control, where filipin was distributed rather equally all over the cell, treatment with archazolid B revealed significant fluorescent inclusions. The filipin intensity increased from 24 h to 72 h treatment, indicating progressive accumulation of free cholesterol within these intracellular compartments. For quantification of the filipin signal, the ratios of MFI of the area with high fluorescence to the MFI of the area with low fluorescence were calculated.

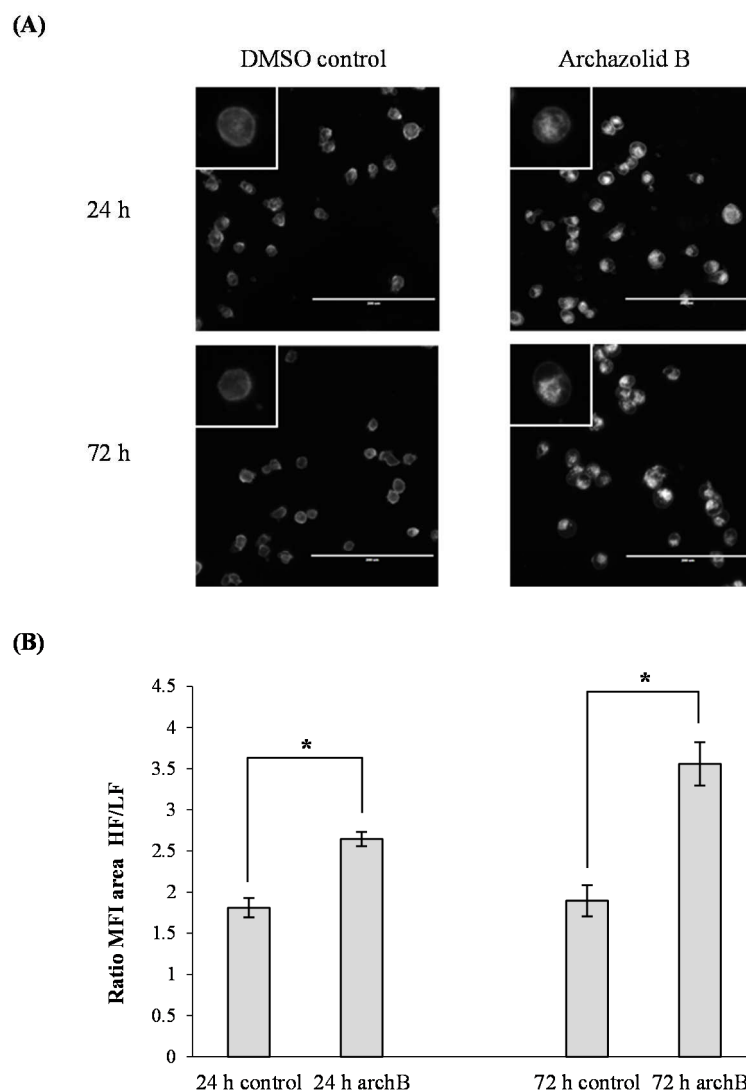


Figure 43: Distribution of free cholesterol in U87MG.ΔEGFR cells after treatment with archazolid B. U87MG.ΔEGFR cells were seeded 20 h before, treated with 154 nM archazolid B (archB) for 24 h and 72 h, fixed and stained with filipin. (A) Distribution of filipin within the cells was visualized using fluorescence microscopy. Scale bar equals 200 μm . (B) Accumulation of filipin within cellular compartments after treatment with archazolid B was quantified by calculating the ratio of MFI of the area with high fluorescence (HF) to MFI of the area with low fluorescence (LF). Ratios of 10 cells were calculated for each experiment and are represented by mean \pm SD of three independent experiments (*Significantly different according to Student's t-test, $P < 0.05$)

3.2.3 Summary: Cholesterol synthesis as a new resistance mechanism

In this part of the work, cholesterol biosynthesis was identified as a new resistance mechanism in response to archazolid B treatment. Validation experiments were carried out on two different cancer types, bladder cancer and glioblastoma.

*Omic*s analysis performed on T24 bladder cancer cells indicated drastic disturbances in cholesterol homeostasis, affecting cholesterol biosynthesis, uptake and transport upon archazolid B treatment. This was confirmed by several experiments, revealing accumulation of free cholesterol in intracellular compartments, SREBP-2 activation and enhanced expression of cholesterol biosynthesis genes. In addition to that, archazolid B led to LDL uptake inhibition and decreased LDLR surface expression, thus severely affecting extracellular cholesterol supply. The importance of cholesterol biosynthesis for cell survival was successfully validated combining archazolid B with fluvastatin, an HMGCR inhibitor, leading to reduced levels of free cholesterol and diminished cell survival.

Gene expression profiles of U87MG and EGFR mutated U87MG.ΔEGFR cells treated with archazolid B displayed the same alterations in cholesterol homeostasis found in T24 cells and accumulation of free cholesterol was observed likewise. Although deregulations affecting cholesterol occurred to the same extent in both glioblastoma cell lines under archazolid B treatment, basic expression of cholesterol-associated genes was found to be elevated in U87MG.ΔEGFR cells, probably contributing to increased archazolid B resistance compared to wild-type cells.

4 Discussion

4.1 Role of established resistance mechanisms

4.1.1 Cytotoxicity of archazolid B towards tumor and non-tumor cells

The efficacy and specificity of archazolid B in the context of chemotherapy was investigated by comparing cytotoxicity of the drug towards tumor cells from different origin (breast, blood, colon, liver) to non-tumorous pendants. Normal breast and liver cells were considerably more resistant to breast cancer and liver cancer cells. Normal colon cells and peripheral mononuclear blood cells, however, were only weakly resistant or sensitive compared to colon cancer and leukemia cells indicating that archazolid B might also exert toxic effects against hematopoietic and colon tissues in the clinical setting.

The deregulation of pH in cancer cells and in their environment is closely related to tumor proliferation, migration and invasion [51]. Archazolid B, as a potent inhibitor of the V-ATPase proton pump, displayed cytotoxicity on all tested cancer cells in the low nanomolar range confirming its potential as a novel and promising anticancer drug. Compared to normal cells, cancer cells often overexpress distinct subunits of V-ATPase or display different splice variants [53]. Especially V-ATPase subunit c, the subunit targeted by archazolid B, has been related to proliferation and metastasis [142]. It can be surmised that enhanced subunit c expression in the tested breast and liver cancer cells, compared to their non-cancerous pendants, likely contributes to greater efficacy of archazolid B. Determination of V-ATPase subunit c expression would therefore be a valuable tool to estimate the response of different tumor types to archazolid B.

Kinetic studies on cytotoxicity of archazolid B and doxorubicin towards T24 cells revealed a clear time-dependency in case of archazolid B. So, a drastic decrease in cell viability was only observed after 72 h incubation with the drug. This result is in accordance with previous experiments performed with the drug on SKBR3 breast cancer cells [62]. In contrast to the DNA-intercalating drug doxorubicin, archazolid B does not cause an instant stop in DNA replication. It can be rather surmised that inhibition of the V-ATPase by archazolid B progressively disturbs cellular functions due to impaired pH regulation, finally resulting in cell death. Furthermore it is quite likely that the cells exert possible resistance mechanisms towards archazolid B that maintain cell survival over long incubation times.

4.1.2 Archazolid B and ABC transporters

Archazolid B exhibited different effects on ABC transporters: ABCB1 (P-gp)- and ABCG2 (BCRP)-expressing cells revealed resistance towards the drug, whereas ABCB5-expressing cells showed hypersensitivity. In general, the interaction of archazolid B with ABC transporters is quite reasonable. Archazolid B possesses strong hydrophobic qualities displaying a partition coefficient (logP value) of 7.1 (PubChem database; <http://pubchem.ncbi.nlm.nih.gov>). As already mentioned, archazolids bind to V-ATPase subunit c, which is part of the proteolipid ring buried within the membrane [60, 61]. Similar to this, drug binding sites of ABC transporters are also located intramembranous [143].

Experiments on the leukemic CEM/ADR5000 cell line identified archazolid B as a possible substrate of P-gp. This result is consistent with earlier experiments on P-gp expressing KB-V1 cervix carcinoma cells showing that verapamil reverses resistance towards archazolid B, concanamycin A and bafilomycin [37]. Transport by P-gp is an unwanted feature of drugs leading to reduced levels of chemotherapeutics within the cell. However, it is to note that resistance of P-gp expressing cells towards archazolid B (40-fold) was rather low in contrast to doxorubicin (600-fold). Comparing archazolid B to other cytotoxic drugs (vincristine, docetaxel, epirubicin) on CEM/ADR5000 cells also confirmed the resistance index to be in the lower range [144]. Molecular docking predicted a probable binding of archazolid B to P-gp at the same site as verapamil. However, the drug did not exert modulatory effects on the P-gp-mediated efflux of doxorubicin, since it failed to reverse its resistance in CEM/ADR5000 cells. One possible explanation for the different effects of archazolid B and verapamil on doxorubicin transport is provided by the flippase model of P-gp, which is based on the assumption that a substrate is transported (flipped) from the inner leaflet to the outer leaflet of the membrane or to the external medium resulting in a concentration gradient [145]. Crucial for this gradient formation is the equilibration rate of a substance across the lipid bilayers. Chemosensitizers (like verapamil) have been reported to rapidly diffuse back into the cell, whereas the equilibration of substrates is slow enough to form a concentration gradient [131]. It can be surmised that verapamil is able to reverse doxorubicin resistance, since P-gp is busy in the futile cycle of verapamil transport and hence not being able to extrude doxorubicin. In case of archazolid B, however, the equilibration may be rather slow, so that P-gp is still able to transport doxorubicin.

BCRP-expressing MDA-MB-231 cells only displayed a resistance index of 1.9, indicating a weak interplay of archazolid B with this transporter. This may be explained by structural and

sequential differences between ABC transporters that influence the transporter-drug interaction. Sustaining this hypothesis, experiments with P-gp and BCRP have shown that even single amino acid substitutions have a great impact on substrate specificity [72, 146].

In contrast to P-gp- and BCRP-mediated resistance towards archazolid B, HEK231 cells, expressing the ABCB5 transporter, showed increased sensitivity towards the drug. Hypersensitivity (also termed collateral sensitivity) of multidrug-resistant cells towards V-ATPase inhibitors has been previously reported [103, 105]. Multidrug-resistant cells often overexpress V-ATPase subunits and expression levels are correlated with increased cytotoxicity towards V-ATPase inhibitors [105, 147]. In case of ABCB5, it can be surmised that collateral sensitivity may not be conferred by the drug transporter itself, but by targeting abundantly expressed V-ATPase in these cells by archazolid B. However, an interaction with ABCB5 cannot be completely excluded and clarification by future experiments is necessary.

4.1.3 Role of tumor suppressor p53 and oncogene EGFR

Loss of tumor suppressor function as well as activation of oncogenes are known to contribute effectively to drug resistance [148]. Therefore, the influence of the tumor suppressor p53 and the oncogene EGFR in the cellular response towards archazolid B was investigated.

The central role of the tumor suppressor p53 is underlined by the fact that the encoding gene *TP53* is mutated in about 50% of all human cancers and that *TP53* mutations can cause resistance to chemo- and radiotherapy [86, 87]. P53 is usually activated in response to various cellular events including DNA damage, hypoxia, viral infection or oncogene activation [85]. However, our data displayed similar cytotoxicity in p53 wild-type and knockout cells, indicating that archazolid B sensitivity or resistance is independent of the p53 status of the cell. It has been previously reported that inactivation of p53 leads to enhanced resistance to doxorubicin, cisplatin, angiogenesis inhibitors and other anticancer drugs [149-151]. Considering the fact that p53 knockout cells are not resistant to archazolid B opens the possibility to treat otherwise drug-resistant p53-mutated tumor cells with archazolid B.

The influence of archazolid B on EGFR signaling was investigated using glioblastoma cells expressing EGFR wild-type and constitutively active EGFR (EGFRvIII mutation). Drug resistance conferred by this mutation is not only limited to kinase inhibitors, but has also been reported for drugs with a completely different mode of action, such as cisplatin [101]. In our

study, cells expressing the EGFRvIII mutant displayed a 10-fold higher archazolid B resistance and showed survival of twice as much cells compared to the wild-type. In SKBR3 breast cancer cells, treatment of cells with archazolid has been shown to affect EGFR internalization and localization and led to reduced duration of Akt signaling [63]. Akt signaling is important for several cellular processes including proliferation and survival [152]. In general, the EGFR mutant displays a slower internalization compared to EGFR wild-type [153]. It is quite likely that signaling through the EGFR mutant is less affected by archazolid B treatment, thus leading to increased cell survival.

Contribution to cell survival by activation of SREBP-1 via the EGFR/PI3K/Akt pathway is discussed in 4.2.2.

4.1.4 MCF-7ArchB cells and acquired resistance mechanisms

The acquirement of cellular resistance mechanisms towards anticancer drugs constitutes a severe problem and often results in loss of effectiveness or complete failure of chemotherapy. Therefore, in addition to direct cellular responses to archazolid B, the induction of resistance mechanisms after repeated drug treatment was investigated. MCF-7ArchB cells displayed a 2.7-fold higher resistance towards the drug compared to MCF-7 control cells. Interestingly, it was not possible to further increase drug resistance by the use of the mutagen EMS. Similar resistance indices have also been reported for MCF-7 cells resistant to doxorubicin (16-fold) and cisplatin (4-fold) [154]. Compared to these common chemotherapeutics, however, the low resistance index of archazolid B is quite favorable and qualifies the drug as a promising therapeutic agent. Investigating the underlying mechanisms, acquired resistance to archazolid B turned out not to be conferred by aberrant expression or DNA mutations of the gene encoding V-ATPase subunit c, the direct target of archazolids. Instead, long-term treatment with archazolid B led to a slight increase of *ABCB1*, encoding P-gp, and a significant overexpression of *EGFR* as well as reduced proliferation. Since archazolid B was confirmed to be effluxed by P-gp, overexpression of this transporter would further decrease the amount of intracellular archazolid B thus contributing to drug resistance. The up-regulation of *EGFR* is likely a consequence of affected EGFR internalization and impaired Akt signaling caused by archazolid B. However, it is not clear to which extent this survival attempt really contributes to drug resistance. Enhanced proliferation and cell growth is often due to metabolic reprogramming of cancer cells [107]. Archazolid B has been reported to cause energy stress and disturb glucose

metabolism [62]. Furthermore, the influence of archazolid B on cholesterol homeostasis is discussed in 4.2. Reduced proliferation, as observed under long-term treatment with archazolid B, may therefore be a result of metabolic adaption of the cells to guarantee cell survival.

4.2 Cholesterol synthesis as a new resistance mechanism

4.2.1 Accumulation of free cholesterol

Staining of T24 bladder cancer and U87MG.ΔEGFR glioblastoma cells with filipin showed that treatment with archazolid B led to an accumulation of free cholesterol within intracellular compartments. Free cholesterol is unesterified cholesterol, generated e.g. by hydrolysis of LDL cholesterol esters in lysosomes [155]. The staining pattern resembled the one observed in NPC1-null CHO (Chinese hamster ovary) cells [156]. NPC1, an integral membrane protein, is responsible for the transport of cholesterol out of late endosomes/lysosomes to the plasma membrane and to the endoplasmic reticulum [157]. In 90-95% of NPC cases, the NPC1 gene is mutated leading to accumulation of extensive amounts of free cholesterol within late endosomes and lysosomes [158]. Archazolid B likely causes a failure of cholesterol export – not by mutation, but rather by disturbance of transport systems resulting from V-ATPase inhibition as already surmised for the inhibitor bafilomycin A₁ [159]. Blockage of V-ATPase action by archazolid B prevents acidification resulting in elevated lysosomal pH levels [37]. The lysosomal NPC1 protein utilizes proton motive forces for effluxing molecules [160]. Accordingly, NPC1 would likely be a candidate protein affected by V-ATPase function [161].

In addition to LDL-derived cholesterol, plasma membrane-derived cholesterol may also get trapped in endosomes/lysosomes due to disturbances in cholesterol recycling caused by V-ATPase inhibition [162]. The contribution of the different cholesterol sources to total levels of free cholesterol are discussed in 4.2.4.

4.2.2 Up-regulation of cholesterol-associated genes

Omics data revealed a remarkable increase of cholesterol-associated genes upon archazolid B treatment. 18 of these genes were deregulated in both, bladder cancer and glioblastoma cells. Especially genes involved in cholesterol biosynthesis and uptake displayed a clear up-

regulation. These results are in agreement with previous gene expression studies performed on the V-ATPase inhibitor bafilomycin A [163]. The main sources of cellular cholesterol involve uptake of extracellular LDL particles and endogenous cholesterol biosynthesis [164]. Cholesterol homeostasis is controlled by the action of SREBPs and LXR transcription factor [113]. Our data showed that in T24 cells 16 out of 20 cholesterol-associated genes were known targets of SREBPs [165, 166]. For glioblastoma cells, this was the case for 14 out of 21 cholesterol-associated genes. Two genes, *SREBF-1* and *SREBF-2*, encode three different proteins, SREBP-1a, SREBP-1c and SREBP-2 [167]. Although target genes of SREBPs display a vast overlap, SREBP-1 seems to be preferentially involved in fatty acid metabolism and lipogenesis, whereas SREBP-2 favors target genes important for cholesterol biosynthesis and homeostasis [168]. This is in accordance with our Western Blot results showing enhanced nuclear accumulation of SREBP-2, but not of SREBP-1, after 2 h treatment of T24 cells with archazolid B. The drastic decrease of nuclear SREBP-2 after 24 h treatment can be explained by negative feedback control. This is supported by the fact that INSIG1 is amongst the top up-regulated genes after 24 h treatment with archazolid B in T24 but also in U87MG and U87MG.ΔEGFR cells. INSIG1 is a negative regulator of SREBPs, preventing their processing by mediating their retention in the endoplasmic reticulum [137]. Comparing 24 h and 48 h microarrays of glioblastoma cells, only a slight decrease in cholesterol-associated gene expression was observed, stressing the importance of cholesterol response under archazolid B treatment.

In addition to regulation of cholesterol homeostasis by SREBPs, our data also pointed to an impaired activation of LXR upon archazolid B treatment. So, T24 as well as U87MG.ΔEGFR displayed clear down-regulation of the gene encoding the LDLR degrader MYLIP. In addition to that, *ABCA1*, encoding a cholesterol transporter, was down-regulated in both glioblastoma cell lines indicating that the cells try to prevent cholesterol export.

Taken together, the response of bladder cancer and glioblastoma cells to archazolid B treatment involves genes responsive to lowered cholesterol levels. These decreased cholesterol levels are likely due to accumulation of free cholesterol in lysosomes. This result is in accordance with NPC-deficient cells which reveal enhanced cholesterol biosynthesis and LDL uptake, since cholesterol cannot reach the endoplasmic reticulum for regulation of homeostasis [169].

Archazolid B disturbed cholesterol homeostasis in both glioblastoma cell lines to about the same extent. However, U87MG.ΔEGFR cells displayed a 10-fold higher resistance towards the drug and showed survival of twice as much cells compared to the wild-type. Obviously, the

mutant cell line exhibits features that contribute to the effectiveness of archazolid B. Gene expression analysis of control samples, not treated with archazolid B, revealed significant up-regulation of 15 cholesterol-associated genes in the EGFR mutant, including 11 genes of the cholesterol biosynthetic pathway as well as *LDLR*, *ACAT2*, *INSIG1* and *SREBF1* and *ABCA1*. Increased HMGCR expression or LDL-binding and expression compared to normal brain tissue have been shown for certain GBMs [170]. In particular, EGFR signaling through PI3K and Akt was reported to be hyper-activated and of great importance in GBMs bearing EGFRvIII mutation [171]. In accordance to that, U87MG.ΔEGFR cells displayed enhanced expression of genes involved in EGFR/PI3K/Akt signaling. The EGFR/PI3K/Akt pathway is closely related to cholesterol, since its activation leads to cleavage and nuclear translocation of SREBP-1 [172, 173]. Especially the uptake of extracellular cholesterol is essential for GBMs and the EGFRvIII mutant has been shown to obtain sufficient amounts of cholesterol by stimulating LDLR expression through hyper-activation of the PI3K/Akt/SREBP-1 pathway [174]. Our microarray data from control samples are in accordance with this finding displaying 11 out of 15 up-regulated genes in U87MG.ΔEGFR cells under SREBP-1 control, including *LDLR* and *SREBF1*. It is quite likely that due to enhanced cholesterol metabolism of U87MG.ΔEGFR cells, these cells may have a greater survival advantage after archazolid B treatment. Considering enhanced SREBP-1 activation and *SREBF-1* expression, it is possible that cholesterol responses evoked by archazolid B are exerted earlier and more efficiently in the mutant cell line.

4.2.3 LDL uptake and LDLR surface expression

Beside the influence of archazolid B on cholesterol biosynthesis, *omics* data indicated disturbances in clathrin-mediated endocytosis. LDL uptake is known to be carried out by clathrin-mediated endocytosis [112]. Indeed, uptake experiments showed that cells pretreated with archazolid B for 24 h were not able to internalize LDL particles any longer. This finding is in accordance with previous experiments showing that transferrin uptake, which is also clathrin-mediated, was progressively abrogated by archazolid B within 24 h [63, 64]. Impaired uptake may be explained by the recent finding that V-ATPase inhibition disturbs clathrin-mediated endocytosis due to failure of cholesterol recycling from non-acidified endosomes thus leading to formation of non-constricted clathrin-coated structures at the plasma membrane [162]. According to this, cholesterol itself represents the limiting factor for cholesterol uptake. In the context of recycling disturbances, we also observed reduced LDLR surface expression

after 24 h treatment with archazolid B. Experiments with concanamycin A and bafilomycin A₁ showed that V-ATPase inhibition disturbs receptor recycling processes causing a decrease in receptor surface expression [175, 176]. Furthermore, archazolid itself has been reported to affect the HER2 receptor in the same way [177]. Thus, under archazolid B treatment, external cholesterol supply is lost on the one hand by progressive LDL uptake inhibition and on the other hand by impaired recycling of internalized LDLR.

Cholesterol uptake is closely related to cancer. So high dietary cholesterol correlates with the risk of numerous cancer types, including stomach, colon, rectum, pancreas, lung, breast, kidney and bladder cancer [119, 178]. A recent study with 876 patients suffering from renal cell carcinoma revealed that low preoperative serum cholesterol levels are associated with worse survival [179]. The determination of serum cholesterol as an independent prognostic factor has therefore been claimed as a meaningful adjunct in clinical practice [179].

4.2.4 Free cholesterol levels under archazolid B treatment

Filipin staining of T24 cells displayed impaired levels of free cholesterol within the first 24 h of treatment with archazolid B. This lack of cholesterol is likely caused by progressive abrogation of LDL uptake within this time span. In case of U87MG.ΔEGFR cells, however, free cholesterol levels were even higher than in control cells after 24 h treatment. Since microarray data revealed an aberrant expression of cholesterol-associated genes in this cell line, it can be surmised that U87MG.ΔEGFR cells are able to exert a faster response to archazolid B induced cholesterol shortage. Thus, in contrast to T24 cells, an earlier compensation of free cholesterol levels is possible. Long-time exposure of both cell lines to archazolid B continuously increased cholesterol accumulation, even though LDL uptake was abolished after 24 h drug treatment. A possible explanation might be that the number of LDL receptors is increased due to SREBP activation and that clathrin-mediated endocytosis is partly rescued by newly synthesized cholesterol resulting from enhanced cholesterol biosynthesis. This newly synthesized cholesterol may then also get trapped by the endocytotic pathway and contribute to cholesterol accumulation [180]. However, even if LDL uptake is partly restored, LDL hydrolysis at high pH is rather unlikely [181]. Nevertheless, LDL-derived cholesterol remains trapped within lysosomes due to failure of cholesterol transport. Therefore, it can be surmised that cholesterol biosynthesis is the main source of cholesterol in archazolid B-treated cells and consequently a critical factor of cell survival.

4.2.5 Combination of archazolid B with fluvastatin

Identification of cholesterol biosynthesis as a target for cancer therapy has revealed a new role for statins, originally developed to treat hypercholesterolemia [129]. Especially combinations of statins with common anticancer drugs like doxorubicin, cisplatin and 5-fluoruracil bear immense potential by displaying synergistic and drug potentiating effects [182]. In accordance to that, combination of archazolid B with the HMGCR inhibitor fluvastatin significantly decreased intracellular free cholesterol levels in T24 cells which correlated with clearly reduced cell viability. It is noteworthy that fluvastatin only displayed an impact when effective doses of archazolid B were used. Therefore, it can be assumed that at high archazolid B concentrations cells are dependent on newly-synthesized cholesterol due to failure of the endocytotic system. *In vitro* experiments with U87MG and U87MG.ΔEGFR cells and the HMGCR inhibitor atorvastatin in lipoprotein-deficient serum have shown that statin treatment led to significant inhibition of cell growth [174]. *In vivo*, however, an LDL-free tumor environment is difficult to achieve. Here, therapeutic strategies might profit from the fact that archazolid B retains LDL cholesterol in lysosomes, thus, imitating the absence of extracellular cholesterol. Assuming that cholesterol biosynthesis represents a critical factor of cell survival, the combination of archazolid B with statins might be a promising approach in cancer treatment that is worth investigating in more detail in future studies.

4.3 Side effects of archazolid B on normal tissue

A basic principle of cancer chemotherapy is that drugs preferentially exert their detrimental effects to the tumor compared to the normal organs. The experience in clinical oncology, however, is that cancer chemotherapy frequently causes severe side effects including myelosuppression, gastrointestinal damage, hair loss, vomiting, nausea and fever [14]. Some cytotoxic drugs also lead to damage of specific organs (e.g. nephrotoxicity – cisplatin, cardiotoxicity – doxorubicin, daunorubicin). Furthermore, neurotoxicity has been reported for *Vinca* alkaloids and taxanes as well as for the myxobacterial class of epothilones [14, 183]. In case of myxobacteria-derived tubulysins, recent studies on mouse models displayed side effects comprising weight loss as well as abdominal swelling [184]. Our *in vitro* data showed that normal colon cells and peripheral mononuclear blood cells were weakly resistant or sensitive to archazolid B in comparison with colon cancer and leukemia cells, respectively. These results indicate that archazolid B might therefore cause myelosuppression and exert toxic effects

against hematopoietic and colon tissue *in vivo*. This aspect should be born in mind, if archazolid B would enter clinical Phase I trials. The target of archazolid B, the V-ATPase, is located in the membrane of intracellular compartments playing an important role in endocytotic processes [43]. Expressed in the plasma membrane, this proton pump also plays a fundamental role in some specialized cells including osteoclasts, renal intercalated cells and macrophages [43]. Loss of V-ATPase function, as it may also occur by archazolid B treatment, is related to osteopetrosis (overproduction of bone), distal renal tubular acidosis and impairment of macrophage activity [50, 185-187].

In the present thesis, archazolid B has been shown to drastically disturb cholesterol homeostasis. Cholesterol is a major component of the brain, which contains about 25% of the body's total cholesterol [188]. Similar to NPC-deficient cells, archazolid B led to accumulation of free cholesterol in lysosomes. Aberrant cholesterol storage as it is present in NPC disease is known to cause progressive neurodegeneration and massive loss of nerve cells leading to premature death and dementia [189, 190]. However, there are main differences between NPC disease and archazolid B treatment. In NPC-disease, cholesterol trafficking is originally impaired by mutation of NPC genes [158]. In contrast to that archazolid B is only harmful when it is directly taken up by cells. Regarding the brain, the blood brain barrier represents an effective prevention from circulating agents [191]. Though archazolid B is quite lipophilic it can be surmised that a passage is not possible due to its molecular weight. Another difference is that the uptake of LDL cholesterol is not impaired in NPC-deficient cells, whereas inhibition of the V-ATPase inhibits the whole endocytotic system. With regards to the capillary system, the inhibition of LDL uptake by archazolid B may therefore lead to elevated serum cholesterol levels, which are known to contribute to atherosclerosis [192].

In vivo studies with V-ATPase inhibitors are rare due to their high toxicity [57]. Yet, first experiments with intravenous application of archazolid in mice showed that a dosage of 1 mg/kg was quite tolerable [63]. Furthermore even an injection of 3 mg archazolid A/kg did not cause acute toxicity [193]. The evaluation of limiting dosages as well as the precise documentation of side effects should be included in oncoming experiments to elucidate the suitability of archazolid B for clinical application.

5 Summary and Conclusion

In this study, the novel V-ATPase inhibitor archazolid B was investigated in regard to resistance of cancer cells against chemotherapy. In addition to the evaluation of classical intrinsic as well as acquired resistance mechanisms relevant in the cellular response to archazolid B, cholesterol biosynthesis was identified as a new defense mechanism evoked by the drug.

Cell viability assays revealed the high anticancer potential of archazolid B. The drug displayed cytotoxicity in the low nanomolar range on a panel of different cancer cell types, including breast, blood, colon and liver. Except for blood cells, archazolid B showed enhanced cytotoxic activity against all cancerous cells compared to their non-cancerous pendants. Although archazolid B turned out to be a substrate of the drug-efflux mediating ABC-transporters ABCB1 (P-gp) and ABCG2 (BCRP), the degree of resistance was rather low compared to other classical anticancer drugs. Furthermore, in case of ABCB5, archazolid B even caused hypersensitivity. Archazolid B exerted its detrimental effects independent of the cellular p53 tumor suppressor status. This fact constitutes a great advantage and provides the possibility to treat drug-resistant p53-mutated tumors with archazolid B. However, experiments on cells expressing constitutively active EGFR displayed significantly increased resistance towards archazolid B. This result indicates that a therapeutic outcome of archazolid B on tumors expressing this EGFRvIII mutant (e.g. GBMs) will not be favorable.

Acquired drug resistance was studied by establishing an archazolid B-resistant MCF-7 cell line. Though it was possible to induce resistance to archazolid B, the resistance index remained low and stable over the whole experimental period and was irresponsive to additional treatment with the mutagen EMS. Gene expression analysis revealed that acquired archazolid B resistance may result from slight *ABCB1* and significant *EGFR* overexpression. Moreover, growth kinetic curves tend to exhibit a decreased proliferation. In contrast to that, a contribution of the direct target of archazolid B, the V-ATPase subunit c, could be excluded, showing neither aberrant expression nor mutation of the encoding gene.

In addition to classical resistance mechanisms, the identification of new resistance strategies exerted by cells in response to archazolid B was a further aim of this thesis. Analysis of *omics* data revealed that archazolid B severely disturbs cholesterol homeostasis in T24 bladder cancer cells, affecting cholesterol biosynthesis, clathrin-mediated LDL uptake and cholesterol transport. Similar deregulation of cholesterol-associated genes was also identified in glioblastoma cells. Figure 44 displays a model for disturbances in cholesterol homeostasis

caused by archazolid B. Inhibition of the V-ATPase by archazolid B results in impaired acidification of endosomal/lysosomal compartments thus disturbing clathrin-mediated endocytosis and receptor recycling. This was validated by experiments showing that archazolid B inhibits LDL uptake and impairs LDLR surface expression. Due to disturbance of the proton gradient, which is likely affecting NPC1, transport of free cholesterol out of lysosomes is inhibited. The lysosomal sequestration of free cholesterol, as shown by filipin staining in bladder and glioblastoma cells, results in low cytosolic cholesterol/oxysterol levels. As a consequence, SREBP-2 processing, validated by Western Blot, and impaired LXR activation mediate cell survival by re-elevation of intracellular cholesterol levels. In case of EGFRvIII mutant glioblastoma cells, this cholesterol response is believed to be enhanced by additional SREBP-1 activation via the EGFR/PI3K/Akt pathway and thus likely contributing to increased cell survival compared to EGFR wild-type cells. Archazolid B inhibits the whole pathway of extracellular cholesterol uptake, thus imitating an LDL-free tumor environment. As a consequence, cells are highly dependent on cholesterol supply via the cholesterol biosynthetic pathway. This was proven by the fact that under archazolid B treatment, total free cholesterol levels as well as cell survival can be significantly reduced by inhibiting HMGCR with fluvastatin. The combination of archazolid B with statins may therefore be an attractive strategy to circumvent the defense mechanism of cholesterol synthesis, thus potentiating the promising anticancer effects of archazolid B.

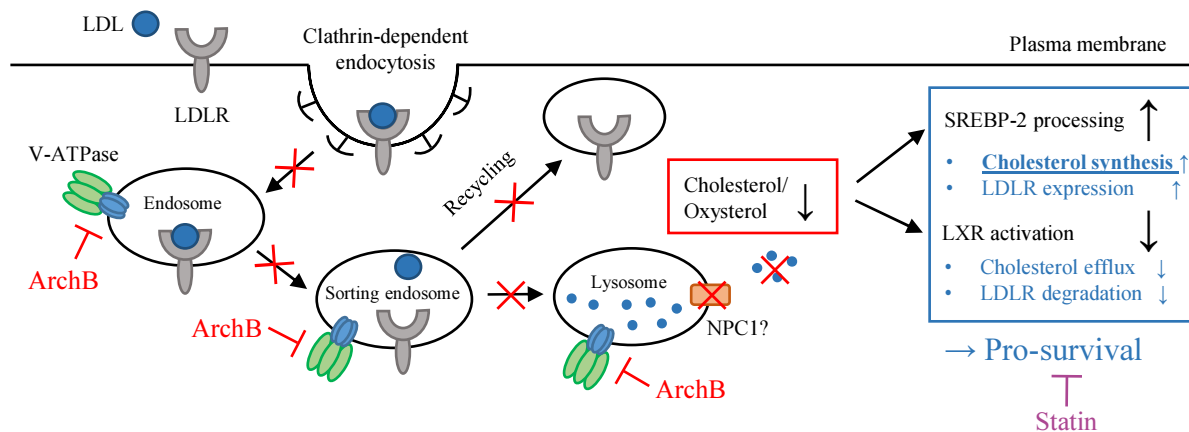


Figure 44: Model for disturbances in cholesterol homeostasis caused by archazolid B. Inhibition of the V-ATPase by archazolid B (archB) results in impaired acidification of endosomal/lysosomal compartments thus disturbing clathrin-mediated endocytosis and recycling of the LDLR receptor. Transport of free cholesterol out of lysosomes is inhibited (due to proton gradient dependency of NPC1?) leading to its lysosomal sequestration and low cytosolic cholesterol/oxysterol levels. As a consequence, SREBP-2 processing and impaired LXR activation mediate cell survival by re-elevation of intracellular cholesterol levels. The central role of cholesterol biosynthesis is displayed by the fact that cell survival after archazolid B treatment can be clearly reduced by inhibiting HMGCR, the key enzyme of this pathway, with a statin.

6 Material and Methods

6.1 Chemicals and equipment

Archazolid B

Archazolid B was provided by Dr. [REDACTED] (Department of Pharmaceutical Biotechnology, Saarland University, Germany), Dr. [REDACTED] (Department of Pharmacy, University of Munich, Germany) and Dr. [REDACTED] (Department of Organic Chemistry, University of Bonn, Germany). Aliquots dissolved in DMSO at concentration of 100 μ M were stored at -20 °C for up to two month. The DMSO content in each experiment did not exceed 1%.

Cell culture media, reagents and disposable material

Table 11: Cell culture media, reagents and disposable material

Product	Producer
6-well cell culture microplate, clear, Nunclon®	Thermo Scientific, Germany
96-well cell culture microplate, clear, Nunclon®	Thermo Scientific, Germany
Cell culture flasks (25 cm ²), Nunclon®	Thermo Scientific, Germany
Cell culture flasks (75 cm ²), Nunclon®	Thermo Scientific, Germany
Cell culture flasks (175 cm ²), Nunclon®	Thermo Scientific, Germany
Cell scraper	Greiner Bio-One, Germany
Centrifuge tube (15 ml)	Sarstedt, Germany
Centrifuge tube (50 ml)	Sarstedt, Germany
Cover Glass 24 × 32 mm	VWR International, Austria
DMEM, High Glucose, GlutaMAX™, pyruvate	Life Technologies, Germany
DPBS, no calcium, no magnesium	Life Technologies, Germany
FACS tubes	BD Biosciences, USA; Sarstedt, Germany
FACS tubes with cell strainer cap	BD Biosciences, USA
Fetal Bovine Serum (FBS)	Life Technologies, Germany
G418 disulfate salt	Sigma-Aldrich, Germany
ibiTreat, μ -Slide 8 well, tissue culture treated, sterile	Ibidi, Germany
Mammary Epithelial Cell Growth Medium (Ready-to-use)	PromoCell, Germany
Micro tubes (1.5 mL, 2.0 mL)	Sarstedt, Germany
McCoy's 5A (Modified) Medium, HEPES	Life Technologies, Germany
Multiply® PCR cup, 0.5 mL, PP	Sarstedt, Germany
Panserin 413	PAN-Biotech, Germany
PCR plates (384-well)	Axon Labortechnik, Germany
PCR plate sealing foils	Axon Labortechnik, Germany

Penicillin (10000 U/mL)/Streptomycin (10000 µg/mL)	Life Technologies, Germany
Phytohemagglutinin M form	Life Technologies, Germany
Roti® PVDF blot membrane (0.45 µm)	Roth, Germany
RPMI 1640	Life Technologies, Germany
Superfrost™ Plus Adhesion Microscope Slides	Thermo Scientific, Germany
Trypsin-EDTA 0.25% (1×), phenol red	Life Technologies, Germany
Zeocin	InvivoGen, CA, USA

Chemicals, dyes, enzymes and kits

Table 12: Chemicals, dyes, antibodies, enzymes and kits

Product	Producer
30% acrylamide/bis solution 29:1	Bio-Rad, Germany
4-(2-hydroxyethyl)-1-piperazineethanesulfonic acid (HEPES)	Sigma-Aldrich, MO, USA
40% acrylamide/bis-acrylamide (37.5:1) solution	Sigma-Aldrich, MO, USA
5 × Hot Start Taq EvaGreen qPCR Mix (no ROX)	Axon Labortechnik, Germany
Acetone ultrapure	AppliChem, Germany
Acetonitrile (ACN)	J. T. Baker Chemicals, NJ, USA
Alexa Fluor® 488 Goat Anti-Mouse IgG (H+L) Antibody	Life Technologies, Germany
Ammonium hydroxide	Sigma-Aldrich, MO, USA
Ammonium persulfate (APS)	Sigma-Aldrich, MO, USA
Anti-SREBP1 antibody (ab28481)	Abcam, UK
Anti-SREBP2 antibody (ab30682)	Abcam, UK
Biotin-16-UTP	Roche, Germany
BODIPY® FL LDL	Life Technologies, Germany
Bovine beta casein	Sigma-Aldrich, MO, USA
Bovine serum albumin (BSA)	Sigma-Aldrich, MO, USA
Bromophenol Blue	Merck, Germany
CellMask™ Orange Plasma Membrane Stain	Life Technologies, Germany
cOmplete Mini protease inhibitor cocktail	Roche, Germany
Cy3-streptavidin	GE Healthcare, UK
Dimethyl sulfoxide (DMSO)	Sigma-Aldrich, Germany
Doxorubicin	JGU Medical Center, Germany
Ethyl methanesulfonate (EMS)	Sigma-Aldrich, Germany
Ethanol (EtOH)	Sigma-Aldrich, Germany
Filipin complex from <i>Streptomyces filipinensis</i>	Sigma-Aldrich, MO, USA
Fluvastatin sodium hydrate	Sigma-Aldrich, Germany
Formaldehyde (37% solution in H ₂ O)	Sigma-Aldrich, MO, USA
Formaldehyde-13C, d2 (20% solution in D ₂ O)	Sigma-Aldrich, MO, USA
Formic acid (FA)	Sigma-Aldrich, MO, USA

Glycerol	AppliChem, Germany
Glycine	AppliChem, Germany
Halt™ Protease Inhibitor Cocktail, EDTA-free (100 x)	Thermo Scientific, IL, USA
Histone H3 antibody	Cell Signaling, UK
Histopaque®	Sigma-Aldrich, MO, USA
HRP-linked anti-rabbit IgG	Cell Signaling, UK
HumanHT-12 v3 Expression BeadChip Kit	Illumina Inc., CA, USA
HumanHT-12 v4 Expression BeadChip Kit	Illumina Inc., CA, USA
Hydrochloric Acid 37% (HCl)	AppliChem, Germany
Ibidi Mounting Medium	Ibidi, Germany
Illumina® TotalPrep™ RNA Amplification Kit	Life Technologies, Germany
InviTrap® Spin Universal RNA Mini kit	STRATEC Biomedical, Germany
LDLR (C7) mouse monoclonal antibody (sc-18823)	Santa Cruz, Germany
Luminata™ Classico Western HRP substrate	Merck Millipore, MA, USA
MagicMark™ XP Western Standard	Life Technologies, CA, USA
M-PER® Mammalian Protein Extraction Reagent	Thermo Scientific, IL, USA
MessageAmp™ II aRNA Amplification Kit	Life Technologies, Germany
Methanol	J. T. Baker, NJ, USA
MicroRNA Expression Profiling Reagent Kit for BeadChips	Illumina Inc., CA, USA
miRNeasy Kit	Qiagen, Germany
NE-PER® Nuclear and Cytoplasmic Extraction Reagents (Kit)	Thermo Scientific, IL, USA
Paraformaldehyde (PFA)	Roth, Germany
Phenazine methosulfate (PMS)	Sigma-Aldrich, Germany
Phusion® High-Fidelity PCR Master Mix with GC Buffer	Thermo Scientific, Germany
QIAquick PCR Purification Kit	Qiagen, Germany
RevertAid H Minus First Strand cDNA Synthesis Kit	Thermo Scientific, Germany
RNeasy Kit	Qiagen, Germany
S-methyl methanethiosulfonate (MMTS)	Sigma-Aldrich, MO, USA
Small RNA Nano chip assay	Agilent Technologies, Germany
Sodium bicarbonate	Sigma-Aldrich, MO, USA
Sodium chloride	Grüssing, Germany
Sodium cyanoborohydride	Sigma-Aldrich, MO, USA
Sodium dodecyl sulfate (SDS)	J. T. Baker, NJ, USA
Tetramethylethylenediamine (TEMED)	Sigma-Aldrich, MO, USA
Total RNA Nano chip assay	Agilent Technologies, Germany
Triethylammonium bicarbonate (TEABC)	Sigma-Aldrich, MO, USA
Trifluoroacetic acid (TFA)	Sigma-Aldrich, MO, USA
Tris (hydroxymethyl) aminomethane (Tris)	AppliChem, Germany
Tris (2-carboxyethyl) phosphine hydrochloride (TCEP)	Sigma-Aldrich, MO, USA
Triton X-100	Sigma-Aldrich, MO, USA
Trypsin (modified, sequencing grade)	Promega, WI, USA
Tween20	Sigma-Aldrich, Germany

Water, nuclease-free	Thermo Scientific, Germany
XTT sodium salt	MP Biomedicals, Germany
XTT sodium salt	Sigma-Aldrich, Germany
β -Mercaptoethanol	AppliChem, Germany
(\pm)-verapamil hydrochloride	Sigma-Aldrich, Germany

Technical equipment and software

Table 13: Technical equipment and software

Device	Producer
Adobe Photoshop CS5 v 12.0.0.2	Adobe Systems, USA
Agilent 2100 Bioanalyzer	Agilent Technologies GmbH, Germany
AlphaView™ Q	Alpha Innotech, CA, USA
AutoDock 4.2 software	Molecular Graphics Laboratory, CA, USA
AutoDockTools 1.5.6rc3 software	Molecular Graphics Laboratory, CA, USA
AutoGrid 4.2 software	Molecular Graphics Laboratory, CA, USA
BD LSRFortessa cell analyzer	BD Biosciences, CA, USA
BeadStudio software	Illumina Inc., CA, USA
BEH C18 reverse phase column (1.7 μ m, 75 μ m \times 250 mm)	Waters, MA, USA
BioFrac™ Fraction Collector	Bio-Rad Laboratories, CA, USA
Centrifuge 5424	Eppendorf, Germany
C1000™ Thermal Cycler	Bio-Rad, Germany
CFX384™ Real-Time PCR Detection System	Bio-Rad, Germany
ChemSketch	ACD, Canada
Chipster software	CSC, Finland
Coulter Counter Z1	Beckman Coulter, Germany
ENVAIR eco air V 0.8m vertical laminar flow workbench	ENVAIR, Germany
EVOS fl microscope	AMG, WA, USA
FACS Calibur Flow Cytometer	BD Biosciences, CA, USA
FlowJo software	Tree Star, USA
FluorChem® Q imaging system	Alpha Innotech, CA, USA
Forma Steri-Cult 3310 CO ₂ -Incubator	Thermo Scientific, Germany
Heraeus Fresco 21 microcentrifuge	Thermo Scientific, Germany
Heraeus Labofuge 400 R centrifuge	Thermo Scientific, Germany
Illumina Human HT-12 v4 BeadChip array	Illumina Inc., CA, USA
Illumina Human miRNA Universal-12 BeadChip array	Illumina Inc., CA, USA
Illumina Human Sentrix HT-12 v3 BeadChip array	Illumina Inc., CA, USA
Illumina BeadStation array scanner	Illumina Inc., CA, USA
ImageJ 1.4.6 software	NIH, MD, USA
Infinite M2000 Pro™ plate reader	Tecan, Germany

Ingenuity Pathway Analysis (IPA)	Ingenuity Systems Inc., CA, USA
LAS AF 2.3.5 software	Leica, Germany
Leica TCS SP5 confocal microscope	Leica, Germany
Mascot software	Matrix Science, MA, USA
Microsoft Office	Microsoft Corporation, WA, USA
Milli-Q ultrapure water purification system	Millipore, Germany
Mini-PROTEAN® Tetra Cell	Bio-Rad, Germany
MODELLER 9.11	University of California, CA, USA
NanoACQUITY UPLC System	Waters, MA, USA
NanoDrop 1000 Spectrophotometer	Thermo Scientific, Germany
Neubauer counting chamber	Marienfeld, Germany
PolySOLFOETHYL A column (200 × 2.1 mm, 5 µm, 300 Å)	PolyLC, MD, USA
Optika XDS-2 trinocular inverted microscope	Optika, Italy
REAX 2000 vortexer	Heidolph, Germany
Safe 2020 Class II Biological Safety Cabinet	Thermo Scientific, Germany
Sartorius R 160 P balance	Sartorius, Germany
Spectrafuge™ Mini Centrifuge	Labnet, Germany
SPSS Statistics version 22	IBM, NY, USA
SUB Aqua 26 waterbath	Grant Scientific, Germany
SYNAPT G2 HDMS Q-TOF Mass Spectrometer	Waters, UK
Thermomixer comfort	Eppendorf, Germany
TopMix vortexer	Fisher Scientific, Germany
Trans Proteomics Pipeline (TPP) 1 version 4.4 rev. 1	Institute for Systems Biology, WA, USA
Universal 32 R centrifuge	Hettich, Germany
Vector NTI® software	Life Technologies, Germany
VMD 1.9 software	University of Illinois at Urbana Champaign, IL, USA

6.2 Cell culture

Cells were maintained in a humidified environment at 37 °C with 5% CO₂. Sub-culturing was performed twice per week and detachment of adherent cells was achieved by treatment with 0.25% trypsin/EDTA solution (Life Technologies). High passage numbers were avoided by thawing new cell aliquots. Experiments were carried out on cells in the logarithmic growth phase. Cell counting was performed using Coulter Counter Z1 (Beckman Coulter) or a Neubauer counting chamber (Marienfeld).

6.2.1 Multidrug-resistant cell lines

Human leukemic CCRF-CEM and ABCB1 (P-gp)-expressing CEM/ADR5000 cells were kindly provided by Dr. [REDACTED] (Department for Pediatrics, University of Jena, Germany). The establishment of resistant sublines has been previously reported [194]. Cells were maintained in RPMI 1640 medium supplemented with 10% FBS and 1% penicillin (1000 U/mL)/streptomycin (100 µg/mL) (P/S) (all Life Technologies). To keep CEM/ADR5000 cells resistant, they were treated once per week with 5000 ng/mL doxorubicin (JGU Medical Center). Human breast cancer cells transduced with a control vector (MDA-MB-231-pcDNA3) or with cDNA encoding BCRP (MDA-MB-231-BCRP) were kindly provided by Dr. [REDACTED] (Department of Medicine and Greenebaum Cancer Center, University of Maryland School of Medicine, Baltimore, MD, USA), cultured in RPMI 1640 medium with 10% FBS and 1% P/S and continuously maintained in 800 ng/mL G418 disulfate salt (Sigma Aldrich). Cell lines were established according to a published protocol [195]. Human embryonic kidney cells HEK293 and the subline HEK293-ABCB5, transfected with the pCAL-MycABCB5-IRES-Zeo plasmid, were a generous gift from Prof. [REDACTED] (Faculty of Pharmacy, Keio University, Tokyo, Japan). Cells were maintained in DMEM (Life Technologies) with 10% FBS and 1% P/S. The generation of HEK293 derived HEK293-ABCB5 cells has been reported previously [81]. HEK293-ABCB5 cells were continuously supplemented with 50 µg/mL zeocin (InvivoGen).

6.2.2 P53 knockout cells

Human HCT116 WT colon cancer cells and p53 knockout HCT116 p53^{-/-} cells were a generous gift from Dr. [REDACTED] (Howard Hughes Medical Institute, Baltimore, MD, USA). The establishment of HCT116 p53^{-/-} by homologous recombination has been described previously [196]. Cells were maintained in DMEM with 10% FBS and 1% P/S. In addition, HCT116 p53^{-/-} cells were supplemented with 400 µg/mL G418 disulfate salt.

6.2.3 EGFR transfected cells

The human glioblastoma cell line U87MG and the transfected subline U87MG.ΔEGFR were used, the latter expressing constitutively active EGFR due to a deletion of exons 2 through 7. The establishment of U87MG.ΔEGFR has been reported previously [197]. Both cell lines were

kindly provided by Dr. [REDACTED] (Ludwig Institute for Cancer Research, San Diego, CA, USA). Cells were maintained in DMEM supplemented with 10% FBS and 1% P/S. U87MG.ΔEGFR cells were maintained in the presence of 400 µg/mL G418 disulfate salt.

6.2.4 Further tumor cell lines

MCF-7 cells (human breast cancer) were obtained from the Institute of Molecular Biology (University of Mainz, Germany). For culturing, DMEM was supplemented with 10% FBS and 1% P/S. The leukemic Jurkat and HL-60 cell lines were maintained in RPMI 1640 medium with 10% FBS and 1% P/S. Human hepatocellular carcinoma cells (HepG2) were cultivated in DMEM supplemented with 10% FBS and 1% P/S. T24 cells (human urinary bladder carcinoma) were obtained from Dr. [REDACTED] (Department of Pharmacy, University of Munich, Germany). The cells were authenticated in April 2013 by the German Collection of Microorganisms and Cell Cultures (DSMZ, Braunschweig, Germany) by DNA profiling of eight highly polymorph short tandem repeats (STR) regions. Cells were maintained in McCoy's 5A medium (Life Technologies) supplemented with 10% FBS and 1% P/S.

6.2.5 Non-tumor cell lines

CCD-18Co human colon and AML12 mouse liver cells were cultured in DMEM with 10% FBS and 1% P/S. For MCF-10a cells (human breast cells), Mammary Epithelial Cell Growth Medium (Ready to use) (PromoCell) was used without any further supplements.

6.2.6 Human peripheral mononuclear cells (PMNC)

Human peripheral mononuclear cells (PMNC) were extracted from fresh blood samples of two healthy donors by centrifugation using Histopaque[®] (Sigma-Aldrich). In brief, 6 mL blood was layered with 6 mL Histopaque[®] and centrifuged (400 × g) for 30 min at 4 °C. The opaque interface, containing lymphocytes and other mononuclear cells, was transferred into a new tube and washed several times. Isolated PMNC were kept in Panserin 413 medium (PAN-Biotech) supplemented with 2% phytohemagglutinin M (Life Technologies).

6.3 Generation of archazolid B-resistant MCF-7 cells (MCF-7ArchB)

To investigate mechanisms of acquired resistance, an archazolid B-resistant cell line was established. MCF-7 cells were repeatedly treated with archazolid B (in the following referred to as MCF-7ArchB cells) and cultivated over a period of about 10 month. MCF-7ArchB cells were maintained in DMEM supplemented with 10% FBS and 1% P/S. The starting dosage of 1 nM was increased up to 10 nM during this time: until P6 (1 nM), until P16 (2 nM/3 nM), until P20 (3 nM/4 nM), until P26 (5 nM/10 nM). Archazolid B was always added to the cells for 72 h. The procedure was repeated when cells completely recovered from the previous treatment.

Parallel to cells treated with archazolid B alone, a combined treatment with ethyl methanesulfonate (EMS) was performed in order to enhance the mutation rate. The use of EMS in the generation of drug-resistant sublines has been described before [198]. Cells were treated with 2.5 mg EMS in a total volume of 10 mL. 24 h later, medium was removed and cells were incubated for five days in EMS-free medium. Then archazolid B was added to the cells for 72 h. EMS treatment was performed three times.

6.4 Growth kinetic studies

MCF-7 (P0) and MCF-7ArchB cells (P6, P16, P20, P26) were seeded in low density (25,000 cells/well) in a 6-well plate. Over a period of 9 days, the number of cells was determined using a Neubauer chamber (Marienfeld). Growth curves were created using Microsoft Excel. Three independent experiments were performed.

6.5 Cytotoxicity assay

The XTT (2, 3-Bis-(2-methoxy-4-nitro-5-sulfophenyl)-2H-tetrazolium-5-carboxanilide) assay was used to determine viability of the different cell lines under treatment with archazolid B. In contrast to dead cells, viable cells are able to metabolize tetrazolium salts by mitochondrial dehydrogenases [199, 200]. The reduction of XTT is enhanced by the electron-coupling reagent phenazine methosulfate (PMS) and the product, an orange formazan compound, can be analyzed by photometry [201].

Adherent cells were seeded 24 h before treatment in appropriate density (breast: 1,500 cells/well; liver: 2,500 cells/96-well; colon: 2,500 cells/96-well; kidney: 5,000 cells/96-well;

brain: 2,500 cells/96-well). Suspension cells (blood) were seeded directly prior to the assay in a density of 10,000 cells/96-well for leukemia cells and 60,000 cells/96-well for PMNC. Cells were incubated with varying concentrations of archazolid B in a total volume of 100 μ L/96-well. Except for liver (AML12 and HepG2) and MDA-MB-231pcDNA3/-BCRP cells, which had to be treated for 96 h in order to obtain IC₅₀ values, the general incubation time was 72 h. Experiments with doxorubicin as well as combination experiments with archazolid B, fluvastatin sodium hydrate, (\pm)-verapamil hydrochloride and doxorubicin were performed in the same way. However, in case of high doxorubicin concentrations, the influence of its fluorescent properties on the measurement was corrected considering control wells with only medium and doxorubicin. Cytotoxicity of archazolid B and doxorubicin on T24 urinary bladder cancer cells was evaluated for different incubation times. Cells were seeded 24 h before treatment as follows: 5,000 cells/96-well (24 h); 2,500 cells/96-well (48 h); 1,500 cells/96-well (72 h); 1,500 cells/96-well (96 h); 750 cells/96-well (120 h). Treatment was performed as described before.

For detection of cell viability, an aqueous solution was prepared out of XTT sodium salt (MP Biomedicals or Sigma-Aldrich) and PMS (Sigma-Aldrich). XTT (1 mg/mL in H₂O) was mixed with 0.5% v/v PMS (1.53 mg/mL in DBPS) and 50 μ L of it were added for about 2 h to each well. Using an Infinite M2000 ProTM plate reader (Tecan), the absorbance was measured at 490 nm and 655 nm and the difference between E490 and E655 was calculated. Comparing treated cells to untreated cells, cell viability was evaluated. Each assay was performed three times with three parallel measurements each. IC₅₀ values were calculated for each experiment from a calibration curve by linear regression using Microsoft Excel and are represented as mean values \pm SD.

6.6 Omics assays: transcriptomics and proteomics

6.6.1 mRNA microarray

6.6.1.1 RNA isolation

T24 cells: RNA samples were obtained from Dr. [REDACTED] (Department of Pharmacy, University of Munich, Germany). T24 cells were seeded 24 h before treatment in a density of 250,000 cells/6-well. The next day, cells were treated with 10 nM archazolid B or DMSO solvent control. Total RNA was isolated using RNeasy Kit (Qiagen) according to the

manufacturer's instruction. RNA was eluted in water. RNA concentrations were determined using NanoDrop 1000 spectrophotometer (Thermo Scientific). The experiment was performed in triplicates for treated samples and in duplicates for control samples.

U87MG and U87MG. Δ EGFR cells: U87MG and U87MG. Δ EGFR cells were seeded one day prior to treatment in 25 cm² flasks (for 24 h treatment: 660,000 cells; for 48 h treatment: 330,000 cells). Cells were treated for 24 h and 48 h with 20 \times IC₅₀ (72 h) concentration of archazolid B (U87MG: 16.2 nM; U87MG. Δ EGFR: 154 nM) or DMSO solvent control. Then, total RNA was isolated and eluted in water using InviTrap[®] Spin Universal RNA Mini kit (STRATEC Biomedical). RNA concentrations were determined using NanoDrop 1000 spectrophotometer (Thermo Scientific). The experiment was performed in duplicates for treated samples and for control samples.

6.6.1.2 Probe labeling and hybridization

MRNA microarrays were performed by the Genomics and Proteomics Core Facility at the German Cancer Research Center (DKFZ, Heidelberg, Germany).

The quality of total RNA was confirmed by gel analysis using the total RNA Nano chip assay on an Agilent 2100 Bioanalyzer (Agilent Technologies GmbH). Samples with RNA index values greater than 8.5 were selected for gene expression profiling. RNA concentrations were determined using NanoDrop 1000 spectrophotometer (Thermo Scientific). Biotin-labeled cRNA samples for hybridization were prepared according to Illumina's recommended sample labeling procedure based on the modified Eberwine protocol [202]. In brief, 250 – 500 ng total RNA was used for complementary DNA (cDNA) synthesis, followed by an amplification/labeling step (*in vitro* transcription) to generate biotin-labeled complementary RNA (cRNA) with the use of MessageAmp II aRNA Amplification kit (Life Technologies) and Biotin-16-UTP (Roche). The cRNA was column purified using Illumina[®] TotalPrep[™] RNA Amplification Kit (Life Technologies). Quality of cRNA (eluted in 60-80 μ L water) was controlled with the RNA Nano Chip Assay on an Agilent 2100 Bioanalyzer (Agilent Technologies GmbH). Quantification was performed using NanoDrop 1000 spectrophotometer (Thermo Scientific). Samples from T24 cells were hybridized on Illumina Human Sentrix HT-12 v3 BeadChip arrays (Illumina Inc.). For samples from U87MG and U87MG. Δ EGFR cells, Illumina Human HT-12 v4 BeadChip arrays were used. Hybridization and washing steps were

carried out according to manufacturer's instructions. For signal detection, arrays were incubated with Cy3-streptavidin (GE Healthcare, UK). After a final wash, arrays were dried and scanned.

6.6.1.3 Scanning and data processing

Microarray scanning was performed by the Genomics and Proteomics Core Facility at the German Cancer Research Center (DKFZ, Heidelberg, Germany) using a Beadstation array scanner (Illumina Inc.), setting adjusted to a scaling factor of 1 and photomultiplier settings at 430. Data extraction was done for all beads individually, and outliers were removed when the median absolute deviation exceeded 2.5. Then mean average signals and standard deviations were calculated for each probe. Data processing was performed by normalization of the signals using the quantile normalization algorithm without background subtraction, and differentially regulated genes were defined by calculating the standard deviation differences of a given probe in a one-by-one comparison of samples or groups.

6.6.2 miRNA microarray

6.6.2.1 RNA isolation

RNA samples were obtained from Dr. [REDACTED] (Department of Pharmacy, University of Munich, Germany). T24 cells, seeded one day prior, were treated for 24 h with 10 nM archazolid B or DMSO solvent control. RNA was isolated using miRNeasy Kit (Qiagen) according to the manufacturer's instruction.

6.6.2.2 Probe labeling and hybridization

The miRNA microarray was performed by the Genomics and Proteomics Core Facility at the German Cancer Research Center (DKFZ, Heidelberg, Germany).

MiRNA quality was confirmed by gel analysis using the Small RNA Nano chip assay on an Agilent 2100 Bioanalyzer (Agilent Technologies GmbH). Probe labeling and hybridization were performed according to the MicroRNA Expression Profiling Assay Guide (Illumina, Inc.). Briefly, 100-200 ng total RNA were polyadenylated using Poly-A polymerase and converted to biotinylated cDNA by standard methods. As a next step, the cDNA was hybridized to

miRNA-specific oligos and the mixture was bound to streptavidin-conjugated paramagnetic particles to select the cDNA/oligo complexes. miRNA specific primer extension was performed and after PCR amplification, the fluorescent labelled, single-stranded product was hybridized on Illumina Human miRNA Universal-12 BeadChip array (1536, Illumina, Inc.) according to manufacturer's instructions.

6.6.2.3 Scanning and data processing

Scanning of the chip was performed on Illumina BeadStation array scanner (Illumina, Inc.). Normalization of the signals was performed using the quantile normalization algorithm.

6.6.3 Proteomics analysis

6.6.3.1 Protein extraction

T24 cells ($5,75 \times 10^6$) were seeded in 175 cm² flasks 24 h before treatment. The next day, old medium was replaced and 10 nM archazolid B or DMSO solvent control were added to the flasks. Samples were prepared in duplicates. After 24 h treatment, cells were washed once with DPBS and proteins were extracted using M-PER[®] Mammalian Protein Extraction Reagent (Thermo Scientific) provided with cOmplete Mini protease inhibitor cocktail (Roche). Cells were incubated for 5 min, harvested with a cell scraper and transferred to a vial. Further incubation was carried out for ½ h on Thermomixer comfort (Eppendorf) at 4 °C. Following centrifugation ($14,000 \times g$, 15 min, 4 °C), the pellet was discarded and the proteins in the supernatant were precipitated by adding cold acetone. After 4 h at -20 °C, precipitation was completed and remaining acetone was removed by centrifugation (3,000 rpm, 10 min, 4 °C).

6.6.3.2 Stable isotope dimethyl labeling

Dimethyl labeling was performed by Dr. [REDACTED] and Prof. [REDACTED] (Agricultural Biotechnology Research Center, Academia Sinica, Taipei, Taiwan).

The protein pellet was dissolved in 50 mM triethylammonium bicarbonate (TEABC, Sigma-Aldrich) up to a final concentration of 1 µg/µL. After a reduction with 5 mM tris (2-carboxyethyl) phosphine hydrochloride (TCEP, Sigma-Aldrich) for 1 h at 37 °C, alkylation

with 2 mM S-methyl methanethiosulfonate (MMTS, Sigma Aldrich) was performed for 45 min at room temperature. The modified tube-gel digestion protocol was used for the proteolytic digestion and the detergent residue was checked as previously described [203]. Two protein mixtures (200 µg) from cells treated with DMSO and archazolid B were dissolved in 200 µL of 100 mM TEABC (pH 8.5) and 20 µL of formaldehyde (Sigma-Aldrich) and formaldehyde-¹³C, ²D (Sigma-Aldrich, diluted to 4% with H₂O) were added. After 5 min vortexing and centrifugation, 20 µL of a 600 mM sodium cyanoborohydride (Sigma-Aldrich) solution was added to each sample. After vortexing (10 min) and centrifugation, samples were incubated for 30 min at 25 °C. For quenching, 10 µL ammonium hydroxide (Sigma-Aldrich, diluted to 7% with H₂O) was added. 16 µL of formic acid (FA, Sigma-Aldrich) was added for acidification and two samples were combined for strong cation exchange (SCX) fractionation. For SCX fractionation, the mobile phase consisted of the buffers SCX-A (5mM KH₂PO₄ in 25% acetonitrile (ACN) at pH 3) and SCX-B (5 mM KH₂PO₄ and 350 nM KCl in 25% ACN at pH 3). After reconstitution in buffer SCX-A, the peptide mixtures were loaded into a PolySOLFOETHYL A column (200 × 2.1 mm, 5 µm, 300 Å, PolyLC) for 10 min at the flow rate of 0.2 mL/min. With a 75 min gradient from 0 to 100% of buffer SCX-B, peptides were fractionated and fractions were collected every three minutes from the retention time of 10 to 55 min by BioFrac™ Fraction Collector (Bio-Rad Laboratories). For further analysis of the peptide mixtures in each of the fractions, liquid chromatography-mass spectrometry/mass spectrometry (LC-MS/MS) was used. LC-MS/MS analysis was carried out using nanoACQUITY UPLC system (Waters) which was coupled online to the nanoelectrospray source of a hybrid quadrupole time-of-flight mass spectrometer (Q-TOF-MS) (SYNAPT G2 HDM Q-TOF-MS, Waters). As a mobile phase, water with 0.1% FA and ACN with 0.1% FA were used. After injection into a trap column (Symmetry C18, 5 µm, 180 µm × 20 mm, Waters, Milford, MA, USA), the sample was separated online with BEH C18 reverse phase column (1.7 µm, 75 µm × 250 mm, Waters) at the flow rate of 300 nL/min using 95 min 5-90% ACN/water gradient. The mass spectrometry instruments were all operated in the positive ion mode. Data dependent acquisition methods were used for all experiments as well. The acquisition method was set to one full MS scan (350-1600 m/z) and a scan time of one second. The setting was switched to six product ion scans (50-1900 m/z) with 0.4 second scan time when a precursor ion charge was 2+, 3+ or 4+ and the intensity was higher than 200 counts.

6.6.3.3 Data processing

Data files were processed using UniQua and further analyzed by Mascot (Matrix Science) and Trans Proteomics Pipeline (TPP) 1 version 4.4 rev. 1 (Institute for Systems Biology). Data processing was described previously in more detail [204].

6.6.4 Omics data analysis

6.6.4.1 Chipster analysis

The expression data sets generated in mRNA microarrays were further processed using Chipster software (CSC). Chipster software allows filtering of genes by standard deviation. Furthermore, data significance can be assessed by performing statistical testing.

T24 cells (mRNA data): Genes were filtered by three times standard deviation and significance was assessed using empirical Bayes t-test ($P < 0.05$) with Benjamini-Hochberg correction.

U87MG and U87MG. Δ EGFR cells (mRNA data): For the comparison of archazolid B treated samples to control samples, genes were filtered by two times standard deviation and empirical Bayes t-test ($P < 0.05$) with Bonferroni correction was applied. When U87MG. Δ EGFR control samples were compared to U87MG control samples, genes were filtered by three times standard deviation and significance was assessed using empirical Bayes t-test ($P < 0.05$) with Benjamini-Hochberg correction.

6.6.4.2 Ingenuity Pathway Analysis

Omics data were analyzed using Ingenuity Pathway Analysis (IPA, Ingenuity Systems Inc.). IPA software relies on the Ingenuity Knowledge Base, a frequently updated database containing biological and chemical interactions and functional annotations gathered from literature.

T24 cells (mRNA, miRNA, protein quantification): Of the three datasets, only molecules with an expression fold change ≥ 1.5 were considered for IPA analysis. For information on cellular functions, networks and affected pathways, IPA offers the Core Analysis tool. At first, Core Analyses were carried out separately for each dataset. Then, mRNA, miRNA and protein datasets were merged to one dataset and also analyzed by this tool. In addition, for miRNA

dataset, the Ingenuity microRNA Target Filter tool was used. This tool associates the deregulated miRNAs with experimentally observed and predicted targets.

U87MG and U87MG.ΔEGFR cells (mRNA data): For IPA analysis, datasets obtained for 24 h treatment with archazolid B were filtered to a fold change $\geq \pm 1.74$. In case of 48 h treatment, only genes with a fold change $\geq \pm 1.82$ were considered for analysis. Core Analyses using the Core Analysis tool were performed for all datasets. The results of the Core Analyses were further studied using the Comparison Analysis tool, offering the possibility to compare datasets of samples with the same incubation time. When U87MG.ΔEGFR control samples were compared to U87MG control samples, complete datasets were considered for Core Analyses.

6.7 Real-time RT-PCR

Primers for real-time RT-PCR were designed using GenScript Real Time PCR Primer Design tool (<https://www.genscript.com/ssl-bin/app/primer>) and Roche Universal Probe Design (<http://www.roche-applied-science.com/sis/rtPCR/upl/index.jsp?id=UP030000>). Oligo Property Scans (MOPS) (<https://ecom.mwgdna.com/services/webgist/mops.tcl>) were performed to assure primer usability. Amplification specificities were checked with Primer Blast (<http://www.ncbi.nlm.nih.gov/tools/primer-blast>) using the sequence data from the NCBI RefSeq Human mRNA data base (<http://www.ncbi.nlm.nih.gov/refseq/>). The housekeeping gene *RPS13*, encoding the 40S ribosomal protein S13, served as reference for standardization [205]. Oligonucleotides were synthesized by Eurofins MWG Operon and primer sequences are shown in Table 14.

Table 14: Primer sequences used for real-time RT-PCR.

Target gene	Primer sequences
<i>HMGCR</i>	FW: 5'-GTTCGGTGGCCTCTAGTGAG-3' REV: 5'-CATGCATTGCGAAAAAGTCTTGACAAC-3'
<i>HMGCS1</i>	FW: 5'-TCTGTCTACTGCAAAAAGATCCAT-3' REV: 5'-CATGAAGCCAAAATCATTCAAGG-3'
<i>LDLR</i>	FW: 5'-ATGACTGCAAGGACATGAGC-3' REV: 5'-CTTGAAGTTGTTGGGTCCCT-3'
<i>SQLE</i>	FW: 5'-CACAGATGATTCCTGCATCAA-3' REV: 5'-AATACAGAAAGCAGCCCAACAG-3'
<i>INSIG1</i>	FW: 5'-GGGCCTTTGGTGGACATTTG-3' REV: 5'-CCTCACAGAAGGGTATCAGCATA-3'
<i>ATP6V0C</i>	FW: 5'-TCAGCCTCTACAAGAGCTTCC-3' REV: 5'-GGATCATGCCACGAATAGTC-3'
<i>EGFR</i>	FW: 5'-CCAGGAACGTACTGGTGAAAA-3' REV: 5'-ATAGGCACTTTGCCTCCTTCT-3'
<i>ABCB1</i>	FW: 5'-AAGGTTCTGGGAAGATCGCTA-3' REV: 5'-TCCAAAGATGTGTGCTTTCCTC-3'
<i>RPS13</i>	FW: 5'-GGTTGAAGTTGACATCTGACGA-3' REV: 5'-CTTGTGCAACACATGTGAAT-3'

6.7.1 mRNA microarray validation

Validation of the microarray data (glioblastoma and T24 cells) was done by real-time RT-PCR for five cholesterol-related genes (*HMGCR*, *HMGCS1*, *LDLR*, *SQLE*, *INSIG1*). In case of glioblastoma cells, real-time RT-PCR was performed with the same samples that were used for microarray experiments. T24 cells, seeded one day prior, were treated for 24 h with 10 nM archazolid B or DMSO solvent control. Total RNA was isolated using InviTrap[®] Spin Universal RNA Mini kit (STRATEC Biomedical) according to the manufacturer's instruction. RNA extracted from glioblastoma and T24 cells was converted to cDNA with random hexamer primers using RevertAid H Minus First Strand cDNA Synthesis Kit (Thermo Scientific). Real-time RT-PCR experiments were performed on CFX384[™] Real-Time PCR Detection System (Bio-Rad). 4 μ L 5 \times Hot Start Taq EvaGreen qPCR Mix (no ROX) (Axon Labor Technik), 250 nM final primer concentration and 300 ng RNA (converted to cDNA) were used per reaction in a total volume of 20 μ L. Real-time RT-PCR was performed as follows: 50 $^{\circ}$ C for 2 min, initial denaturation at 95 $^{\circ}$ C for 10 min, 40 cycles including strand separation at 95 $^{\circ}$ C for

15 sec, annealing at 56.5 °C for 1 min and extension at 72 °C for 1 min following final extension at 95 °C for 1 min. All measurements were done in duplicates and the experiment was repeated once. Standardized C_t (cycle threshold) values for the genes in samples were obtained by dividing the C_t values of genes in drug-treated samples by C_t values of *RPS13* gene in drug-treated samples and multiplying with the C_t value of *RPS13* in the DMSO control. Fold changes were calculated with the ΔC_t (Standardized C_t of the gene in drug-treated sample - C_t of the gene in DMSO control) method where the fold change is equal to $2^{-\Delta C_t}$ for the up-regulated genes and $-(2^{\Delta C_t})$ for the down-regulated genes. R values were determined using Pearson's Correlation Coefficient Calculator (<https://statistics.laerd.com/calculators/pearsons-product-moment-correlation-coefficient-calculator.php>).

6.7.2 Gene expression: *ABCB1*, *EGFR*, *ATP6V0C*

Altered expression of *EGFR*, *ATP6V0C* and *ABCB1* in MCF-7ArchB cells was analyzed performing real-time RT-PCR experiments. Total RNA from MCF-7 (P0) and MCF-7ArchB cells (P6, P16, P20, P26) was isolated using InviTrap® Spin Universal RNA Mini kit (STRATEC Biomedical) according to the manufacturer's instruction. Subsequently, RNA was converted to cDNA with random hexamer primers using RevertAid H Minus First Strand cDNA Synthesis Kit (Thermo Scientific). Real-time RT-PCR experiments were performed on CFX384™ Real-Time PCR Detection System (Bio-Rad). 4 μ L 5 \times Hot Start Taq EvaGreen qPCR Mix (no ROX) (Axon Labortechnik), 250 nM final primer concentration and 300 ng RNA (converted to cDNA) were used per reaction in a total volume of 20 μ L. Real-time RT-PCR was performed as follows: 50 °C for 2 min, initial denaturation at 95 °C for 10 min, 45 cycles including strand separation at 95 °C for 15 s, annealing at 57.5 °C for 1 min and extension at 72 °C for 1 min following final extension at 95 °C for 1 min. Standardized C_t (cycle threshold) values for the genes in samples were obtained by dividing the C_t values of genes in drug-treated samples (MCF-7ArchB) by C_t values of *RPS13* gene in drug-treated samples (MCF-7ArchB) and multiplying with the C_t value of *RPS13* in the MCF-7 control. Fold changes were calculated with the ΔC_t (Standardized C_t of the gene in drug-treated sample - C_t of the gene in MCF-7 control) method where the fold change is equal to $2^{-\Delta C_t}$ for the up-regulated genes and $-(2^{\Delta C_t})$ for the down-regulated genes. The experiment was performed in quadruplicates for each passage (P0, P6, P16, P20, P26) and repeated once. Data is represented as mean \pm SD of gene expression (% of MCF-7 control) in MCF-7ArchB passages (P6, P16, P20 and P26).

6.8 Sequencing

In order to investigate if long-term archazolid B treatment leads to mutation of *ATP6V0C*, total RNA was extracted from MCF-7 (P0) and MCF-7ArchB cells (P6, P16, P20, P26) using InviTrap® Spin Universal RNA Mini kit (STRATEC Biomedical). Extracted RNA was converted to cDNA with RevertAid H Minus First Strand cDNA Synthesis Kit (Thermo Scientific) with random hexamer primers according to manufacturer's protocol. PCR primers for *ATP6V0C* were designed using GenScript Real Time PCR Primer Design (<https://www.genscript.com/ssl-bin/app/primer>) and an Oligo Property Scan (MOPS) (<https://ecom.mwgdna.com/services/webgist/mops.tcl>) was performed to assure primer usability. Amplification specificities were checked with Primer-Blast (<http://www.ncbi.nlm.nih.gov/tools/primer-blast>) using the sequence data from the NCBI RefSeq Human mRNA data base (NM_001694.3). Primers were synthesized by Eurofins MWG Operon. PCR experiments were performed on C1000™ Thermal Cycler (Bio-Rad). The following primer sequences were used: forward primer: 5'-TGCTGGTATTTAGAGCGCAG-3' and reverse primer: 5'-GGAAACAGACGATGGGCACT-3'. Total reaction volume was 50 µL. PCR reactions were set up using Phusion® High-Fidelity PCR Master Mix with GC Buffer (Thermo Scientific) according to the provided protocol. Final primer concentration (500 nM) and 50 ng RNA (converted to cDNA) were used per reaction. The protocol was as follows: Initial denaturation at 98 °C for 30 s, 30 cycles of denaturation at 98 °C for 10 s, annealing at 64 °C for 20 s and extension at 72 °C for 15 s following final extension at 72 °C for 7.5 min. The PCR product (762 bp) was purified using QIAquick PCR Purification Kit (QIAGEN) and the DNA concentration was determined using NanoDrop1000 Spectrophotometer (Thermo Scientific). PCR products were sequenced by Eurofins MWG Operon. Sequences were assembled for comparison using Vector NTI® software (Life Technologies). Protein sequence alignment of V-ATPase subunit c from *Saccharomyces cerevisiae* (yeast) and *Homo sapiens* was performed using Standard Protein BLAST. (http://blast.ncbi.nlm.nih.gov/Blast.cgi?PROGRAM=blastp&PAGE_TYPE=BlastSearch&LINK_LOC=blasthome). Protein sequences were obtained from NCBI Protein data base.

6.9 Molecular docking

The structure of human ABCB1 (P-gp) was created by homology modelling using the x-ray crystallography-based structure of the mouse P-gp as a template (PDB code: 3G60). Homology

modelling was performed by [REDACTED] (Department of Pharmaceutical Biology, University of Mainz, Germany) as previously described [206]. In short, the protein sequences were aligned using EMBOSS Needle (http://www.ebi.ac.uk/Tools/psa/emboss_needle/) and homology models were created using the alignment file with the help of MODELLER 9.11 software (University of California) and Swiss MODEL alignment mode (<http://swissmodel.expasy.org/interactive>). The best homology model was then selected by the Swiss-MODEL structure assessment tool and used for molecular docking. Structures of the ligands (archazolid B, S-verapamil, R-verapamil, doxorubicin) were drawn and 3-D versions of them were created with CORINA online demo (http://www.molecular-networks.com/online_demos/corina_demo). Molecular docking was performed following a previously reported protocol [207]. In brief, human P-gp was set as the rigid receptor molecule. Human P-gp as well as the ligands were first processed with AutodockTools 1.5.6rc3, the graphical user interface for Autodock 4.2 software (Molecular Graphics Laboratory) [208]. The output files were in PDBQT format. The grid box, defining the docking space, was constructed in the way that it covered substrate and modulator binding sites of P-gp [143]. The grid box consisted of 120 grid points in X, 166 grid points in Y and 124 grid points in Z direction, separated by a distance of 0.75 Å between each one. Docking parameters were set to 100 runs and 2,500,000 energy evaluations for each cycle. Grid files were prepared using AutoGrid 4.2 software (Molecular Graphics Laboratory). Docking was performed by Autodock 4.2 software (Molecular Graphics Laboratory) using the Lamarckian Algorithm and binding energies were attained from the docking log files (dlg). Pictures were created with VMD 1.9 (University of Illinois at Urbana Champaign) and Adobe Photoshop CS5 v 12.0.0.2 (Adobe Systems).

6.10 Nuclear expression of SREBPs (Western blot)

The experiment was conducted in collaboration with [REDACTED] (Department of Pharmaceutical Biology, University of Mainz, Germany), who performed cell seeding and treatment.

6.10.1 Sample preparation

Cells were seeded one day before treatment in appropriate density. After 2 h, 24 h and 72 h incubation with 10 nM archazolid B or DMSO (control), cells were harvested and nuclear

proteins were extracted using NE-PER[®] Nuclear and Cytoplasmic Extraction Reagents (Thermo Scientific) supplemented with 1% Halt[™] Protease Inhibitor Cocktail (Thermo Scientific). Nuclear protein concentrations were determined using NanoDrop 1000 spectrophotometer.

6.10.2 SDS-PAGE

For electrophoresis, the Mini-PROTEAN[®] Tetra Cell system from Bio-Rad was used. 12 μ L protein solution was mixed with 4 μ L 6 \times sample loading buffer and water was added to a final volume of 24 μ L. Prior to gel loading, samples were boiled at 95 °C for 10 min. To estimate the molecular weights of the separated protein, 2.5 μ L of MagicMark[™] XP Western Standard protein ladder (Life Technologies) were put on the gel as well. Samples were run through the stacking gel with 50-70 V, then the voltage was increased up to 100 V.

Table 15: Preparation of SDS-PAGE

Stacking gel		Running gel	
H ₂ O	3.075 mL	H ₂ O	3.075 mL
0.5 M Tris-HCl (pH 6.8)	1.25 mL	1.5 M Tris-HCl (pH 8.8)	1.875 mL
20% SDS (w/v)	0.025 mL	20% SDS (w/v)	0.0375 mL
30% acrylamide/bis solution, 29:1	0.67 mL	30% acrylamide/bis solution, 29:1	2.475 mL
10% APS	0.025 mL	10% APS	0.0375 mL
TEMED	0.005 mL	TEMED	0.005 mL

Table 16: Buffers for SDS-PAGE

6 \times sample loading buffer		Electrophoresis buffer	
SDS	1.2 g	Tris-HCl	25 mM
Bromophenol Blue	0.006 g	Glycin	200 mM
Glycerol	4.7 mL	SDS (w/v)	0.1%
1 M Tris-HCl (pH 6.8)	0.6 mL	in H ₂ O	
H ₂ O	2.7 mL		
β -Mercaptoethanol	5%		

6.10.3 Tank blotting

After separating the samples by SDS-PAGE, proteins were transferred to a PVDF blot membrane (Roth). For tank blotting, the Mini Trans-Blot[®] Cell, a component of the Mini-PROTEAN[®] Tetra Cell system (Bio-Rad), was used. The PVDF membrane was rinsed with methanol and water at first. Sponges, papers and the membrane were equilibrated with transfer buffer, before a blotting sandwich was prepared as follows (cathode → anode): sponge, paper, protein gel (from SDS-PAGE), PVDV membrane, paper, sponge. The transfer was carried out within 1.5 h at 300 mA.

Table 17: Transfer buffer

Transfer buffer (Towbin buffer)	
Tris	25 mM
Glycine	192 mM
Methanol	20%
in H ₂ O	

6.10.4 Antibody staining and detection

After protein transfer, the membrane was incubated with blocking solution (2% BSA in Tris-buffered saline-Tween20 (TBS-T)) for 1 h at room temperature. After washing with TBS-T, incubation with the primary rabbit antibody, anti-SREBP1 / anti-SREBP2 antibody (both abcam), was performed for 1.5 h at room temperature. Antibodies were diluted 1:1000 in blocking solution. The membrane was washed three times 10 min with TBS-T. For secondary antibody, HRP-linked anti-rabbit IgG (Cell Signaling) was used (1:2000 in blocking solution) and the membrane was incubated for 1 h at room temperature. After washing with TBST-T (3 × 10 min), 750 µL Luminata[™] Classico Western HRP substrate (Merck Millipore) was added and the blot was detected using the imaging system FluorChem[®]Q (Alpha Innotech).

To ensure comparable sample loading, the blot was additionally stained with Histone H3 antibody (Cell Signaling), diluted 1:5000, in the same way.

Protein bands were quantified using ImageJ 1.4.6 software (NIH). The experiment was performed two times for each SREBP antibody.

Table 18: TBS-T

TBS-T	
Tris-HCl (pH 7.5)	20 mM
NaCl	500 mM
Tween20	0.1%
in H ₂ O	

6.11 Staining of free cholesterol with filipin

6.11.1 Cell seeding and treatment

T24 cells and U87MG.ΔEGFR cells were seeded one day prior to treatment in appropriate density. T24 cells were incubated with 10 nM archazolid B or DMSO solvent control for 12 h, 24 h, 48 h, 60 h, 72 h, 96 h and 120 h. U87MG.ΔEGFR cells were treated with 154 nM archazolid B or DMSO solvent control for 24 h and 72 h.

Combination experiments with archazolid B and fluvastatin were performed by [REDACTED] (Department of Pharmaceutical Biology, University of Mainz, Germany). T24 cells were treated with 10 nM archazolid, DMSO solvent control, 0.5 μM fluvastatin and 10 nM archazolid B/0.5 μM fluvastatin combination and incubated for 72 h.

6.11.2 Staining

After incubation time, cells were harvested and incubated with 1% paraformaldehyde (PFA; Roth) solution for 30 min at room temperature. Fixed cells were washed once with DPBS and subsequently stained with 50 μg/500 μL filipin complex from *Streptomyces filipinensis* (Sigma-Aldrich). Due to its instability, the filipin solution was always freshly prepared. After staining for 2 h at room temperature, cells were centrifuged (1300 rpm, 5 min) and washed twice with DPBS.

6.11.3 Flow cytometry

For FACS (fluorescence-activated cell sorting) analysis, the cell pellet was re-suspended in DPBS and cells were transferred to a FACS tube (BD Biosciences). To detect auto-

fluorescence, cells without staining were prepared as well. The measurements were performed on BD LSRFortessa cell analyzer (BD Biosciences) at the Institute of Molecular Biology (Mainz). The filipin signal was detected with excitation at 355 nm and emission at 450/50 nm. MFIs were calculated and pictures were created with FlowJo software (Tree star). The experiment was performed two times for archazolid B/fluvastatin combination and three times for archazolid B treatment alone. For each experiment, samples were prepared in duplicates.

6.11.4 Fluorescence microscopy

For fluorescence microscopy, the cell pellet was re-suspended in DPBS and cells were pipetted on a microscope slide with cover glass. To detect auto-fluorescence, cells without staining were prepared as well. Pictures were taken on an EVOS fl microscope (AMG) with EVOS fl 20× NA 0.45 objective (AMG) using EVOS light cube DAPI (AMG) with excitation at 357/44 nm and emission at 447/60 nm. Filipin distribution was quantified by calculating the ratio of MFI of the area with high fluorescence to the MFI of the area with low fluorescence using ImageJ 1.4.6 software (NIH). Per experiment with archazolid B alone, the ratios of 10 cells were determined and experiments were performed three times. For archazolid B/fluvastatin combination, ratios of 5 cells from two experiments were considered.

6.12 LDL uptake (Confocal microscopy)

To investigate LDL uptake, T24 cells were seeded in a density of 12,500 cells/well on μ -slides ibiTreat (ibidi). The working volume was always 300 μ L. The next day, cells were treated with 10 nM archazolid B or DMSO solvent control for 24 h. After starving for 2 h in DMEM without FBS, 4.5 μ g/300 μ L BODIPY[®] FL LDL (Life Technologies) was added for 15 min at 37 °C. Cells were washed with DPBS and subsequently incubated with 0.6 μ g/300 μ L CellMask[™] Orange Plasma Membrane Stain (Life Technologies) for 5 min at 37 °C. After two washing steps with DPBS, cells were fixed with 4% PFA for 10 min at room temperature. Cells were washed again with DPBS and covered with mounting medium (ibidi). To detect auto-fluorescence, cells without staining were prepared as well. Pictures were taken with a Leica TCS SP5 confocal microscope (Leica), controlled by LAS AF 2.3.5 software (Leica), using an HCX PL APO CS 63× NA 1.4 OIL UV objective (Leica). BODIPY[®] FL LDL was excited at 488 nm and emission between 498 nm and 530 nm was considered. CellMask[™] Orange Plasma

Membrane Stain was excited at 561 nm and emission between 571 nm and 630 nm was measured. Images were processed using ImageJ 1.4.6 software (NIH). The experiment was performed three times in total.

6.13 LDLR surface expression (Flow cytometry)

LDLR surface expression experiments were performed in collaboration with Dr. [REDACTED] (Department of Pharmaceutical Biology, University of Mainz, Germany), who performed antibody staining and FACS measurement.

T24 cells were seeded in a density of 1,950,000 cells/75 cm² flask. The next day cells were treated with 10 nM archazolid B or DMSO solvent control and harvested after 24 h incubation. After fixation with 4% PFA for 30 min at room temperature cells were washed twice with 0.5% BSA (Sigma-Aldrich) in DPBS. Staining for 1 h at 4 °C was performed using mouse monoclonal LDLR (C7) primary antibody (Santa Cruz) at dilution of 1:50 (in 0.5% BSA/DPBS). As secondary antibody, anti-mouse conjugated with Alexa 488 (Life Technologies) was used for 45 min at 4 °C (1:250 dilution in 0.5% BSA/DPBS). To detect auto-fluorescence, cells without staining were prepared as well. The measurements were performed on FACS Calibur Flow Cytometer (BD Biosciences). The signal was detected with excitation at 488 nm and emission at 530 nm. The experiment was performed two times and for each experiment samples were prepared in duplicates.

6.14 Statistical analysis

Results are represented as mean \pm SD. P-values were calculated by Student's t-test or right-tailed Fisher's exact test (IPA data). Differences were considered as significant at $P < 0.05$.

7 References

- [1] J. Ferlay, H. R. Shin, F. Bray, D. Forman, C. Mathers, and D. M. Parkin, "Estimates of worldwide burden of cancer in 2008: GLOBOCAN 2008," *Int J Cancer*, vol. 127, pp. 2893-917, Dec 2010.
- [2] M. J. Thun, J. O. DeLancey, M. M. Center, A. Jemal, and E. M. Ward, "The global burden of cancer: priorities for prevention," *Carcinogenesis*, vol. 31, pp. 100-10, Jan 2010.
- [3] C. L. Chaffer and R. A. Weinberg, "A perspective on cancer cell metastasis," *Science*, vol. 331, pp. 1559-64, Mar 2011.
- [4] D. Hanahan and R. A. Weinberg, "The hallmarks of cancer," *Cell*, vol. 100, pp. 57-70, Jan 2000.
- [5] D. Hanahan and R. A. Weinberg, "Hallmarks of cancer: the next generation," *Cell*, vol. 144, pp. 646-74, Mar 2011.
- [6] B. Vogelstein and K. W. Kinzler, "The multistep nature of cancer," *Trends Genet*, vol. 9, pp. 138-41, Apr 1993.
- [7] P. A. Futreal, L. Coin, M. Marshall, T. Down, T. Hubbard, R. Wooster, *et al.*, "A census of human cancer genes," *Nat Rev Cancer*, vol. 4, pp. 177-83, Mar 2004.
- [8] S. Sharma, T. K. Kelly, and P. A. Jones, "Epigenetics in cancer," *Carcinogenesis*, vol. 31, pp. 27-36, Jan 2010.
- [9] P. Anand, A. B. Kunnumakkara, A. B. Kunnumakara, C. Sundaram, K. B. Harikumar, S. T. Tharakan, *et al.*, "Cancer is a preventable disease that requires major lifestyle changes," *Pharm Res*, vol. 25, pp. 2097-116, Sep 2008.
- [10] B. A. Chabner and T. G. Roberts, "Timeline: Chemotherapy and the war on cancer," *Nat Rev Cancer*, vol. 5, pp. 65-72, Jan 2005.
- [11] V. T. DeVita and E. Chu, "A history of cancer chemotherapy," *Cancer Res*, vol. 68, pp. 8643-53, Nov 2008.
- [12] R. J. Papac, "Origins of cancer therapy," *Yale J Biol Med*, vol. 74, pp. 391-8, 2001 Nov-Dec 2001.
- [13] T. Efferth, *Molekulare Pharmakologie und Toxikologie: Biologische Grundlagen von Arzneimitteln und Giften*. Heidelberg: Springer, 2006.
- [14] K. Aktories, U. Förstermann, F. B. Hofmann, and K. Starke, *Repetitorium: Allgemeine und spezielle Pharmakologie und Toxikologie*. München: Elsevier, 2006.
- [15] D. E. Gerber, "Targeted therapies: a new generation of cancer treatments," *Am Fam Physician*, vol. 77, pp. 311-9, Feb 2008.
- [16] M. Huang, A. Shen, J. Ding, and M. Geng, "Molecularly targeted cancer therapy: some lessons from the past decade," *Trends Pharmacol Sci*, vol. 35, pp. 41-50, Jan 2014.
- [17] C. Sawyers, "Targeted cancer therapy," *Nature*, vol. 432, pp. 294-7, Nov 2004.
- [18] D. J. Newman and G. M. Cragg, "Natural products as sources of new drugs over the 30 years from 1981 to 2010," *J Nat Prod*, vol. 75, pp. 311-35, Mar 2012.
- [19] M. Pandey, M. Debnath, S. Gupta, and S. K. Chikara, "Phytomedicine: An ancient approach turning into future potential source of therapeutics," *J Pharmacognosy Phytother*, vol. 3, pp. 113-17, Feb 2011.
- [20] B. Sandhya, S. Thomas, W. Isabel, and R. Shenbagarathai, "Ethnomedicinal plants used by the Valaiyan community of Piranmalai hills (Reserved Forest), Tamilnadu, India. - A pilot study " *Afr J Trad CAM*, vol. 3, pp. 101-14, Dec 2006.
- [21] N. Savithramma, M. Linga Rao, and D. Suhrulatha, "Screening of Medicinal Plants for Secondary Metabolites," *Middle-East J Sci Res*, vol. 8, pp. 579-84, 2011.
- [22] T. Efferth, P. C. Li, V. S. Konkimalla, and B. Kaina, "From traditional Chinese medicine to rational cancer therapy," *Trends Mol Med*, vol. 13, pp. 353-61, Aug 2007.

- [23] G. M. Cragg and D. J. Newman, "Natural products: a continuing source of novel drug leads," *Biochim Biophys Acta*, vol. 1830, pp. 3670-95, Jun 2013.
- [24] A. L. Demain and S. Sanchez, "Microbial drug discovery: 80 years of progress," *J Antibiot (Tokyo)*, vol. 62, pp. 5-16, Jan 2009.
- [25] L. A. Giddings and D. J. Newman, "Microbial natural products: molecular blueprints for antitumor drugs," *J Ind Microbiol Biotechnol*, vol. 40, pp. 1181-210, Nov 2013.
- [26] H. Reichenbach, "The ecology of the myxobacteria," *Environ Microbiol*, vol. 1, pp. 15-21, Feb 1999.
- [27] H. Reichenbach, "Myxobacteria, producers of novel bioactive substances," *J Ind Microbiol Biotechnol*, vol. 27, pp. 149-56, Sep 2001.
- [28] H. B. Bode and R. Müller, "Analysis of myxobacterial secondary metabolism goes molecular," *J Ind Microbiol Biotechnol*, vol. 33, pp. 577-88, Jul 2006.
- [29] K. J. Weissman and R. Müller, "Myxobacterial secondary metabolites: bioactivities and modes-of-action," *Nat Prod Rep*, vol. 27, pp. 1276-95, Sep 2010.
- [30] K. C. Nicolaou, J. S. Chen, and S. M. Dalby, "From nature to the laboratory and into the clinic," *Bioorg Med Chem*, vol. 17, pp. 2290-303, Mar 2009.
- [31] E. Mukhtar, V. M. Adhami, and H. Mukhtar, "Targeting microtubules by natural agents for cancer therapy," *Mol Cancer Ther*, vol. 13, pp. 275-84, Feb 2014.
- [32] F. Sasse, H. Steinmetz, J. Heil, G. Höfle, and H. Reichenbach, "Tubulysins, new cytostatic peptides from myxobacteria acting on microtubuli. Production, isolation, physico-chemical and biological properties," *J Antibiot (Tokyo)*, vol. 53, pp. 879-85, Sep 2000.
- [33] Y. A. Elnakady, F. Sasse, H. Lünsdorf, and H. Reichenbach, "Disorazol A1, a highly effective antimetabolic agent acting on tubulin polymerization and inducing apoptosis in mammalian cells," *Biochem Pharmacol*, vol. 67, pp. 927-35, Mar 2004.
- [34] A. H. Maurer, P. Elsinga, S. Fanti, B. Nguyen, W. J. Oyen, and W. A. Weber, "Imaging the folate receptor on cancer cells with ^{99m}Tc-etarfolatide: properties, clinical use, and future potential of folate receptor imaging," *J Nucl Med*, vol. 55, pp. 701-4, May 2014.
- [35] F. Sasse, B. Kunze, T. M. Gronewold, and H. Reichenbach, "The chondramides: cytostatic agents from myxobacteria acting on the actin cytoskeleton," *J Natl Cancer Inst*, vol. 90, pp. 1559-63, Oct 1998.
- [36] T. M. Gronewold, F. Sasse, H. Lünsdorf, and H. Reichenbach, "Effects of rhizopodin and latrunculin B on the morphology and on the actin cytoskeleton of mammalian cells," *Cell Tissue Res*, vol. 295, pp. 121-9, Jan 1999.
- [37] M. Huss, F. Sasse, B. Kunze, R. Jansen, H. Steinmetz, G. Ingenhorst, *et al.*, "Archazolid and apicularen: novel specific V-ATPase inhibitors," *BMC Biochem*, vol. 6, p. 13, 2005.
- [38] F. Sasse, H. Steinmetz, G. Höfle, and H. Reichenbach, "Archazolids, new cytotoxic macrolactones from *Archangium gephyra* (Myxobacteria). Production, isolation, physico-chemical and biological properties," *J Antibiot (Tokyo)*, vol. 56, pp. 520-5, Jun 2003.
- [39] D. Menche, J. Hassfeld, H. Steinmetz, M. Huss, H. Wieczorek, and F. Sasse, "Archazolid-7-O- β -D-glucopyranoside - Isolation, structural elucidation and solution conformation of a novel V-ATPase inhibitor from the myxobacterium *Cystobacter violaceus*," *Eur J Org Chem*, vol. 2007, pp. 1196-202, Mar 2007.
- [40] D. Menche, J. Hassfeld, H. Steinmetz, M. Huss, H. Wieczorek, and F. Sasse, "The first hydroxylated archazolid from the myxobacterium *Cystobacter violaceus*: isolation, structural elucidation and V-ATPase inhibition," *J Antibiot (Tokyo)*, vol. 60, pp. 328-31, May 2007.
- [41] N. Horstmann, S. Essig, S. Bockelmann, H. Wieczorek, M. Huss, F. Sasse, *et al.*, "Archazolid A-15-O- β -D-glucopyranoside and iso-archazolid B: potent V-ATPase

- inhibitory polyketides from the myxobacteria *Cystobacter violaceus* and *Archangium gephyra*," *J Nat Prod*, vol. 74, pp. 1100-5, May 2011.
- [42] M. Huss, O. Vitavska, A. Albertmelcher, S. Bockelmann, C. Nardmann, K. Tabke, *et al.*, "Vacuolar H(+)-ATPases: intra- and intermolecular interactions," *Eur J Cell Biol*, vol. 90, pp. 688-95, Sep 2011.
- [43] T. Nishi and M. Forgac, "The vacuolar (H+)-ATPases--nature's most versatile proton pumps," *Nat Rev Mol Cell Biol*, vol. 3, pp. 94-103, Feb 2002.
- [44] T. H. Stevens and M. Forgac, "Structure, function and regulation of the vacuolar (H+)-ATPase," *Annu Rev Cell Dev Biol*, vol. 13, pp. 779-808, 1997.
- [45] M. Forgac, "Vacuolar ATPases: rotary proton pumps in physiology and pathophysiology," *Nat Rev Mol Cell Biol*, vol. 8, pp. 917-29, Nov 2007.
- [46] A. Hinton, S. Bond, and M. Forgac, "V-ATPase functions in normal and disease processes," *Pflugers Arch*, vol. 457, pp. 589-98, Jan 2009.
- [47] N. Nelson, "Structural conservation and functional diversity of V-ATPases," *J Bioenerg Biomembr*, vol. 24, pp. 407-14, Aug 1992.
- [48] M. Futai, T. Oka, G. Sun-Wada, Y. Moriyama, H. Kanazawa, and Y. Wada, "Luminal acidification of diverse organelles by V-ATPase in animal cells," *J Exp Biol*, vol. 203, pp. 107-16, Jan 2000.
- [49] K. W. Beyenbach and H. Wiczorek, "The V-type H+ ATPase: molecular structure and function, physiological roles and regulation," *J Exp Biol*, vol. 209, pp. 577-89, Feb 2006.
- [50] E. J. Bowman and B. J. Bowman, "V-ATPases as drug targets," *J Bioenerg Biomembr*, vol. 37, pp. 431-5, Dec 2005.
- [51] B. A. Webb, M. Chimenti, M. P. Jacobson, and D. L. Barber, "Dysregulated pH: a perfect storm for cancer progression," *Nat Rev Cancer*, vol. 11, pp. 671-7, Sep 2011.
- [52] R. Martínez-Zaguilan, R. M. Lynch, G. M. Martínez, and R. J. Gillies, "Vacuolar-type H(+)-ATPases are functionally expressed in plasma membranes of human tumor cells," *Am J Physiol*, vol. 265, pp. C1015-29, Oct 1993.
- [53] X. Lu and W. Qin, "Vacuolar H(+)-ATPase in cancer cells: structure and function," *Atlas Genet Cytogenet Oncol Haematol*, vol. 16, pp. 252-9, 2012.
- [54] S. Fais, A. De Milito, H. You, and W. Qin, "Targeting vacuolar H+-ATPases as a new strategy against cancer," *Cancer Res*, vol. 67, pp. 10627-30, Nov 2007.
- [55] S. R. Sennoune, D. Luo, and R. Martínez-Zaguilán, "Plasmalemmal vacuolar-type H+-ATPase in cancer biology," *Cell Biochem Biophys*, vol. 40, pp. 185-206, 2004.
- [56] M. Pérez-Sayáns, J. M. Somoza-Martín, F. Barros-Angueira, J. M. Rey, and A. García-García, "V-ATPase inhibitors and implication in cancer treatment," *Cancer Treat Rev*, vol. 35, pp. 707-13, Dec 2009.
- [57] S. Dröse and K. Altendorf, "Bafilomycins and concanamycins as inhibitors of V-ATPases and P-ATPases," *J Exp Biol*, vol. 200, pp. 1-8, Jan 1997.
- [58] D. Menche, J. Hassfeld, J. Li, K. Mayer, and S. Rudolph, "Modular total synthesis of archazolid A and B," *J Org Chem*, vol. 74, pp. 7220-9, Oct 2009.
- [59] P. A. Roethle, I. T. Chen, and D. Trauner, "Total synthesis of (-)-archazolid B," *J Am Chem Soc*, vol. 129, pp. 8960-1, Jul 2007.
- [60] S. Bockelmann, D. Menche, S. Rudolph, T. Bender, S. Grond, P. von Zezschwitz, *et al.*, "Archazolid A binds to the equatorial region of the c-ring of the vacuolar H+-ATPase," *J Biol Chem*, vol. 285, pp. 38304-14, Dec 2010.
- [61] S. Dreisigacker, D. Latek, S. Bockelmann, M. Huss, H. Wiczorek, S. Filipek, *et al.*, "Understanding the inhibitory effect of highly potent and selective archazolides binding to the vacuolar ATPase," *J Chem Inf Model*, vol. 52, pp. 2265-72, Aug 2012.
- [62] K. von Schwarzenberg, R. M. Wiedmann, P. Oak, S. Schulz, H. Zischka, G. Wanner, *et al.*, "Mode of cell death induction by pharmacological vacuolar H+-ATPase (V-ATPase) inhibition," *J Biol Chem*, vol. 288, pp. 1385-96, Jan 2013.

- [63] R. M. Wiedmann, K. von Schwarzenberg, A. Palamidessi, L. Schreiner, R. Kubisch, J. Liebl, *et al.*, "The V-ATPase-inhibitor archazolid abrogates tumor metastasis via inhibition of endocytic activation of the Rho-GTPase Rac1," *Cancer Res*, vol. 72, pp. 5976-87, Nov 2012.
- [64] R. M. Wiedmann, "Anticancer effects of the V-ATPase inhibitor Archazolid B," Dissertation, LMU München, 2011.
- [65] R. S. Kerbel, H. Kobayashi, and C. H. Graham, "Intrinsic or acquired drug resistance and metastasis: are they linked phenotypes?," *J Cell Biochem*, vol. 56, pp. 37-47, Sep 1994.
- [66] M. M. Gottesman, "Mechanisms of cancer drug resistance," *Annu Rev Med*, vol. 53, pp. 615-27, 2002.
- [67] J. I. Fletcher, M. Haber, M. J. Henderson, and M. D. Norris, "ABC transporters in cancer: more than just drug efflux pumps," *Nat Rev Cancer*, vol. 10, pp. 147-56, Feb 2010.
- [68] M. Dean, Y. Hamon, and G. Chimini, "The human ATP-binding cassette (ABC) transporter superfamily," *J Lipid Res*, vol. 42, pp. 1007-17, Jul 2001.
- [69] G. Szakács, J. K. Paterson, J. A. Ludwig, C. Booth-Genthe, and M. M. Gottesman, "Targeting multidrug resistance in cancer," *Nat Rev Drug Discov*, vol. 5, pp. 219-34, Mar 2006.
- [70] T. Murakami and M. Takano, "Intestinal efflux transporters and drug absorption," *Expert Opin Drug Metab Toxicol*, vol. 4, pp. 923-39, Jul 2008.
- [71] S. G. Aller, J. Yu, A. Ward, Y. Weng, S. Chittaboina, R. Zhuo, *et al.*, "Structure of P-glycoprotein reveals a molecular basis for poly-specific drug binding," *Science*, vol. 323, pp. 1718-22, Mar 2009.
- [72] S. V. Ambudkar, S. Dey, C. A. Hrycyna, M. Ramachandra, I. Pastan, and M. M. Gottesman, "Biochemical, cellular, and pharmacological aspects of the multidrug transporter," *Annu Rev Pharmacol Toxicol*, vol. 39, pp. 361-98, 1999.
- [73] D. R. Ferry and D. J. Kerr, "Multidrug resistance in cancer," *BMJ*, vol. 308, pp. 148-9, Jan 1994.
- [74] F. J. Sharom, "Complex Interplay between the P-Glycoprotein Multidrug Efflux Pump and the Membrane: Its Role in Modulating Protein Function," *Front Oncol*, vol. 4, 2014.
- [75] C. F. Higgins and K. J. Linton, "The ATP switch model for ABC transporters," *Nat Struct Mol Biol*, vol. 11, pp. 918-26, Oct 2004.
- [76] M. Yu, A. Ocana, and I. F. Tannock, "Reversal of ATP-binding cassette drug transporter activity to modulate chemoresistance: why has it failed to provide clinical benefit?," *Cancer Metastasis Rev*, vol. 32, pp. 211-27, Jun 2013.
- [77] T. Nakanishi and D. D. Ross, "Breast cancer resistance protein (BCRP/ABCG2): its role in multidrug resistance and regulation of its gene expression," *Chin J Cancer*, vol. 31, pp. 73-99, Feb 2012.
- [78] K. Kage, T. Fujita, and Y. Sugimoto, "Role of Cys-603 in dimer/oligomer formation of the breast cancer resistance protein BCRP/ABCG2," *Cancer Sci*, vol. 96, pp. 866-72, Dec 2005.
- [79] T. Litman, T. E. Druley, W. D. Stein, and S. E. Bates, "From MDR to MXR: new understanding of multidrug resistance systems, their properties and clinical significance," *Cell Mol Life Sci*, vol. 58, pp. 931-59, Jun 2001.
- [80] N. Y. Frank, S. S. Pendse, P. H. Lapchak, A. Margaryan, D. Shlain, C. Doeing, *et al.*, "Regulation of progenitor cell fusion by ABCB5 P-glycoprotein, a novel human ATP-binding cassette transporter," *J Biol Chem*, vol. 278, pp. 47156-65, Nov 2003.
- [81] T. Kawanobe, S. Kogure, S. Nakamura, M. Sato, K. Katayama, J. Mitsushashi, *et al.*, "Expression of human ABCB5 confers resistance to taxanes and anthracyclines," *Biochem Biophys Res Commun*, vol. 418, pp. 736-41, Feb 2012.

- [82] D. B. Longley and P. G. Johnston, "Molecular mechanisms of drug resistance," *J Pathol*, vol. 205, pp. 275-92, Jan 2005.
- [83] B. Vogelstein, D. Lane, and A. J. Levine, "Surfing the p53 network," *Nature*, vol. 408, pp. 307-10, Nov 2000.
- [84] F. Chen, W. Wang, and W. S. El-Deiry, "Current strategies to target p53 in cancer," *Biochem Pharmacol*, vol. 80, pp. 724-30, Sep 2010.
- [85] W. S. El-Deiry, "Regulation of p53 downstream genes," *Semin Cancer Biol*, vol. 8, pp. 345-57, 1998.
- [86] W. S. El-Deiry, "The role of p53 in chemosensitivity and radiosensitivity," *Oncogene*, vol. 22, pp. 7486-95, Oct 2003.
- [87] T. Soussi and C. Bérout, "Assessing TP53 status in human tumours to evaluate clinical outcome," *Nat Rev Cancer*, vol. 1, pp. 233-40, Dec 2001.
- [88] G. Blandino, A. J. Levine, and M. Oren, "Mutant p53 gain of function: differential effects of different p53 mutants on resistance of cultured cells to chemotherapy," *Oncogene*, vol. 18, pp. 477-85, Jan 1999.
- [89] H. Song, M. Hollstein, and Y. Xu, "p53 gain-of-function cancer mutants induce genetic instability by inactivating ATM," *Nat Cell Biol*, vol. 9, pp. 573-80, May 2007.
- [90] R. S. Herbst, "Review of epidermal growth factor receptor biology," *Int J Radiat Oncol Biol Phys*, vol. 59, pp. 21-6, 2004.
- [91] G. Lurje and H. J. Lenz, "EGFR signaling and drug discovery," *Oncology*, vol. 77, pp. 400-10, 2009.
- [92] T. Servidei, A. Riccardi, S. Mozzetti, C. Ferlini, and R. Riccardi, "Chemoresistant tumor cell lines display altered epidermal growth factor receptor and HER3 signaling and enhanced sensitivity to gefitinib," *Int J Cancer*, vol. 123, pp. 2939-49, Dec 2008.
- [93] N. Normanno, A. De Luca, C. Bianco, L. Strizzi, M. Mancino, M. R. Maiello, *et al.*, "Epidermal growth factor receptor (EGFR) signaling in cancer," *Gene*, vol. 366, pp. 2-16, Jan 2006.
- [94] R. I. Nicholson, J. M. Gee, and M. E. Harper, "EGFR and cancer prognosis," *Eur J Cancer*, vol. 37, pp. 9-15, Sep 2001.
- [95] R. Nishikawa, X. D. Ji, R. C. Harmon, C. S. Lazar, G. N. Gill, W. K. Cavenee, *et al.*, "A mutant epidermal growth factor receptor common in human glioma confers enhanced tumorigenicity," *Proc Natl Acad Sci U S A*, vol. 91, pp. 7727-31, Aug 1994.
- [96] K. Schwchheimer, S. Huang, and W. K. Cavenee, "EGFR gene amplification--rearrangement in human glioblastomas," *Int J Cancer*, vol. 62, pp. 145-8, Jul 1995.
- [97] N. Sugawa, A. J. Ekstrand, C. D. James, and V. P. Collins, "Identical splicing of aberrant epidermal growth factor receptor transcripts from amplified rearranged genes in human glioblastomas," *Proc Natl Acad Sci U S A*, vol. 87, pp. 8602-6, Nov 1990.
- [98] C. J. Wikstrand, C. J. Reist, G. E. Archer, M. R. Zalutsky, and D. D. Bigner, "The class III variant of the epidermal growth factor receptor (EGFRvIII): characterization and utilization as an immunotherapeutic target," *J Neurovirol*, vol. 4, pp. 148-58, Apr 1998.
- [99] H. W. Lo, "EGFR-targeted therapy in malignant glioma: novel aspects and mechanisms of drug resistance," *Curr Mol Pharmacol*, vol. 3, pp. 37-52, Jan 2010.
- [100] M. W. Pedersen, N. Pedersen, L. H. Ottesen, and H. S. Poulsen, "Differential response to gefitinib of cells expressing normal EGFR and the mutant EGFRvIII," *Br J Cancer*, vol. 93, pp. 915-23, Oct 2005.
- [101] M. Nagane, A. Levitzki, A. Gazit, W. K. Cavenee, and H. J. Huang, "Drug resistance of human glioblastoma cells conferred by a tumor-specific mutant epidermal growth factor receptor through modulation of Bcl-XL and caspase-3-like proteases," *Proc Natl Acad Sci U S A*, vol. 95, pp. 5724-9, May 1998.

- [102] H. Izumi, T. Torigoe, H. Ishiguchi, H. Uramoto, Y. Yoshida, M. Tanabe, *et al.*, "Cellular pH regulators: potentially promising molecular targets for cancer chemotherapy," *Cancer Treat Rev*, vol. 29, pp. 541-9, Dec 2003.
- [103] Z. Ouar, M. Bens, C. Vignes, M. Paulais, C. Pringel, J. Fleury, *et al.*, "Inhibitors of vacuolar H⁺-ATPase impair the preferential accumulation of daunomycin in lysosomes and reverse the resistance to anthracyclines in drug-resistant renal epithelial cells," *Biochem J*, vol. 370, pp. 185-93, Feb 2003.
- [104] H. You, J. Jin, H. Shu, B. Yu, A. De Milito, F. Lozupone, *et al.*, "Small interfering RNA targeting the subunit ATP6L of proton pump V-ATPase overcomes chemoresistance of breast cancer cells," *Cancer Lett*, vol. 280, pp. 110-9, Jul 2009.
- [105] T. Murakami, I. Shibuya, T. Ise, Z. S. Chen, S. Akiyama, M. Nakagawa, *et al.*, "Elevated expression of vacuolar proton pump genes and cellular PH in cisplatin resistance," *Int J Cancer*, vol. 93, pp. 869-74, Sep 2001.
- [106] F. Valeriote and L. van Putten, "Proliferation-dependent cytotoxicity of anticancer agents: a review," *Cancer Res*, vol. 35, pp. 2619-30, Oct 1975.
- [107] R. J. DeBerardinis, J. J. Lum, G. Hatzivassiliou, and C. B. Thompson, "The biology of cancer: metabolic reprogramming fuels cell growth and proliferation," *Cell Metab*, vol. 7, pp. 11-20, Jan 2008.
- [108] M. Upadhyay, J. Samal, M. Kandpal, O. V. Singh, and P. Vivekanandan, "The Warburg effect: insights from the past decade," *Pharmacol Ther*, vol. 137, pp. 318-30, Mar 2013.
- [109] J. R. Cantor and D. M. Sabatini, "Cancer cell metabolism: one hallmark, many faces," *Cancer Discov*, vol. 2, pp. 881-98, Oct 2012.
- [110] C. R. Santos and A. Schulze, "Lipid metabolism in cancer," *FEBS J*, vol. 279, pp. 2610-23, Aug 2012.
- [111] J. L. Goldstein and M. S. Brown, "Regulation of the mevalonate pathway," *Nature*, vol. 343, pp. 425-30, Feb 1990.
- [112] J. L. Goldstein, M. S. Brown, R. G. Anderson, D. W. Russell, and W. J. Schneider, "Receptor-mediated endocytosis: concepts emerging from the LDL receptor system," *Annu Rev Cell Biol*, vol. 1, pp. 1-39, 1985.
- [113] A. J. Brown and W. Jessup, "Oxysterols: Sources, cellular storage and metabolism, and new insights into their roles in cholesterol homeostasis," *Mol Aspects Med*, vol. 30, pp. 111-22, Jun 2009.
- [114] M. S. Brown and J. L. Goldstein, "The SREBP pathway: regulation of cholesterol metabolism by proteolysis of a membrane-bound transcription factor," *Cell*, vol. 89, pp. 331-40, May 1997.
- [115] L. J. Millatt, V. Bocher, J. C. Fruchart, and B. Staels, "Liver X receptors and the control of cholesterol homeostasis: potential therapeutic targets for the treatment of atherosclerosis," *Biochim Biophys Acta*, vol. 1631, pp. 107-18, Mar 2003.
- [116] N. Zelcer, C. Hong, R. Boyadjian, and P. Tontonoz, "LXR regulates cholesterol uptake through Idol-dependent ubiquitination of the LDL receptor," *Science*, vol. 325, pp. 100-4, Jul 2009.
- [117] D. Gal, P. C. MacDonald, J. C. Porter, and E. R. Simpson, "Cholesterol metabolism in cancer cells in monolayer culture. III. Low-density lipoprotein metabolism," *Int J Cancer*, vol. 28, pp. 315-9, Sep 1981.
- [118] O. Larsson, "HMG-CoA reductase inhibitors: role in normal and malignant cells," *Crit Rev Oncol Hematol*, vol. 22, pp. 197-212, Apr 1996.
- [119] J. Hu, C. La Vecchia, M. de Groh, E. Negri, H. Morrison, L. Mery, *et al.*, "Dietary cholesterol intake and cancer," *Ann Oncol*, vol. 23, pp. 491-500, Feb 2012.
- [120] H. Y. Li, F. R. Appelbaum, C. L. Willman, R. A. Zager, and D. E. Banker, "Cholesterol-modulating agents kill acute myeloid leukemia cells and sensitize them to therapeutics by blocking adaptive cholesterol responses," *Blood*, vol. 101, pp. 3628-34, May 2003.

- [121] A. Hryniewicz-Jankowska, K. Augoff, A. Biernatowska, J. Podkalicka, and A. F. Sikorski, "Membrane rafts as a novel target in cancer therapy," *Biochim Biophys Acta*, vol. 1845, pp. 155-165, Apr 2014.
- [122] J. A. Menendez and R. Lupu, "Fatty acid synthase and the lipogenic phenotype in cancer pathogenesis," *Nat Rev Cancer*, vol. 7, pp. 763-77, Oct 2007.
- [123] N. S. Parkar, B. S. Akpa, L. C. Nitsche, L. E. Wedgewood, A. T. Place, M. S. Sverdlov, *et al.*, "Vesicle formation and endocytosis: function, machinery, mechanisms, and modeling," *Antioxid Redox Signal*, vol. 11, pp. 1301-12, Jun 2009.
- [124] A. Subtil, I. Gaidarov, K. Kobylarz, M. A. Lampson, J. H. Keen, and T. E. McGraw, "Acute cholesterol depletion inhibits clathrin-coated pit budding," *Proc Natl Acad Sci USA*, vol. 96, pp. 6775-80, Jun 1999.
- [125] S. K. Rodal, G. Skretting, O. Garred, F. Vilhardt, B. van Deurs, and K. Sandvig, "Extraction of cholesterol with methyl-beta-cyclodextrin perturbs formation of clathrin-coated endocytic vesicles," *Mol Biol Cell*, vol. 10, pp. 961-74, Apr 1999.
- [126] S. J. McTaggart, "Isoprenylated proteins," *Cell Mol Life Sci*, vol. 63, pp. 255-67, Feb 2006.
- [127] J. W. Clendening, A. Pandya, P. C. Boutros, S. El Ghamrasni, F. Khosravi, G. A. Trentin, *et al.*, "Dysregulation of the mevalonate pathway promotes transformation," *Proc Natl Acad Sci USA*, vol. 107, pp. 15051-6, Aug 2010.
- [128] P. C. Lee, A. D. Nguyen, and R. A. Debose-Boyd, "Mutations within the membrane domain of HMG-CoA reductase confer resistance to sterol-accelerated degradation," *J Lipid Res*, vol. 48, pp. 318-27, Feb 2007.
- [129] J. W. Clendening and L. Z. Penn, "Targeting tumor cell metabolism with statins," *Oncogene*, vol. 31, pp. 4967-78, Nov 2012.
- [130] S. Pisanti, P. Picardi, E. Ciaglia, A. D'Alessandro, and M. Bifulco, "Novel prospects of statins as therapeutic agents in cancer," *Pharmacol Res*, Jul 2014.
- [131] F. J. Sharom, "The P-glycoprotein efflux pump: how does it transport drugs?," *J Membr Biol*, vol. 160, pp. 161-75, Dec 1997.
- [132] W. T. Bellamy, W. S. Dalton, J. M. Kailey, M. C. Gleason, T. M. McCloskey, R. T. Dorr, *et al.*, "Verapamil reversal of doxorubicin resistance in multidrug-resistant human myeloma cells and association with drug accumulation and DNA damage," *Cancer Res*, vol. 48, pp. 6365-70, Nov 1988.
- [133] A. E. Lykkesfeldt, M. W. Madsen, and P. Briand, "Altered expression of estrogen-regulated genes in a tamoxifen-resistant and ICI 164,384 and ICI 182,780 sensitive human breast cancer cell line, MCF-7/TAMR-1," *Cancer Res*, vol. 54, pp. 1587-95, Mar 1994.
- [134] Y. S. Min, E. H. Yi, J. K. Lee, J. W. Choi, J. H. Sim, J. S. Kang, *et al.*, "CK20 expression enhances the invasiveness of tamoxifen-resistant MCF-7 cells," *Anticancer Res*, vol. 32, pp. 1221-8, Apr 2012.
- [135] G. A. Sega, "A review of the genetic effects of ethyl methanesulfonate," *Mutat Res*, vol. 134, pp. 113-42, 1984 Sep-Nov 1984.
- [136] Y. Huang, X. J. Shen, Q. Zou, S. P. Wang, S. M. Tang, and G. Z. Zhang, "Biological functions of microRNAs: a review," *J Physiol Biochem*, vol. 67, pp. 129-39, Mar 2011.
- [137] T. Yang, P. J. Espenshade, M. E. Wright, D. Yabe, Y. Gong, R. Aebersold, *et al.*, "Crucial step in cholesterol homeostasis: sterols promote binding of SCAP to INSIG-1, a membrane protein that facilitates retention of SREBPs in ER," *Cell*, vol. 110, pp. 489-500, Aug 2002.
- [138] L. Liscum and K. W. Underwood, "Intracellular cholesterol transport and compartmentation," *J Biol Chem*, vol. 270, pp. 15443-6, Jun 1995.

- [139] C. P. Muller, D. A. Stephany, D. F. Winkler, J. M. Hoeg, S. J. Demosky, and J. R. Wunderlich, "Filipin as a flow microfluorometry probe for cellular cholesterol," *Cytometry*, vol. 5, pp. 42-54, Jan 1984.
- [140] J. M. Robinson and M. J. Karnovsky, "Evaluation of the polyene antibiotic filipin as a cytochemical probe for membrane cholesterol," *J Histochem Cytochem*, vol. 28, pp. 161-8, Feb 1980.
- [141] J. P. Desyhpere, "The role of HMG-CoA reductase inhibitors in the treatment of hyperlipidemia: a review of fluvastatin," *Curr Ther Res*, vol. 56, pp. 111-28, 1995.
- [142] H. Zhan, K. Yokoyama, H. Otani, K. Tanigaki, N. Shirota, S. Takano, *et al.*, "Different roles of proteolipids and 70-kDa subunits of V-ATPase in growth and death of cultured human cells," *Genes Cells*, vol. 8, pp. 501-13, Jun 2003.
- [143] R. J. Ferreira, M. J. Ferreira, and D. J. dos Santos, "Molecular docking characterizes substrate-binding sites and efflux modulation mechanisms within P-glycoprotein," *J Chem Inf Model*, vol. 53, pp. 1747-60, Jul 2013.
- [144] T. Efferth, V. B. Konkimalla, Y. F. Wang, A. Sauerbrey, S. Meinhardt, F. Zintl, *et al.*, "Prediction of broad spectrum resistance of tumors towards anticancer drugs," *Clin Cancer Res*, vol. 14, pp. 2405-12, Apr 2008.
- [145] C. F. Higgins and M. M. Gottesman, "Is the multidrug transporter a flippase?," *Trends Biochem Sci*, vol. 17, pp. 18-21, Jan 1992.
- [146] Y. Honjo, C. A. Hrycyna, Q. W. Yan, W. Y. Medina-Pérez, R. W. Robey, A. van de Laar, *et al.*, "Acquired mutations in the MXR/BCRP/ABCP gene alter substrate specificity in MXR/BCRP/ABCP-overexpressing cells," *Cancer Res*, vol. 61, pp. 6635-9, Sep 2001.
- [147] L. Ma and M. S. Center, "The gene encoding vacuolar H(+)-ATPase subunit C is overexpressed in multidrug-resistant HL60 cells," *Biochem Biophys Res Commun*, vol. 182, pp. 675-81, Jan 1992.
- [148] C. Holohan, S. Van Schaeybroeck, D. B. Longley, and P. G. Johnston, "Cancer drug resistance: an evolving paradigm," *Nat Rev Cancer*, vol. 13, pp. 714-26, Oct 2013.
- [149] X. Lin, K. Ramamurthi, M. Mishima, A. Kondo, R. D. Christen, and S. B. Howell, "P53 modulates the effect of loss of DNA mismatch repair on the sensitivity of human colon cancer cells to the cytotoxic and mutagenic effects of cisplatin," *Cancer Res*, vol. 61, pp. 1508-16, Feb 2001.
- [150] J. L. Yu, B. L. Coomber, and R. S. Kerbel, "A paradigm for therapy-induced microenvironmental changes in solid tumors leading to drug resistance," *Differentiation*, vol. 70, pp. 599-609, Dec 2002.
- [151] V. Kuete, P. D. Tchakam, B. Wiench, B. Ngameni, H. K. Wabo, M. F. Tala, *et al.*, "Cytotoxicity and modes of action of four naturally occurring benzophenones: 2,2',5,6'-tetrahydroxybenzophenone, guttiferone E, isogarcinol and isoxanthochymol," *Phytomedicine*, vol. 20, pp. 528-36, Apr 2013.
- [152] D. A. Altomare and J. R. Testa, "Perturbations of the AKT signaling pathway in human cancer," *Oncogene*, vol. 24, pp. 7455-64, Nov 2005.
- [153] M. V. Grandal, R. Zandi, M. W. Pedersen, B. M. Willumsen, B. van Deurs, and H. S. Poulsen, "EGFRvIII escapes down-regulation due to impaired internalization and sorting to lysosomes," *Carcinogenesis*, vol. 28, pp. 1408-17, Jul 2007.
- [154] N. Y. Lukyanova, N. V. Rusetskya, N. A. Tregubova, and V. F. Chekhun, "Molecular profile and cell cycle in MCF-7 cells resistant to cisplatin and doxorubicin," *Exp Oncol*, vol. 31, pp. 87-91, Jun 2009.
- [155] M. S. Brown, Y. K. Ho, and J. L. Goldstein, "The cholesteryl ester cycle in macrophage foam cells. Continual hydrolysis and re-esterification of cytoplasmic cholesteryl esters," *J Biol Chem*, vol. 255, pp. 9344-52, Oct 1980.

- [156] J. Zhang, N. Dudley-Rucker, J. R. Crowley, E. Lopez-Perez, M. Issandou, J. E. Schaffer, *et al.*, "The steroidal analog GW707 activates the SREBP pathway through disruption of intracellular cholesterol trafficking," *J Lipid Res*, vol. 45, pp. 223-31, Feb 2004.
- [157] J. C. Cruz, S. Sugii, C. Yu, and T. Y. Chang, "Role of Niemann-Pick type C1 protein in intracellular trafficking of low density lipoprotein-derived cholesterol," *J Biol Chem*, vol. 275, pp. 4013-21, Feb 2000.
- [158] J. E. Wraith, N. Guffon, M. Rohrbach, W. L. Hwu, G. C. Korenke, B. Bembi, *et al.*, "Natural history of Niemann-Pick disease type C in a multicentre observational retrospective cohort study," *Mol Genet Metab*, vol. 98, pp. 250-4, Nov 2009.
- [159] T. Furuchi, K. Aikawa, H. Arai, and K. Inoue, "Bafilomycin A1, a specific inhibitor of vacuolar-type H(+)-ATPase, blocks lysosomal cholesterol trafficking in macrophages," *J Biol Chem*, vol. 268, pp. 27345-8, Dec 1993.
- [160] J. P. Davies, F. W. Chen, and Y. A. Ioannou, "Transmembrane molecular pump activity of Niemann-Pick C1 protein," *Science*, vol. 290, pp. 2295-8, Dec 2000.
- [161] D. Halter, "Transport and Translocation of Glycosylceramide," Dissertation, Utrecht University, 2007.
- [162] P. Kozik, N. A. Hodson, D. A. Sahlender, N. Simecek, C. Soromani, J. Wu, *et al.*, "A human genome-wide screen for regulators of clathrin-coated vesicle formation reveals an unexpected role for the V-ATPase," *Nat Cell Biol*, vol. 15, pp. 50-60, Jan 2013.
- [163] S. Straud, I. Zubovych, J. K. De Brabander, and M. G. Roth, "Inhibition of iron uptake is responsible for differential sensitivity to V-ATPase inhibitors in several cancer cell lines," *PLoS One*, vol. 5, p. e11629, 2010.
- [164] B. Mesmin and F. R. Maxfield, "Intracellular sterol dynamics," *Biochim Biophys Acta*, vol. 1791, pp. 636-45, Jul 2009.
- [165] J. D. Horton, N. A. Shah, J. A. Warrington, N. N. Anderson, S. W. Park, M. S. Brown, *et al.*, "Combined analysis of oligonucleotide microarray data from transgenic and knockout mice identifies direct SREBP target genes," *Proc Natl Acad Sci U S A*, vol. 100, pp. 12027-32, Oct 2003.
- [166] N. Gévry, K. Schoonjans, F. Guay, and B. D. Murphy, "Cholesterol supply and SREBPs modulate transcription of the Niemann-Pick C-1 gene in steroidogenic tissues," *J Lipid Res*, vol. 49, pp. 1024-33, May 2008.
- [167] P. A. Edwards, D. Tabor, H. R. Kast, and A. Venkateswaran, "Regulation of gene expression by SREBP and SCAP," *Biochim Biophys Acta*, vol. 1529, pp. 103-13, Dec 2000.
- [168] T. F. Osborne, "Sterol regulatory element-binding proteins (SREBPs): key regulators of nutritional homeostasis and insulin action," *J Biol Chem*, vol. 275, pp. 32379-82, Oct 2000.
- [169] K. B. Peake and J. E. Vance, "Defective cholesterol trafficking in Niemann-Pick C-deficient cells," *FEBS Lett*, vol. 584, pp. 2731-9, Jul 2010.
- [170] M. J. Rudling, B. Angelin, C. O. Peterson, and V. P. Collins, "Low density lipoprotein receptor activity in human intracranial tumors and its relation to the cholesterol requirement," *Cancer Res*, vol. 50, pp. 483-7, Feb 1990.
- [171] C. G. A. R. Network, "Comprehensive genomic characterization defines human glioblastoma genes and core pathways," *Nature*, vol. 455, pp. 1061-8, Oct 2008.
- [172] T. Porstmann, B. Griffiths, Y. L. Chung, O. Delpuech, J. R. Griffiths, J. Downward, *et al.*, "PKB/Akt induces transcription of enzymes involved in cholesterol and fatty acid biosynthesis via activation of SREBP," *Oncogene*, vol. 24, pp. 6465-81, Sep 2005.
- [173] D. Guo, R. M. Prins, J. Dang, D. Kuga, A. Iwanami, H. Soto, *et al.*, "EGFR signaling through an Akt-SREBP-1-dependent, rapamycin-resistant pathway sensitizes glioblastomas to antilipogenic therapy," *Sci Signal*, vol. 2, p. ra82, 2009.

- [174] D. Guo, F. Reinitz, M. Youssef, C. Hong, D. Nathanson, D. Akhavan, *et al.*, "An LXR agonist promotes glioblastoma cell death through inhibition of an EGFR/AKT/SREBP-1/LDLR-dependent pathway," *Cancer Discov*, vol. 1, pp. 442-56, Oct 2011.
- [175] H. A. Tawfeek and A. B. Abou-Samra, "Important role for the V-type H(+)-ATPase and the Golgi apparatus in the recycling of PTH/PTHrP receptor," *Am J Physiol Endocrinol Metab*, vol. 286, pp. E704-10, May 2004.
- [176] K. Tveten, T. Ranheim, K. E. Berge, T. P. Leren, and M. A. Kulseth, "The effect of bafilomycin A1 and protease inhibitors on the degradation and recycling of a Class 5-mutant LDLR," *Acta Biochim Biophys Sin (Shanghai)*, vol. 41, pp. 246-55, Mar 2009.
- [177] K. von Schwarzenberg, T. Lajtos, L. Simon, R. Müller, G. Vereb, and A. M. Vollmar, "V-ATPase inhibition overcomes trastuzumab resistance in breast cancer," *Mol Oncol*, vol. 8, pp. 9-19, Feb 2014.
- [178] H. A. Risch, J. D. Burch, A. B. Miller, G. B. Hill, R. Steele, and G. R. Howe, "Dietary factors and the incidence of cancer of the urinary bladder," *Am J Epidemiol*, vol. 127, pp. 1179-91, Jun 1988.
- [179] M. de Martino, C. V. Leitner, C. Seemann, S. L. Hofbauer, I. Lucca, A. Haitel, *et al.*, "Preoperative serum cholesterol is an independent prognostic factor for patients with renal cell carcinoma (RCC)," *BJU Int*, Apr 2014.
- [180] J. C. Cruz and T. Y. Chang, "Fate of endogenously synthesized cholesterol in Niemann-Pick type C1 cells," *J Biol Chem*, vol. 275, pp. 41309-16, Dec 2000.
- [181] J. L. Goldstein and M. S. Brown, "The LDL receptor," *Arterioscler Thromb Vasc Biol*, vol. 29, pp. 431-8, Apr 2009.
- [182] M. Jakobisiak and J. Golab, "Statins can modulate effectiveness of antitumor therapeutic modalities," *Med Res Rev*, vol. 30, pp. 102-35, Jan 2010.
- [183] A. A. Argyriou, J. Bruna, P. Marmiroli, and G. Cavaletti, "Chemotherapy-induced peripheral neurotoxicity (CIPN): an update," *Crit Rev Oncol Hematol*, vol. 82, pp. 51-77, Apr 2012.
- [184] J. A. Reddy, R. Dorton, A. Dawson, M. Vetzal, N. Parker, J. S. Nicoson, *et al.*, "In vivo structural activity and optimization studies of folate-tubulysin conjugates," *Mol Pharm*, vol. 6, pp. 1518-25, 2009 Sep-Oct 2009.
- [185] Y. Hu, J. Nyman, P. Muhonen, H. K. Väänänen, and T. Laitala-Leinonen, "Inhibition of the osteoclast V-ATPase by small interfering RNAs," *FEBS Lett*, vol. 579, pp. 4937-42, Sep 2005.
- [186] F. E. Karet, "Inherited distal renal tubular acidosis," *J Am Soc Nephrol*, vol. 13, pp. 2178-84, Aug 2002.
- [187] C. J. Swallow, S. Grinstein, R. A. Sudsbury, and O. D. Rotstein, "Modulation of the macrophage respiratory burst by an acidic environment: the critical role of cytoplasmic pH regulation by proton extrusion pumps," *Surgery*, vol. 108, pp. 363-8; discussion 368-9, Aug 1990.
- [188] Z. Korade and A. K. Kenworthy, "Lipid rafts, cholesterol, and the brain," *Neuropharmacology*, vol. 55, pp. 1265-73, Dec 2008.
- [189] R. Distl, S. Treiber-Held, F. Albert, V. Meske, K. Harzer, and T. G. Ohm, "Cholesterol storage and tau pathology in Niemann-Pick type C disease in the brain," *J Pathol*, vol. 200, pp. 104-11, May 2003.
- [190] F. W. Pfrieger, "Cholesterol homeostasis and function in neurons of the central nervous system," *Cell Mol Life Sci*, vol. 60, pp. 1158-71, Jun 2003.
- [191] W. M. Pardridge, "The blood-brain barrier: bottleneck in brain drug development," *NeuroRx*, vol. 2, pp. 3-14, Jan 2005.
- [192] J. L. Goldstein and M. S. Brown, "The low-density lipoprotein pathway and its relation to atherosclerosis," *Annu Rev Biochem*, vol. 46, pp. 897-930, 1977.

- [193] R. Kubisch, T. Fröhlich, G. J. Arnold, L. Schreiner, K. von Schwarzenberg, A. Roidl, *et al.*, "V-ATPase inhibition by archazolid leads to lysosomal dysfunction resulting in impaired cathepsin B activation in vivo," *Int J Cancer*, vol. 134, pp. 2478-88, May 2014.
- [194] A. Kimmig, V. Gekeler, M. Neumann, G. Frese, R. Handgretinger, G. Kardos, *et al.*, "Susceptibility of multidrug-resistant human leukemia cell lines to human interleukin 2-activated killer cells," *Cancer Res*, vol. 50, pp. 6793-9, Nov 1990.
- [195] L. A. Doyle, W. Yang, L. V. Abruzzo, T. Krogmann, Y. Gao, A. K. Rishi, *et al.*, "A multidrug resistance transporter from human MCF-7 breast cancer cells," *Proc Natl Acad Sci U S A*, vol. 95, pp. 15665-70, Dec 1998.
- [196] F. Bunz, A. Dutriaux, C. Lengauer, T. Waldman, S. Zhou, J. P. Brown, *et al.*, "Requirement for p53 and p21 to sustain G2 arrest after DNA damage," *Science*, vol. 282, pp. 1497-501, Nov 1998.
- [197] H. S. Huang, M. Nagane, C. K. Klingbeil, H. Lin, R. Nishikawa, X. D. Ji, *et al.*, "The enhanced tumorigenic activity of a mutant epidermal growth factor receptor common in human cancers is mediated by threshold levels of constitutive tyrosine phosphorylation and unattenuated signaling," *J Biol Chem*, vol. 272, pp. 2927-35, Jan 1997.
- [198] S. Akiyama, A. Fojo, J. A. Hanover, I. Pastan, and M. M. Gottesman, "Isolation and genetic characterization of human KB cell lines resistant to multiple drugs," *Somat Cell Mol Genet*, vol. 11, pp. 117-26, Mar 1985.
- [199] T. F. Slater, B. Sawyer, and U. Straeli, "Studies on succinate-tetrazolium reductase systems: III. Points of coupling of four different tetrazolium salts," *Biochim Biophys Acta*, vol. 77, pp. 383-93, Nov 1963.
- [200] T. Mosmann, "Rapid colorimetric assay for cellular growth and survival: application to proliferation and cytotoxicity assays," *J Immunol Methods*, vol. 65, pp. 55-63, Dec 1983.
- [201] D. A. Scudiero, R. H. Shoemaker, K. D. Paull, A. Monks, S. Tierney, T. H. Nofziger, *et al.*, "Evaluation of a soluble tetrazolium/formazan assay for cell growth and drug sensitivity in culture using human and other tumor cell lines," *Cancer Res*, vol. 48, pp. 4827-33, Sep 1988.
- [202] J. Eberwine, H. Yeh, K. Miyashiro, Y. Cao, S. Nair, R. Finnell, *et al.*, "Analysis of gene expression in single live neurons," *Proc Natl Acad Sci U S A*, vol. 89, pp. 3010-4, Apr 1992.
- [203] C. J. Chen, M. C. Tseng, H. J. Lin, T. W. Lin, and Y. R. Chen, "Visual indicator for surfactant abundance in MS-based membrane and general proteomics applications," *Anal Chem*, vol. 82, pp. 8283-90, Oct 2010.
- [204] W. H. Chang, C. Y. Lee, C. Y. Lin, W. Y. Chen, M. C. Chen, W. S. Tzou, *et al.*, "UniQua: a universal signal processor for MS-based qualitative and quantitative proteomics applications," *Anal Chem*, vol. 85, pp. 890-7, Jan 2013.
- [205] F. Jacob, R. Guertler, S. Naim, S. Nixdorf, A. Fedier, N. F. Hacker, *et al.*, "Careful selection of reference genes is required for reliable performance of RT-qPCR in human normal and cancer cell lines," *PLoS One*, vol. 8, p. e59180, 2013.
- [206] Y. Tajima, H. Nakagawa, A. Tamura, O. Kadioglu, K. Satake, Y. Mitani, *et al.*, "Nitensidine A, a guanidine alkaloid from *Pterogyne nitens*, is a novel substrate for human ABC transporter ABCB1," *Phytomedicine*, vol. 21, pp. 323-32, Feb 2014.
- [207] Q. Zhao, M. Zeino, T. Eichhorn, J. Herrmann, R. Müller, and T. Efferth, "Molecular docking studies of myxobacterial disorazoles and tubulysins to tubulin," *J Biosci Med*, vol. 3, pp. 31-43, 2013.
- [208] G. M. Morris, R. Huey, W. Lindstrom, M. F. Sanner, R. K. Belew, D. S. Goodsell, *et al.*, "AutoDock4 and AutoDockTools4: Automated docking with selective receptor flexibility," *J Comput Chem*, vol. 30, pp. 2785-91, Dec 2009.

Lebenslauf

Der Lebenslauf ist in der elektronischen Fassung der Dissertation nicht enthalten.

Permissions to publish

Permissions to publish have been granted by the following copyright holders:

Figure 1: Reprinted from: Cell, vol. 144 (5), D. Hanahan and R. A. Weinberg, "Hallmarks of cancer: the next generation," pp. 646-74, Mar 2011, Copyright 2011, with permission from Elsevier. doi:10.1016/j.cell.2011.02.013;

<http://www.sciencedirect.com/science/article/pii/S0092867411001279>

Figure 2: Reprinted by permission from Macmillan Publishers Ltd [Nature Reviews Molecular Cell Biology]: T. Nishi and M. Forgac, "The vacuolar (H⁺)-ATPases--nature's most versatile proton pumps," Nat Rev Mol Cell Biol, vol. 3, pp. 94-103, Feb 2002. Copyright 2002. doi:10.1038/nrm729; <http://www.nature.com/nrm/journal/v3/n2/abs/nrm729.html>

Figure 3: With kind permission from Springer Science+Business Media: Pflugers Arch, "V-ATPase functions in normal and disease processes," vol. 457 (3), 2009, pp. 589-98, A. Hinton, S. Bond, and M. Forgac, Figure 1. Copyright 2007. doi:10.1007/s00424-007-0382-4; <http://link.springer.com/article/10.1007/s00424-007-0382-4>

Figure 5: From S. G. Aller, J. Yu, A. Ward, Y. Weng, S. Chittaboina, R. Zhuo, et al., "Structure of P-glycoprotein reveals a molecular basis for poly-specific drug binding," Science, vol. 323 (5922), pp. 1718-22, Mar 2009. Reprinted with permission from AAAS. doi:10.1126/science.1168750; <http://www.sciencemag.org/content/323/5922/1718.short>

Text, figures and tables from own publications:

Reprinted from: Biochem Pharm, vol. 91 (1), R. Hamm, Y.-R. Chen, E.-J. Seo, M. Zeino, C.-F. Wu, R. Müller, N.-S. Yang, "Induction of cholesterol biosynthesis by archazolid B in T24 bladder cancer cells," pp. 18-30, 2014. Copyright 2014, with permission from Elsevier. doi:10.1016/j.bcp.2014.06.018;

<http://www.sciencedirect.com/science/article/pii/S000629521400361X>

Reprinted from: Toxicol Appl Pharmacol, vol. 281 (1), R. Hamm, M. Zeino, S. Frewert, T. Efferth, "Up-regulation of cholesterol associated genes as novel resistance mechanism in glioblastoma cells in response to archazolid B," pp. 78-86, 2014. Copyright 2014, with permission from Elsevier. doi:10.1016/j.taap.2014.08.033; <http://www.sciencedirect.com/science/article/pii/S0041008X14003251>

With kind permission from Springer Science+Business Media: Invest New Drugs, "Resistance mechanisms of cancer cells to the novel vacuolar H⁺-ATPase inhibitor archazolid B," vol. 32 (5), 2014, pp. 893-903, R. Hamm, Y. Sugimoto, H. Steinmetz, T. Efferth. Copyright 2014. doi:10.1007/s10637-014-0134-1; <http://link.springer.com/article/10.1007/s10637-014-0134-1>